MODELLING OF STORM SURGE DUE TO HURRICANES IN MISSISSIPPI (USA)

BY
ÁLVARO PRIDA GUILLÉN

FEBRUARY 2020

MODELLING OF STORM SURGE DUE TO HURRICANES IN MISSISSIPPI (USA)

BY
ÁLVARO PRIDA GUILLÉN

Department of Hydraulic Engineering
Section of Hydraulic Structures and Flood Risk

in partial fulfillment of the requirements for the degree of

Master of Science
in Civil Engineering

at the Delft University of Technology,
to be defended publicly on February 14, 2020 at 10:00 AM.

Student number:	4583302	
Project duration:	May 15, 2019 – February 14, 2020	
Committee chairman:	Dr. Ir. Bricker, J.	TU Delft
Committee members:	Dr. Ir. Meynadier, R.	AXA GRM
	Prof. Dr. Ir. Ranasinghe, R.	IHE Delft
	Dr. Ir. Duong, T.	IHE Delft
	Dr. Ir. Morales-Nápoles, O.	TU Delft
	Dr. Ir. Díaz Loaiza, A.	TU Delft
	Dr. Ir. Luijendijk, A.	TU Delft

This thesis is confidential and cannot be made public until February 14, 2020.

An electronic version of this thesis is available at `http://repository.tudelft.nl/`.

TU Delft Delft University of Technology

AXA

Preface

With this project, I close a chapter of three years and a half in The Netherlands. I arrived back in August 2016 for an Exchange Programme of one year. The courses I took on the first months of the Programme were mostly oriented to Hydraulic Engineering, and I discovered the wide range of applications of this branch of Civil Engineering. The Department of Hydraulic Engineering concentrated highly experienced professionals from the field in hydraulics coming from worldwide. Considering this a unique atmosphere to learn and grow as engineer, I applied for the MSc in Civil Engineering, with specialization in Hydraulic Engineering. I am very grateful to Fundación "La Caixa" and the Delft University of Technology for funding my MSc studies, by means of the *Scholarship for studies in Europe* and the *Faculty Excellence Scholarship*, respectively. I really appreciate your confidence along the whole MSc period.

My studies in Delft have finished with a graduation project of 9 months of duration. Along this project, I set up a physical and stochastic model to predict storm surge due to hurricanes. Since the beginning, I knew it was going to be a challenging project. I worked with softwares that I never used before, in programming languages that were new for me. Despite the obstacles, I have been able to succeed in modelling coastal phenomena, which was one of my main objectives of the MSc. This would have not been possible without the project proposal from Jeremy Bricker. I really appreciate your enthusiasm to help and giving me advice. Your comments along the process have been crucial to continuously improve the outcomes of the project. Many thanks for your excellent guidance along this complex project.

I am also very grateful to Rémi Meynadier who has given me the opportunity to work in the Group Risk Management department of AXA, in Paris. Since the very first day, I felt very comfortable in the team thanks to the fantastic atmosphere of the office. Many thanks for the constructive discussions we had about the project and the support along the six months of internship. My stay in Paris has been an unforgettable experience.

I am very glad to have been supervised by Andrés Díaz Loaiza. I can definitely say that without your help I could not have finished this project, due to the large amount of simulations and repetitions I had to perform in the physical modelling part of the project. You have given me a new insight in the physical modelling, by using high performance computers.

I would like to thank Trang Duong, Rosh Ranasinghe and Arjen Luijendijk for their help with Delft3D FM along the project and their comments during the meetings. Thanks to you I have gotten more familiarized with coastal engineering modelling and the processes behind it.

I really appreciate the insight given by Oswaldo Morales-Nápoles in the probabilistic part of the project. I firmly believe that the future of hydraulic engineering will be every time more associated to stochastic models such as Bayesian Networks, and I am very happy to have learnt from your expertise in this field of knowledge.

I do not forget the support of David Rodríguez, Qian Ke and Maialen Irazoqui, who kindly helped me to overcome several difficulties I have encountered during the modelling in Delft3D FM.

Finally, I am very thankful to my mother Eva, my father Fernando and my brothers Fernando and Pelayo for their unconditional support along the whole MSc. You have been able to transmit me the motivation I needed in the toughest moments of the thesis, and I feel very fortunate for that. Thanks also to all the people that I met during the MSc and my friends from Spain, specially Gonzalo and Wouter.

Executive summary

The existing hydrodynamic models consider full physics approaches to calculate storm surge at coastal regions. However, due to the complexity of the equations that model these processes, the computational time and power required to run them can be large, compared to models that consider simplified equations. By contrast, simplified hydraulic models lack physical background, what leads to a minor accuracy in the surge estimations with respect to hydrodynamic models. In this project, a stochastic model has been developed with the objective to estimate surge at the coast of Mississippi (United States) at a reasonable accuracy and time, without solving equations that represent complex physical processes.

The stochastic model needs to be trained by means of hurricane data, including surge levels. This information must be generated beforehand, by simulating a limited number of hurricanes with an hydrodynamic model. In this project, the hydrodynamic model Delft3D Flexible Mesh has been used for this purpose. The approach followed to build the stochastic model has been based on three main steps. The first step has been setting up and validating the hydrodynamic model in Delft3D FM. Hurricane Katrina (2005) has been simulated to calibrate the input parameters of the model, by comparing the maximum simulated water levels at 41 stations along the shoreline of Mississippi to the high water marks observed at the same locations during the event. Tide, surge and wave setup have been considered in the validation. An unstructured mesh with a maximum resolution of 200 meters at the shoreline of Mississippi has been used. This mesh comprises the entire Gulf of Mexico and presents open sea boundaries at the Yucatan Channel and the Florida Strait, where an astronomical tide has been imposed. The adaptation of the Holland model made by Veltcheva [81] is applied to generate the hurricane forcing. The wind drag has been prescribed based on the model of Makin [47]. The results of the validation show a line best fit slope from the origin of 0.912 and an R^2 of 0.996. At Gulfport, the absolute error of the surge estimation is 19 centimeters, equivalent to a relative error of 2.5%.

The second step in the construction of the stochastic model has been the generation of a historical hurricane data base. The hurricane best tracks have been retrieved from the HURDAT2 data base. The variables considered have been the forward speed and the forward direction of the hurricane at landfall, the wind speed at landfall, the distance from landfall location to a reference point (Galveston Bay) and the maximum storm surge during the hurricane. In this case, only the hurricane forcing is considered as external action. The storm surge has been recorded at Gulfport Harbour (central coast of Mississippi). The values of the surge have been obtained by using the validated model to simulate the historical hurricanes making landfall in a rectangular domain of 600 kilometers, being Gulfport Harbour the center of the rectangle. Due to the scarce number of hurricanes making landfall in this region, the tracks of the hurricanes making landfall in the North of the Gulf of Mexico but outside the rectangular domain have been shifted inside the domain, in order to generate a sufficiently large data base to train the stochastic model. A data base with 140 hurricanes has been built, from which the 85% (119 hurricanes) have been used for the training of the stochastic model and the other 15% (21 hurricanes) have been used for the validation of the stochastic model.

The third and last step has been the setup and validation of the stochastic model, by comparing the storm surge obtained from the stochastic model to the surge obtained from the hydrodynamic simulations. The stochastic model used to estimate storm surge has been a Bayesian Network that assumes normal copulas to represent the joint distribution between nodes of the network. The Bayesian Network provides the uncertainty of the estimation by giving a normal distribution of the surge. The calculated slope of the best fit line for the mean surge values has been 0.861, with an R^2 of 0.885. Moreover, the average standard deviation of the estimations is 1.16 meters. These results indicate a reasonable estimation of the surge by means of the Bayesian Network. This estimation can be made in the order of seconds.

Table of contents

List of Figures

List of Tables

CHAPTER 1

Introduction

1.1 Motivation

Global cities are the engine for the economic development of the countries and the global economy. Most of the global cities are located close or on the coast, what has enhanced their commercial relationships with the rest of the world and contributed to their wealth [10]. Many of these cities are also located close to river mouths, benefiting also from the trade flowing in and out of the inland waterway network. However, coastal regions are vulnerable to climate hazards, particularly those cities located in tropical areas, due to the occurrence of tropical cyclones. Amongst the natural hazards, flooding has been reported as the most catastrophic, in monetary terms [52] and in life terms [75].

Coastal flooding due to the storm surge generated by hurricanes has particularly drawn the attention of insurance companies and funds, due to the severity of the consequences of these extreme events. For instance, the Hurricane Katrina hit the Atlantic coast of the United States in August 2005, triggering itself more flood insurance claim payments by the National Flood Insurance Program (NFIP) than the payments made over the life of the program to that point ($16 billion) [42].

Despite the uncertainty in the connection between tropical cyclone frequency and climate change declared by the scientific community, warmer ocean temperatures and higher sea levels are expected to intensify the impact of tropical cyclones [7]. In these circumstances, the improvement of the estimations of storm surge and coastal flood in cyclone-prone areas is an issue of current interest in the coastal engineering field. Moreover, an additional challenge regarding this topic is the reduction of the time of simulation to estimate these water levels.

The flood risk is defined as the product of the probability of occurrence of a flood event and the consequences [38]. The recent increase of the flood risk in tropical areas is due to two reasons:

- **Increase of probability of occurrence of flood events:** As mentioned in [7], there is no sign that indicated that the frequency of tropical cyclones is increasing due to climate change, but records indicate that there is a progressive intensification of the tropical cyclones., Therefore, there are more tropical cyclones causing floods, what boosts the probability of flooding, together with the sea level rise. The tropical cyclone intensity (i.e. more precipitation) is enhanced by the rise of the seawater temperature. This phenomenon accelerates the evaporation of sea water, what leads to more accumulation of water in the clouds and therefore heavier rainfall events. On the other hand, several recent studies suggest that the sea level rise by 2100 can reach the 2 meters [33].
- **Aggravation of the consequences of flood events:** The concentration of population and the economical activity in coastal regions aggravate the consequences of flooding, due to the larger exposure of lives and property to flood.

1.2 Problem definition and research questions

Hydraulic models are used to assess the effects of a flood event in a specific domain. The ideal hydraulic model should be able to predict surge and flooding in a short time span and with high accuracy. However, the existing

models either require large computational time and power to simulate these hydraulic phenomena or they are capable of estimating flood in a shorter time but with larger uncertainty. This fact makes each model suitable for different objectives. For rough estimations of flood, the bucket-fill approach is commonly used. The advantage of this method is the fast speed of calculation. However, the method uses simplifications of the physical laws, what leads to achieve a limited level of accuracy in the results. On the other hand, hydrodynamic models such as Delft3D Flexible Mesh are very accurate due to their strong physical background, but computationally more expensive.

The objective of this project is to develop a model that finds a trade-off between computational time and accuracy in the results. To meet this purpose, a stochastic model is developed. The stochastic model needs to be trained by means of hurricane data, including surge levels. This information must be generated beforehand, by simulating a limited number of hurricanes with an hydrodynamic model. Based on this approach, a main research question is formulated:

Is it possible to estimate storm surge at reasonable accuracy and time in the coast of Mississippi by using a stochastic model?

The research question can be answered by responding several sub-questions:

- How should the different input of the hydrodynamic model be calibrated to simulate surge at high fidelity?
- How should the hurricane data scarcity be tackled in order to generate a sufficiently large data set for the training of the stochastic model?
- What is the accuracy of the surge estimation and the time of computation of the stochastic model?

By answering these questions, the following objectives will be fulfilled:

- Setup and validation of an hydrodynamic model for the coast of Mississippi.
- Generation of a hurricane database, including storm surge levels.
- Setup and validation of a stochastic model capable of estimating storm surge at the coast of Mississippi.

1.3 Research location

According to the objectives outlined above, this project is a first step in the development of a high-fidelity stochastic model that can predict storm surge and coastal flood worldwide. In this project, the area of study is the coast of Mississippi, in the United States (Figure 1.1). Three main reasons have led to select this region as research site:

- **Coastal morphology**: The assumption of alongshore uniform coast in the Mississippi state is reasonable, what simplifies the elaboration of the stochastic model by neglecting the influence of coastal morphology.
- **Absence of flood defences**: The Mississippi coast is characterized by the absence of coastal defences. Consequently, the complex 3D effects on the flow (such as vertical turbulence) that result from the failure of levees or other coastal defences do not need to be considered in the model, simplifying the model setup.
- **Societal interest**: Due to the economic development of the region and the frequent occurrence of hurricanes, the relevance of the research on surge estimation in the area is high.
- **Data availability**: The North Atlantic historical catalogue of hurricanes provided by the National Hurricane Center of the United States (HURDAT2) is extensive and accessible, what guarantees the statistical significance of the hurricane sample.

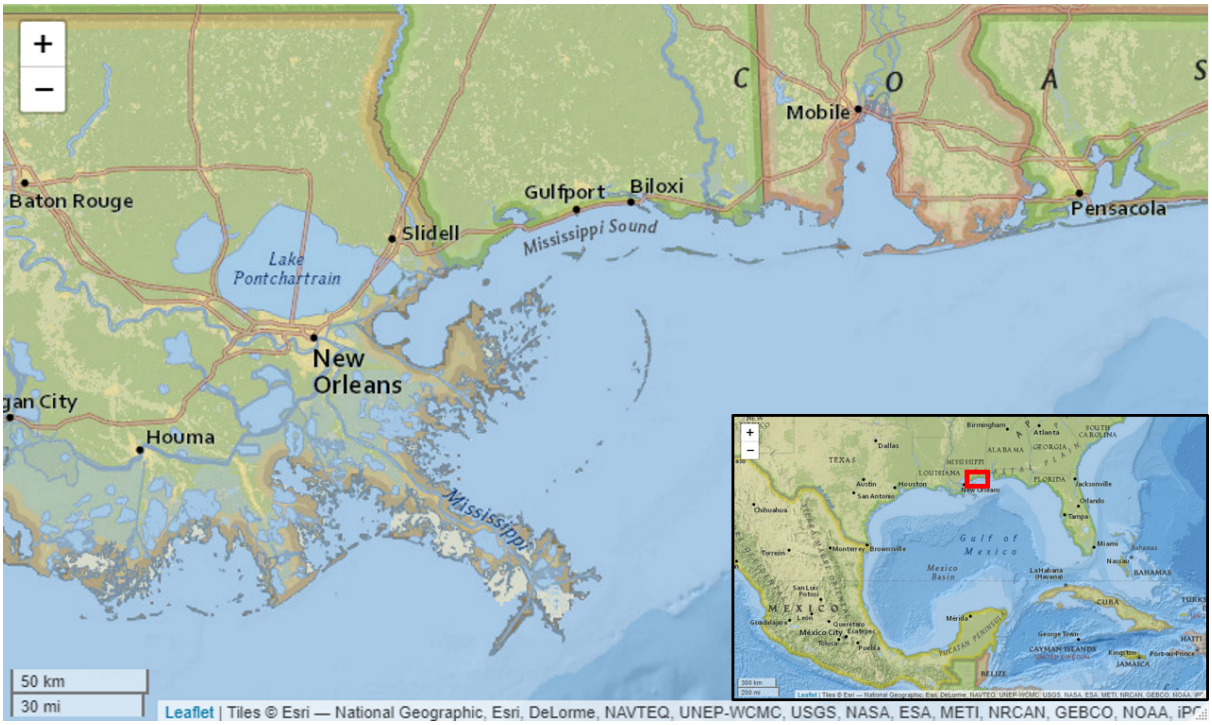

Figure 1.1: The storm surge is modelled for the Mississippi coast, which is shown in this figure.

1.4 Structure of the report

This report starts with an introduction to the project (Chapter 1). The objective of this chapter is to explain the motivation of the project, to define the problem and the research questions to be tackled and to justify the location where the research focuses.

The report proceeds reviewing the state of the art on storm surge modelling, in Chapter 2. First, there are described the physical processes that govern hurricanes and storm surge. Subsequently, the physical modelling and the stochastic modelling of storm surge due to hurricanes is reviewed. For the physical modelling approach, it is gathered information about the inputs to be implemented in Delft3D FM . For the stochastic modelling of surge, relevant theory on Bayesian Networks is summarized. In Chapter 3, it is explained the methodology followed to achieve the stochastic model. The explanation of the methodology is complemented with a flow chart.

Chapter 4 is dedicated to the setup and validation of the physical model. For the calibration and validation of the model, Hurricane Katrina (2005) is simulated. The resulting water levels from the simulations in Delft3D FM are compared to real data . Once the model is validated, the storm surge generated by a finite number of hurricanes can be modelled, and a hurricane data base can be elaborated. This procedure is explained in Chapter 5. In Chapter 6, a Bayesian Network is trained and validated by using the the hurricane catalogue.
In Chapter 7 the results of the physical and stochastic modelling are discussed. The limitations of the models are described. Finally, Chapter 8 gathers the conclusions on the results achieved, by giving answers to the research question and sub-questions formulated at the beginning of the project.

CHAPTER 2

Literature review

To build a stochastic model capable of predicting storm surge due to hurricanes, it is essential to understand beforehand the physical phenomena that govern the generation and development of these atmospheric events. Chapter 2.1 includes a review of concepts related to hurricanes, the anatomy process and the life phases of hurricanes. The effects of the hurricane in the sea water level (storm surge) are also explained.

The prediction of the dimension of storm surge and coastal flood events and their related damage is possible thanks to models. The accurate representation of the physics behind the hydraulic processes has been traditionally the main interest of hydraulic engineers. A wide range of physical models are available in literature for this end. To date, there is a growing interest in complementing (or even substituting) the use of physical models by data driven and stochastic models, due to their high speed of calculation. In Chapter 2.2, several physical and probabilistic models are reviewed.

2.1 Description of the physical processes

The subject of study of this project is the identification of the relationship between the variables that describe an atmospheric phenomenon (tropical cyclone) and the subsequent hydraulic phenomenon (storm surge and coastal flooding). The first step in the process is the generation of a low-pressure atmospheric system in the open sea. If the conditions are adequate for its formation, a tropical cyclone is originated (Chapter 2.1.1). The tropical cyclone progresses along the ocean until it makes landfall, where it can provoke a rise in the sea water level, commonly known as storm surge (Chapter 2.1.2). The abnormal height of the sea water level can lead to the flood of coastal areas when the tropical cyclone reaches the coastline, causing property and life damage (Chapter 2.1.3).

2.1.1 Hurricanes

2.1.1.1 Definition

Tropical cyclones are rotating low-pressure weather systems that develop over the warm water of the oceans, typically between the latitudes of 30 degrees Nord and 30 degrees South [48]; [84]. These systems rotate in counterclockwise direction in the northern hemisphere and in clockwise direction in the southern hemisphere, due to the Coriollis force [20]. The generic name *tropical cyclones* may be used anywhere worldwide for tropical storms with peak wind speed exceeding 17 m/s (1-minute average, 10-minute average or gust wind are used depending on the region).

The definition of several concepts related to tropical cyclones are given below [62]:

- **Best track**: representation of a tropical cyclone location and intensity over its lifetime. The best track contains the cyclone eye latitude, longitude, maximum sustained surface winds, and minimum sea-level central pressure at 6-hourly intervals. Best track positions and intensities, which are based on a post-storm assessment of all available data, may differ from values contained in storm advisories. They also generally will not reflect the erratic motion implied by connecting individual center fix positions.

- **Center**: the vertical axis of a tropical cyclone, usually defined by the location of minimum wind or minimum pressure. The cyclone center position can vary with altitude. In advisory products, refers to the center position at the surface.

- **Eye**: the roughly circular area of comparatively light winds that encompasses the center of a severe tropical cyclone. The eye is either completely or partially surrounded by the eyewall cloud.

- **Eyewall or wallcloud**: an organized band or ring of cumulonimbus clouds that surround the eye, or light-wind center of a tropical cyclone.

- **Hurricane season**: the portion of the year having a relatively high incidence of hurricanes. The hurricane season in the Atlantic, Caribbean, and Gulf of Mexico runs from June 1 to November 30. The hurricane season in the Eastern Pacific basin runs from May 15 to November 30. The hurricane season in the Central Pacific basin runs from June 1 to November 30.

- **Inter-Tropical Convergence Zone**: a zonally elongated axis of surface wind confluence of northeasterly and southeasterly trade winds in the tropics.

- **Landfall**: the intersection of the surface center of a tropical cyclone with a coastline. Because the strongest winds in a tropical cyclone are not located precisely at the center, it is possible for a cyclone strongest winds to be experienced over land even if landfall does not occur. Similarly, it is possible for a tropical cyclone to make landfall and have its strongest winds remain over the water.

- **Maximum sustained surface wind**: the standard measure of a tropical cyclone intensity. When the term is applied to a particular weather system, it refers to the highest one-minute average wind (at an elevation of 10 meters with an unobstructed exposure) associated with that weather system at a particular point in time.

- **Radius of maximum winds**: the distance from the center of a tropical cyclone to the location of the cyclone's maximum winds. In well-developed hurricanes, the radius of maximum winds is generally found at the inner edge of the eyewall.

2.1.1.2 Classification

Different names have been traditionally given to tropical cyclones, depending on the world zone where they occur. In the Northwestern Pacific ocean, the tropical cyclones whose peak winds speeds exceed 33 m/s are called *typhoons*. In the North Atlantic and the Northeastern Pacific ocean, the tropical cyclones whose peak winds speeds exceed 33 m/s are referred as *hurricanes*. Finally, in the South Pacific and Indian ocean these events are known as *cyclones*. Since the location of study for this project is the coast of Mississippi, from now on the term *hurricane* will be used. The Saffir-Simpson scale is a scale that classifies the hurricanes according to their maximum sustained winds (1-minute average and 10 meters above the ground) (Table 2.1).

Category	**Wind speeds (1-minute max. sustained winds**			
	m/s	**kn**	**km/h**	**mph**
1	33-43	64-83	119-154	74-96
2	43-50	83-96	154-178	96-111
3	50-58	96-112	178-209	111-130
4	58-70	113-137	209-252	130-157
5	≥ 70	≥ 137	≥ 252	≥ 157

Table 2.1: Saffir-Simpson Hurricane Scale [68]

.

Out of the Saffir-Simpson Hurricane Scale, the *tropical storms* are still considered hurricanes (the maximum sustained wind velocity is between 17 and 33 m/s). The *tropical depressions* are those events whose maximum sustained velocity falls below 17 m/s.

2.1.1.3 Anatomy of the tropical cyclone

Several structural elements are commonly found in all hurricanes: the boundary layer inflow, the eyewall, the cirrus shield, the rainbands and the upper tropospheric outflow. Moreover, a central eye of the storm grows when the intensity of the storm increases. It is possible to observe the eye of the storm by means of satellite photographies [43].

Several phenomena are present in the spiral rainband, depending on the vertical position in the structure. In the lower levels of the tropical cyclone, the wind flows inward cyclonically, while it flows upwards in the zones of deep convection (central eyewall and spiral rainbands), following an helicoidal trajectory. Finally, the wind reaches a region just below the tropopause, where the absolute vorticity is reduced and the cyclone is dispersed to form the cirrus cloud shield.

The eye of the tropical cyclone is a clear region in the center of the cyclone, which is relatively calm, with light winds and with the lowest surface pressure of the system. The storm center is surrounded by an organized band of thunderstorms. This region is called the eyewall, and the strongest winds in the system can be found in the inner flank of the thunderstorm ring.

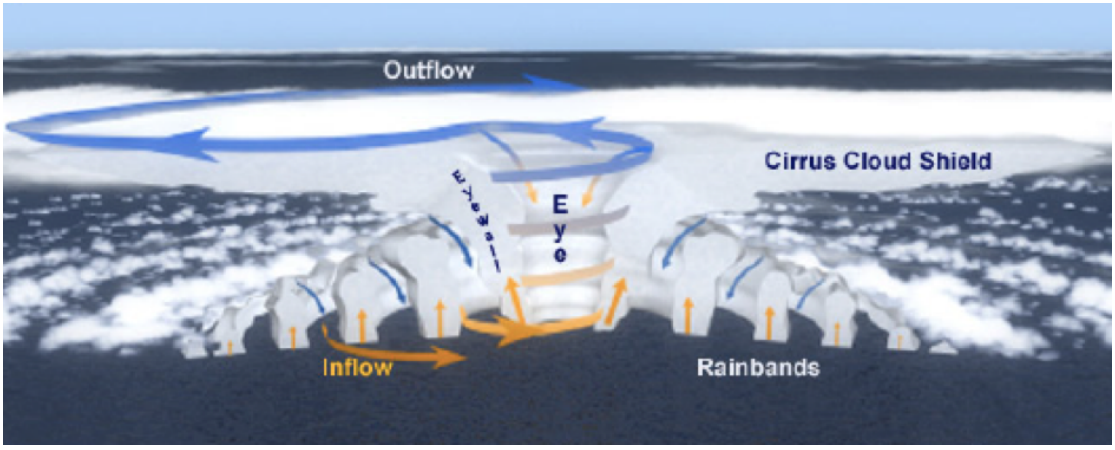

Figure 2.1: Conceptual model of the main structural elements of hurricanes [43].

2.1.1.4 Development of the tropical cyclone

The lifetime of a tropical cyclone can be divided into three phases: cyclone genesis, cyclone propagation and cyclone decay. The first sign of cyclone genesis is the appearance of a group of thunderstorms over the tropical oceans, called tropical disturbances [25]. The generation of tropical disturbances always involve the convergence of surface winds, and can develop in three ways. The first way of development is the convergence of Northern and Southern hemisphere easterly trade winds near the equator, what provokes numerous thunderstorms in the inter-tropical convergence zone (ITCZ) daily. A second way of formation of hurricanes is the convergence of air along the boundary between masses of warm and cold air. However, the most common mechanism of generation of hurricanes is the African easterly wave, a weather disturbance wave that travels along the tropical Atlantic. This disturbance is formed due to a kink in the jet of air that flows out of the African tropical region. The kink is formed due to the large difference in temperature between the Sahara Desert and the Gulf of Guinea. The warm air over the Sahara rises and subsequently it flows towards the south, to the cooler air over the Gulf of Guinea. The rotation of the Earth leads these winds to move westwards. The convergence of these winds generates thunderstorms, which can develop into hurricanes.

[26] identified six necessary (but not sufficient) features for tropical cyclogenesis:

- Sufficient ocean thermal energy: the sea surface temperature should be larger than 26 degrees Celsius to a depth of 60 meters.
- Enhanced mid-troposphere (700 hPa) relative humidity.

- Conditional barotropic instability occurring that breaks down the ITCZ and the associated monsoon breakdown: vortices can be created, either forming groups of several hurricanes or developing one larger hurricane.
- Weak vertical shear of the horizontal winds at the genesis site.
- In most of the cases, the locations at which the cyclons develop are displaced at least 5 degrees latitude away from the equator.

If the conditions are adequate, a unified system is formed and the tropical cyclone is developed. hurricanes intensify when condensation of water vapor in rising air releases heat energy into the storm, setting off a chain reaction. The heat makes the surrounding air more buoyant, causing it to rise further. To compensate for the rising air, surrounding air sinks. The sinking air is compressed by the weight of the air above it, and it warms. The pressure rises at the top of the layer of warmed air, pushing air outward. As the air spreads outward, the total air pressure at the surface drops. The more the pressure drops, the more the winds intensify, drawing more heat and moisture from the ocean surface, what leads to more thunderstorms. This process is retro alimented, triggering stronger winds.

The cyclone decay can occur for several reasons. When the tropical cyclone moves onto regions of cool waters, warm and moist air is not available for the formation of thunderstorms and strong winds in the eyewall inner flank. In the same way, the source of warmth and moist is lost when the cyclone makes landfall. The tropical cyclone also dissipates when moving onto a region of strong winds high in the atmosphere, since these disperse the latent heat, what reduces the warm temperatures above and increases the surface pressure.

In the present research, special attention is given to the development of the tropical cyclone when it makes landfall, since it can influence the extent of the flood. In this sense, apart from the loss of ocean energy source, the increased friction due to the greater roughness of the land surface compared to the sea surface also induces a reduction of the wind strength. The friction effect is larger in mountainous areas than in flat (riverine and deltaic) areas, and also in forest areas rather than in swamp areas. In the case of presence of water, the weakening effects can be delayed and even storms can temporarily intensify [43].

hurricanes can trigger other physical phenomena that can represent a hazard for hinterland areas [43]. For instance, tornadoes can be generated due to the strong moisture gradient between the storm and the landfall environment, combined with the vertical wind shear profile. Landslides have also occurred as a consequence of the topographic enhancement of the already intense rainfall associated with the storm provoking numerous casualties, such as in Hurricane Mitch in 1998 [31].

2.1.2 Storm surge

2.1.2.1 Definition

Storm surge is an abnormal rise of water generated by a storm above the predicted astronomical tide, mainly driven by wind stress and to a lesser extent by falling atmospheric pressures. Storm surges have wave periods ranging from a few minutes to a few days and, as tidal waves, are categorised as long gravity waves [55].

The genesis of the storm surge is produced when the cyclone is far from the coast, in deep waters. The drop of the atmospheric pressure in the center of the eye causes a slight rise in the water level, of the order of 1 centimeter per hPa fall in the air pressure [50]. However, the large depth in these regions makes possible the development of a counter current below the water surface that counters an attempt by the wind to build up the surge [37] (Figure 2.2).

When approaching the coast, the water depth is progressively reduced and the excess of water volume built up by the central pressures in the eye cannot dissipate in the depth, due to the presence of the sea bed (Figure 2.3). At the same time, the force of the winds swirling around the storm push the water towards the coast, generating surge. The level of storm surge that can be reached in a particular area also depends on the slope of the continental shelf. Coastal regions with shallow continental shelf slopes are prone to undergo flooding due to surge, while regions with steeper continental shelf are prone to suffer flooding due to large breaking waves.

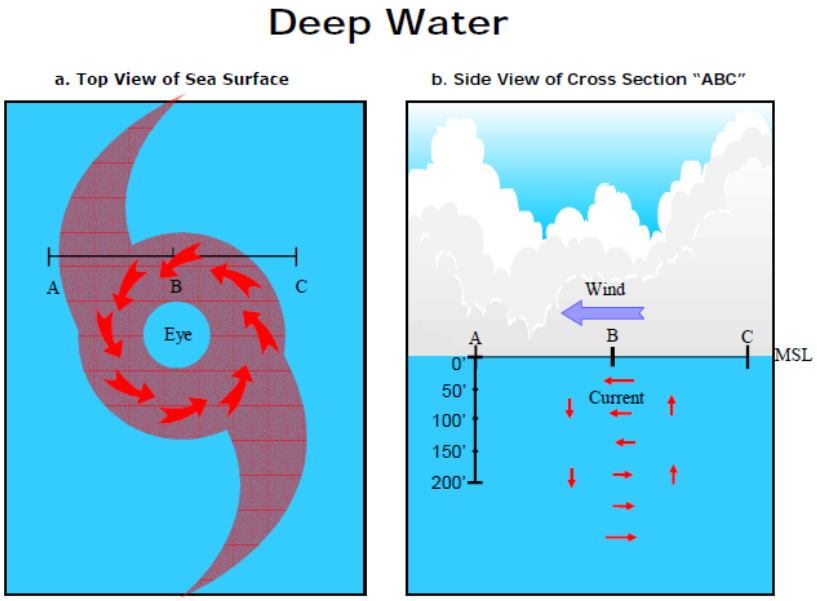

Figure 2.2: Top view of the sea surface and cross section of the sea when a storm travels over deep waters [37].

2.1.2.2 Factors influencing the storm surge

Storm surge is often the greatest threat to life and property from a tropical storm or hurricane event. Storm surge values do not correspond well to the hurricane wind categories (of the Saffir-Simpson Hurricane Wind Scale) that range from 1 to 5. These categories are based only on winds and do not account for storm surge. Tropical storms, category 1 or 2 hurricanes, major (category 3 to 5) hurricanes, and post- hurricanes can all cause life-threatening storm surge [58]. The factors influencing the water levels reached during storm surge events are [63]:

- **Central pressure**: as previously mentioned, the drop in the air pressure can lead to higher surge, of the order of 1 centimeter per hectopascal. However, the contribution to surge of pressure drop is relatively small compared to other factors.
- **Storm intensity**: as also mentioned before, the wind intensity has a main role in the storm surge phenomenon, since water is pushed towards the coast causing the rise in the water level. This phenomenon is particularly important in shallow waters, where the continental shelf is wide.
- **Storm forward speed**: the coastal morphology plays an important roile in this factor. If the coast is open, a storm progressing faster will cause more storm surge than a storm progressing slower, since in the former case water piles up at the coast and does not have time to move aside. If the coastal region is located in an enclosed body such a bay or a sound, water flow aside of the surge body. In this case, a slower motion of the storm would provoke higher storm surge levels.
- **Angle of approach to the coast**: a storm approaching perpendicularly to the shoreline would cause higher storm surge than a storm that progresses at an oblique angle or parallel to the coast. If the storm approaches perpendicularly to the shoreline, the water is pushed towards the shore by the swirling wind, but also by the forward speed of the storm.
- **Storm size**: the winds in a larger storm push on a larger area of the ocean moving a larger volume of water, what leads to generate higher values of surge and to affect a larger stretch of coastline.
- **Shape of the coastline**: storm surge will be higher when a hurricane makes landfall in a curved-inward coastline, rather than in a curved-outward coast, due to possibility to pile up water in a curved-inward coastline.
- **Width and slope of the ocean bottom**: the influence of the width and the slope of the ocean seabed on the storm surge has also been introduced previously. Higher storm surge happens in wide, gently

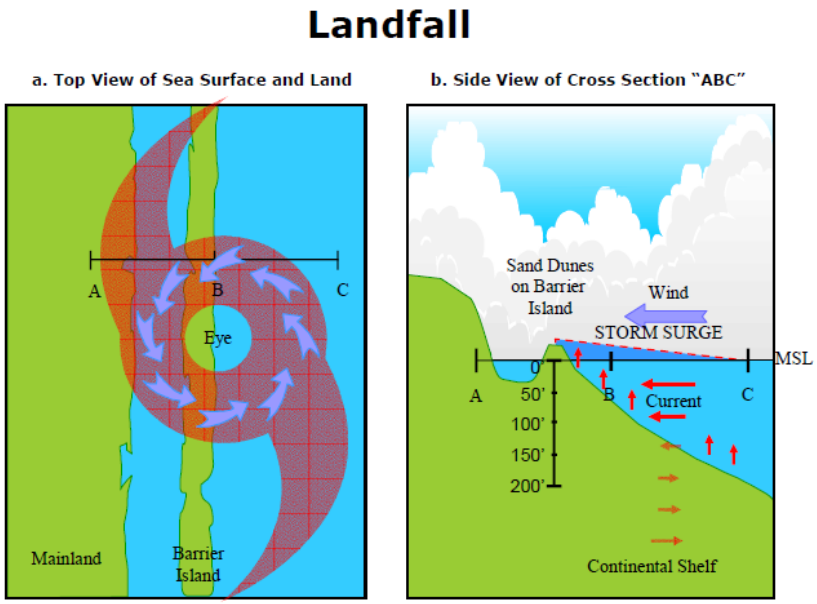

Figure 2.3: Top view of the sea surface and cross section of the sea when a storm makes landfall [37].

sloping continental shelves, rather than in narrow steeply sloping shelves. The coast of Louisiana and Mississippi is particularly prone to high storm surges because of their gentle and wide seabed slopes.

- **Local features**: local features of every specific region can also contribute more or less to the flow of water and the storm surge. As mentioned in [27], barrier islands can constitute a first line of defence against hurricane impacts since they reduce the incoming storm surge and the wind waves.

2.1.2.3 Other phenomena contributing to the rise of the water level

Storm surge can have a major impact in coastal areas when combined with astronomical tides, wind waves and rainfall [63]. The combination of these four elements build up the concept of total water level:

- **Astronomical tides:** The gravitational pull of the moon and the sun causes the rise and fall of the water levels along the coast. Tidal waves are considered long waves, due to their long period (generally around 12 hours). The restoring force that dampens the tidal wave motion is gravity, although these waves are also influenced by the Coriolis force. The characteristics of the tide vary globally. The tidal environments can be classified by two parameters: the magnitude of the tide, which can be characterized by the vertical distance covered by the tide (tidal range), and the tidal character, which which can be determined by the relative influence of diurnal with respect to semi-diurnal tidal components.

  The tidal range and the tidal amplitude are influenced by the local differences in water depth (slope and width of the continental shelf) and the location and shape of the land masses (Figure 2.4). When tidal wave approaches the coast and enters an area with steep continental shelf, the wave length is reduced and the amplitude is increased, due to the concentration of energy in the wave. This effect is comparable to the shoaling effect that wind waves undergo when approaching shallow waters. If the slope of the continental shelf is shallow, the water depth is small and the width of the continental shelf is large, a great amount of wave energy can be dissipated due to bottom friction, leading to small tidal amplitudes.

  The location and shape of land masses can also influence the tidal amplitude. Resonance may occur in basins where the eigen period of the tidal wave and the basin are similar. Moreover, the presence of islands and other land entities at the entrance of a basin can dissipate the energy of the tidal waves, leading to a small tidal range and amplitude.

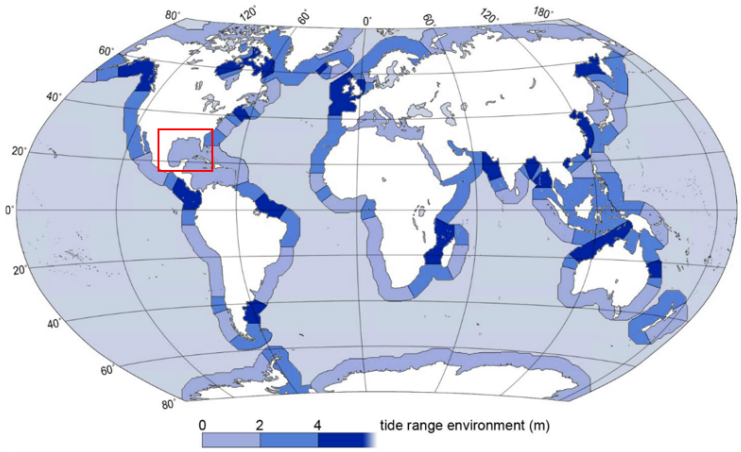

Figure 2.4: World distribution of the mean spring tidal range (MHWS-MLWS) [9]. The emplacement of the project is indicated by a red rectangle.

The tidal character differs also along the globe, governed by a combination of geography and latitude of each location. The declination of the Earth axis introduces the so-known daily inequalities in the tide, by which the water levels during the two high tides within a day differ. This difference is produced by the interaction of diurnal components of the tide with semi-diurnal components. The daily inequality increases with the latitude. However, it can also be large in the equator when the diurnal tidal components excites one of the resonance modes of a basin or bay. This is the reason why several areas in the equator undergo diurnal tidal character, such as in the Gulf of Mexico.

- **Wave setup:** Wave setup is the additional elevation of the water level due to the effects of transferring wave related momentum to the surf zone [19]. Momentum is transferred from winds to waves in the wave generating area and then is conveyed to shore by the waves. A main difference between energy and momentum is that energy is dissipated in the surf zone whereas momentum is transferred to the water column. This transfer is equivalent to a shoreward-directed "push" on the water column that causes a tilt of the water surface. The wave setup is small and negative seaward of the surf zone (setdown) and begins to rise in the surf zone due to the transfer of momentum. If only one wave of a constant height and period were present, the wave setup would be steady.

  Wave setup increases with steeper beach slopes and smaller wave steepness. Steeper profiles accumulate more momentum in the water water column when approaching the coastline. The shorelines exposed to large and long period swells are particularly susceptible to experience large wave setups, which can account for up to 10% of the deep water wave height, in the case of waves of low steepeness. FEMA proposes a guidance to account for wave setup based on the wave steepness and the bottom slope (Figure 2.5).

- **Rainfall:** Heavy rainfall ahead of the hurricane can cause the increase in the river water levels. This situation can be aggravated by the wind setup of the water levels due to a hurricane. The presence of levees and the friction along the wetland overbanks block or hinder the lateral flow, what aggravates the storm surge generated by the hurricanes, as well as the orientation of the river with respect to the storm track [40].

The combination of storm surge and astronomical tide is known as storm tide and achieve their maximum levels during high tides.

2.1.3 Coastal flooding

The storm surge generated by a tropical cyclone can lead to severe flooding in coastal regions, in case of insufficient protection against this type of extreme events. However, storm surge is not just an immediate coastal threat. It can affect inland communities, including some areas that are many miles from the coastline.

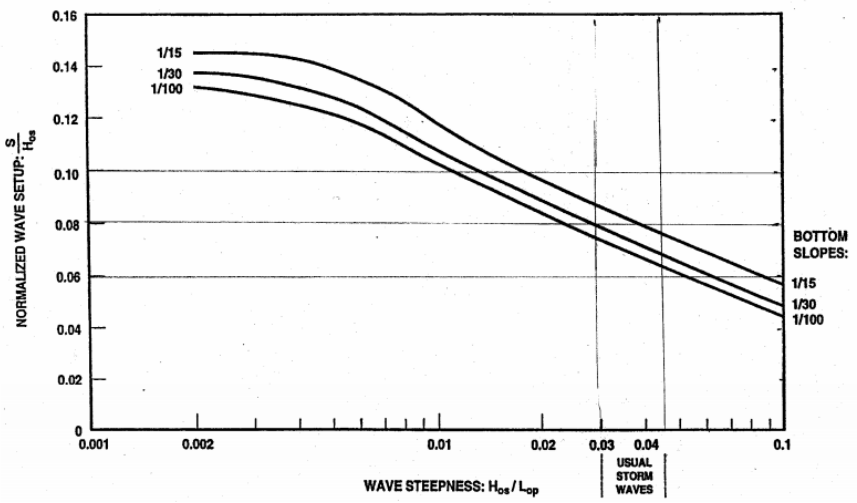

Figure 2.5: Relationship between deep water wave steepness, bottom slope and wave setup [18].

2.1.3.1 Parameters influencing the coastal flooding extent

Several factors can influence the amount, the extent and the impact of tropical cyclone flooding [43]:

- **Antecedent precipitation**: the level of saturation of the soil can influence critically the filtration capacity of the terrain. If recent rainfall occurred in the region affected by the tropical cyclone, the soil pores might be saturated, increasing the runoff and therefore the flooding impact.
- **Speed of movement of the cyclone**: the slower the forward speed of the cyclone in the hinterland direction, the longer the time that the storm surge holds at the coast line. Therefore, the lower the speed of movement of the cyclone the larger the flooding effects.
- **Orographic enhancement**: in regions of higher elevation, additional moist air is lifted up, increasing the precipitation volume.
- **Intensification due to synoptic forcing**: the simultaneous occurrence of a cyclone and other midlatitude synoptic systems can aggravate the floods caused by the storm surge, either due to the additional reduction of lower pressures or due to the increase of precipitation.
- **Hydrology**: narrow river basins are more prone to flood than wide and flat river basins.
- **Land use**: the presence of building foundations in urban areas reduce the soil filtration and enhances the runoff volumes and velocities. Therefore, urban land uses are more exposed to flash floods. Hill slopes without a vegetation cover are more prone to suffer landslides than hill slopes that are covered by vegetation, whose roots increase the stability of the soil.
- **Soil characteristics**: the permeability of the soil depends on the grain size. Impermeable soil materials contribute to larger runoff and flooding.

2.2 Modeling of the physical processes

2.2.1 Hurricane modeling

The trajectory and the features of the hurricanes are gathered in the so-called best tracks records. These data sets contain information about the coordinates of the eye of the tropical cyclone, the maximum sustained wind speeds, the minimum sea-level pressure in the eye and the size of the tropical cyclone at 6-hourly intervals. The best tracks of a tropical cyclone are based on post-storm assessments of available data.

2.2.1.1 The HURDAT2 database

The most complete record of hurricanes occurring in the Gulf of Mexico has been elaborated by the United States National Oceanic and Atmospheric Administration (NOAA) and is known as Atlantic Hurricane Database (HURDAT2) [60]. The Atlantic HURDAT2 database is included in a global tropical cyclone database that has also been developed by NOAA, known as IBTrACKS [61]. These databases are two typical sources to retrieve tropical cyclone best-track data. In this project, the HURDAT2 database has been used, which includes the best track of 1864 hurricanes for the period 1851-2018 (Figure 2.6).

The National Hurricane Center (NHC) is a division of the NOAA dedicated to the elaboration of the HURDAT2 data base [44]. This data base includes a post-storm analysis of each tropical cyclone to determine the official assessment of the cyclone history. Among other uses, the HURDAT database is used for the analysis of potential losses for insurance and business interests [49].

The post-storm assessment is key to elaborate a high fidelity data set. Many types of meteorological data arrive with some latency (e.g., microwave imagery, scatterometer data, and Advanced Microwave Sounding Unit (AMSU) data), and some data do not become available until well after a storm is over. Furthermore, knowing what happened subsequent to a given point in time can be instrumental in the correct assessment of what was occurring at that point in time.

The precision of the parameters of the best track of a tropical cyclone is 5 kt for the intensity (1 kt = 0.514 m/s), 1 hPa for the central pressure, 0.1° for the position (latitude and longitude) and 5 nmi for the size (1 $nmi = 1.852$ km) being the cyclone size the maximum extent of winds of 34, 50 and 64 kt in each of the four quadrants about the center [45]. Best track intensity and position estimates are provided for every synoptic time (00:00, 06:00, 12:00 and 18:00 UTC) for all tropical storms, hurricanes and subtropical storms since 1956. Before this year, tropical cyclone information was only recorded once or twice a day and interpolation was used to obtain best track estimates for the remaining synoptic times when the HURDAT database was constructed in the early 1980s. Central pressure estimates for every synoptic time have been included since 1979. Before 1979, only the observations that could be used explicitly as best track value were included into HURDAT.

Cyclone size records have been included in the database since 2004. The database used in this project is the second generation HURDAT database (HURDAT2), which is an adaptation of the HURDAT database. Apart from the data described, the HURDAT2 database includes also asynoptic points in order to capture landfall and peak intensities that occurred at times other than the synoptic hours. HURDAT2 also includes non-developing tropical depressions.

Figure 2.7 (top) shows the distribution of the 1864 storms of the HURDAT2 database by intensity (Saffir-Simpson Scale). Figure 2.7 (bottom) shows the distribution of the events per year. A trend showing that the number of events has increased in the last 50 years can be observed.

2.2.1.2 The Holland model

Parametric wind models are widely used instead of full physics mesoscale models, due to the extensive resources required to run full physics models. Parametric models are used to simulate wind fields, which can be used as hurricane forcing for storm surge modelling. The hurricane data is commonly given in so-known best tracks (as explained in Chapter 2.2.1.1). This data is used as input for the wind parametric model in order to generate 2D fields of wind and pressure. One common model to describe the time and space varying wind and pressure is the Holland model [34]. The outcome of the model can be written in spiderweb format, which is represented by a grid in polar coordinates, being the radius and the angle the parameters of the grid (Figure 2.8). Each point of the spiderweb includes information about the wind speed, the wind direction and the pressure drop. The eye of the hurricane is the origin of the coordinate system. This format is specially devoted to the representation of cyclonic winds.

The forward speed (FS) and the forward direction (FD) of the tropical cyclone at each time step are calculated as follows:

$$FS = \frac{d}{t_t - t_{t-1}} = \frac{\sqrt{\Delta x^2 + \Delta y^2}}{t_t - t_{t-1}} \tag{2.1}$$

Figure 2.6: Hurricanes included in the HURDAT2 database for the period 1851-2018 (371 hurricanes). The colors indicate the variation in the intensity along the tracks.

$$FD = -atan2(\Delta y, \Delta x) + 90 \tag{2.2}$$

Δx and Δy are the variation in the longitude and latitude coordinates between two points of the best track trajectory of the tropical cyclone (coordinates of the eye) and are defined in Figure 2.10. The expressions given for Δx and Δy are only applicable if the angles θ' and φ' are sufficiently small. In such a case, the infinitesimal equivalence $\theta' \approx \sin(\theta')$ applies (analogous for φ'). t_t and t_{t+1} are the times at the best track point t and $t+1$. It is noted that FD is calculated in degrees and taking the North as reference (Figure 2.11).

[34] observed that the parametric profiles of the normalized pressures of nine hurricanes in Florida (as recorded by [69] resembled a family of rectangular hyperbolas, which could be approximated by:

$$r^B \ln\left(\frac{p_n - p_c}{p - p_c}\right) = A \tag{2.3}$$

where A and B are scaling parameters, p is the pressure at radius r, p_c the minimum pressure at sea level in the eye of the tropical cyclone and p_n the ambient pressure. Rearranging terms, it is obtained:

$$p = p_c + (p_n - p_c)\exp\left(\frac{-A}{r^B}\right) \tag{2.4}$$

Using the gradient wind equations [70], the wind gradient (W_{grad}) can be expressed by:

$$W_{grad} = \left(\frac{AB(p_n - p_c)\exp\left(\frac{-A}{r^B}\right)}{\rho r^B} + \frac{r^2 f^2}{4}\right)^{1/2} - \frac{rf}{2} \tag{2.5}$$

where ρ is the air density and f is the Coriolis parameter. This expression indicates that the Coriollis force generated by the Earth rotation, the pressure gradient caused by the pressure drop and the centrifugal force originated from the cyclonic rotation of the wind are in balance. At the region of maximum winds, the Coriolis force is small compared to the pressure gradient and the centrifugal force. In this situation, the air is in cyclostrophic balance. The wind speed in this region (i.e. cyclostrophic wind) is (W_c):

$$W_c = \left(\frac{AB(p_n - p_c)\exp\left(\frac{-A}{r^B}\right)}{\rho r^B}\right)^{1/2} \tag{2.6}$$

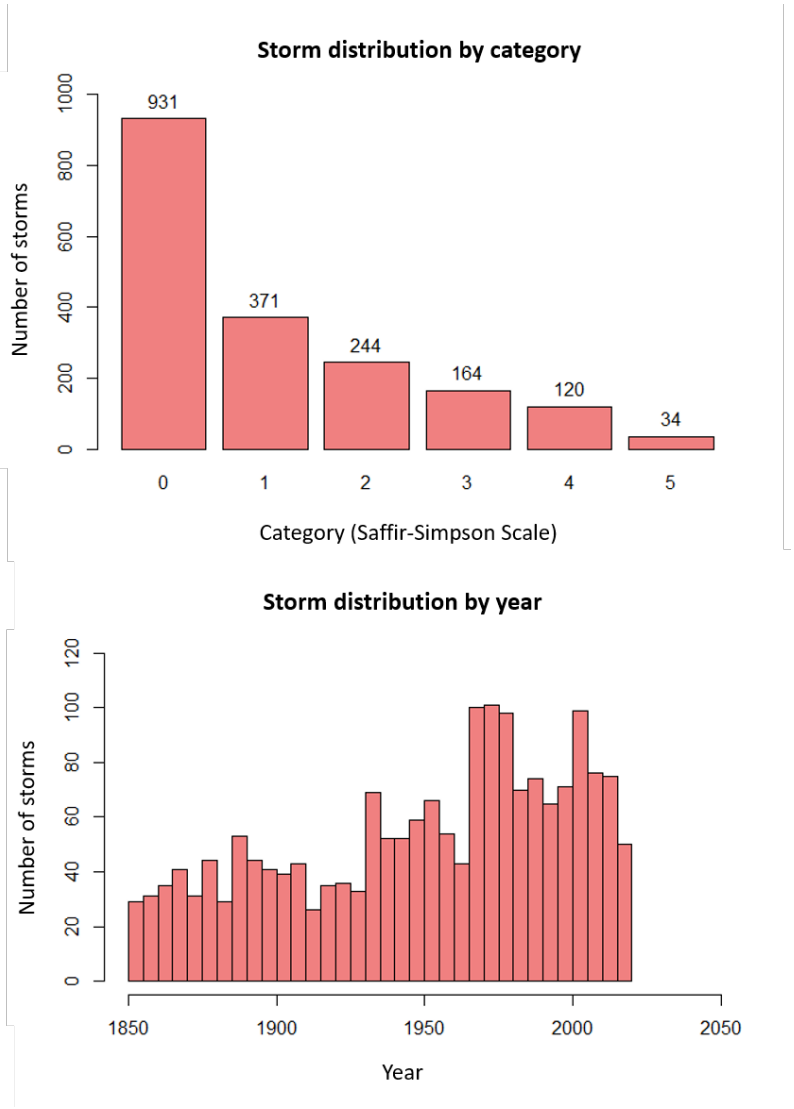

Figure 2.7: Distribution of the hurricanes included in the HURDAT2 database by category, according to the Saffir-Simpson scale (top), and distribution of the hurricanes included in the HURDAT2 database by year (bottom).

Matching the derivative of W_c in function of the radii to 0, it is obtained the radius of maximum winds (R_{max}):

$$R_{max} = A^{1/B} \tag{2.7}$$

which gives an expression relating the parameter A and B of the Holland model. The parameter A determines the location of the hurricane with respect to the origin, while the parameter B determines the profile shape of the tropical cyclone. Substituting Eq. (2.7) into Eq. (2.6) and rearranging terms, the parameter B can be written in function of the maximum sustained wind speed (W_{max}) and the pressure in the eye of the hurricane:

$$B = \left(\frac{\rho e W_{max}^2}{p_n - p_c} \right)^{1/2} \tag{2.8}$$

The effect of the parameter B of the Holland model in the sea pressure profile and the gradient wind profile is shown in Figure 2.12.

W_{max} can be written in a general way as:

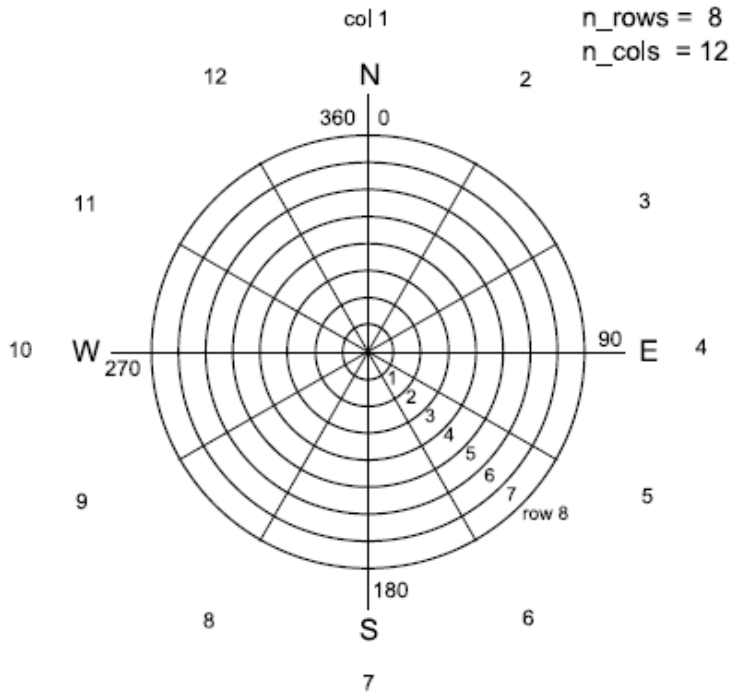

Figure 2.8: Spiderweb grid definition [13].

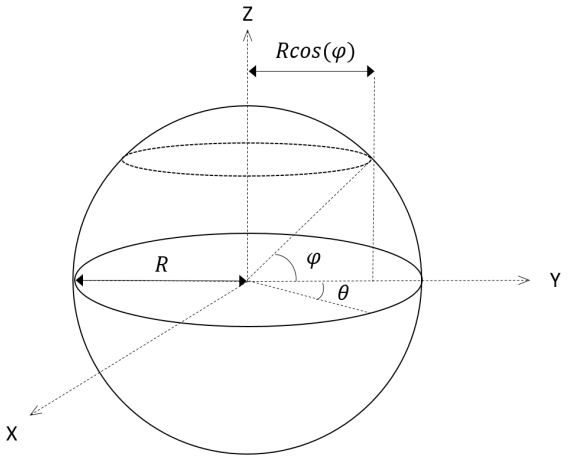

Figure 2.9: Earth reference system. θ represents the longitude and ϕ represents the latitude.

$$W_{max} = C(p_n - p_c)^x \tag{2.9}$$

expression that follows a commonly-used formulation for pressure-wind models [32]. The coefficient C is obtained empirically and the exponent x is adjusted to the observed hurricanes in the region of interest. In the North Atlantic region, [17] proposed a tabular pressure-wind model that relates the W_{max} and p_c, which can be very closely fitted to:

$$W_{max(NA)} = 3.92(1015 - p_c)^{0.644} \tag{2.10}$$

where 1015 is the ambient pressure in hPa assumed by Dvorak in the North Atlantic region and the velocity is expressed in m/s. The HURDAT2 database does not include p_c values before 1989. However, W_{max} is available

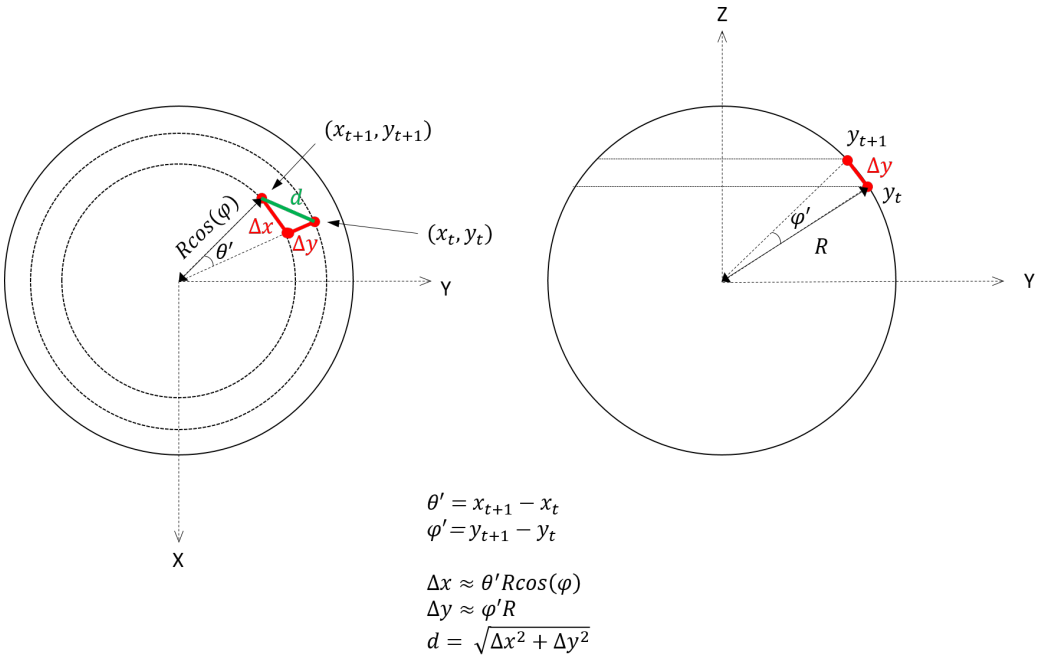

Figure 2.10: Graphical representation of the distance between two points of a hurricane best track.

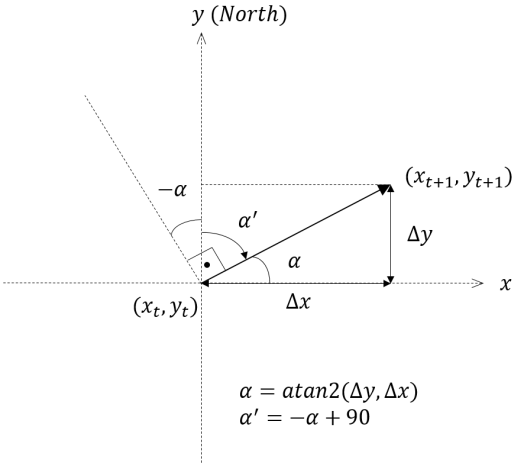

Figure 2.11: Graphical representation of FD in local coordinates (x-y in the Earth surface plane), symbolized by the angle α'. The y-axis heads the North in the local coordinates.

before this year. Eq. (2.10) can be inverted and used to calculate p_c:

$$p_c = 1015 - \exp\left(\frac{\ln(W_{max}) - \ln(3.92))}{0.644}\right) \tag{2.11}$$

[67] derived a practical expression for R_{max} in the Gulf of Mexico which is directly related to the W_{max}:

$$R_{max} = 62.4 - 0.41 W_{max} \tag{2.12}$$

It is noted that although this model improves the available models for the prediction of R_{max} (e.g. [41] and particularizes the estimation for the Gulf area, the analysis of the goodness of fit of the model proposed by [67] shows relevant inaccuracies (Mean Absolute Error of 21.1% and $R^2 = 0.28$). The reasons for such inaccuracies might be the several interactions of the tropical cyclone with land, before making landfall in a region of the Gulf Coast.

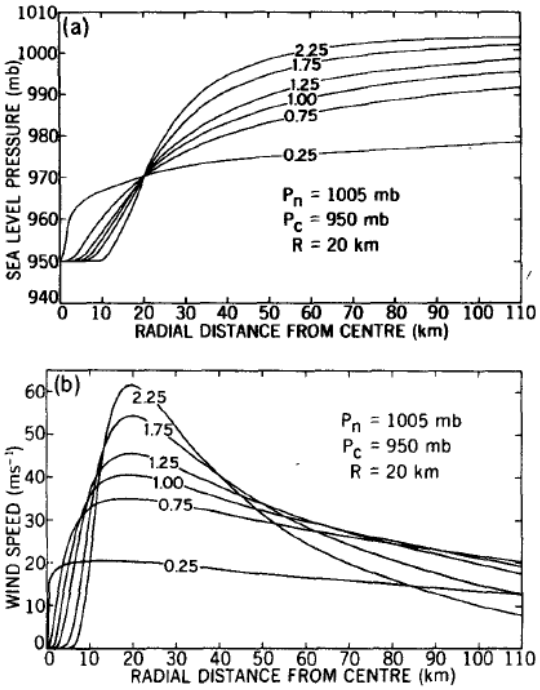

Figure 2.12: Effect of varying the parameter B of the Holland model on the sea level pressure profile (top) and the gradient wind profile (bottom) [34].

The Holland model is a symmetric model. However, real hurricanes hardly ever present a symmetric structure. Asymmetric hurricanes can lead to great errors in the estimation of the surge levels when compared to symmetric hurricanes, in some cases in the order of 15% [85]. One of the main factors that contribute to asymmetry is the hurricane system motion, represented by the forward speed (FS) and the forward direction (FD) of the system. [81] adapts the Holland model to introduce these contributions, in order to consider the hurricane asymmetries in the 2D wind field. The geostrophic wind speed is (W_g):

$$W_g = \left(\frac{AB(p_n - p_c)\exp\left(\frac{-A}{r^B}\right)}{\rho f r^{(B+1)}} \right)^{1/2} \tag{2.13}$$

The combination of cyclostrophic and geostrophic wind speed, FS and FD is considered in the calculation of a parameter γ:

$$\gamma = \frac{1}{2}\left(\frac{FS\sin(\theta')}{W_c} + \frac{W_c}{W_g} \right) \tag{2.14}$$

where θ' is the difference between FD and the angle between the origin and the position of the cell. Finally, the total tangent velocity of the hurricane is found (W):

$$W = W_c\sqrt{\gamma^2 + 1} - \gamma \tag{2.15}$$

Based on the expressions previously developed, the best track of a hurricane can be used to generate a 2D wind and pressure field in spiderweb format.

2.2.2 Storm surge and coastal flood modeling

2.2.2.1 Introduction

Since the beginning of the civilization, the understanding, assessment and prediction of flood events and their impact has been a main concern for the populations settling close to rivers and the sea. Flood inundation models are therefore developed to accomplish these purposes. As flooding accounts for a significant proportion of the total number of reported natural disasters occurring in the world, and over the last 30 years this proportion

has been increasing [21], the development and application of storm surge and flood models has become a global endeavor. Specially since the 1970s, the research community has been involved in the improvement of storm surge and flood models [77]. Since the present research focuses on storm surge modeling, the characteristics of the hydraulic models presented focus mainly on storm surge.

Generally, the interest in any modeling process is focused on the output variables of interest and their time and space scales, the required accuracy of the output and the computational efficiency of the model. In the case of storm surge modeling, applications may require a quick run time and real-time data assimilation. Based on these considerations, the flood modeler can sensibly select a model balancing their demands against model complexity and data requirements.

2.2.2.2 Overview of the main storm surge models

Nowadays, storm surge can be modeled by means of several softwares. In this report, four of the most commonly used models to represent storm surge are described:

- **ADCIRC**: The ADvanced CIRCulation model is capable of solving the equation of motion for a fluid in a global scale. ADCIRC can be run as a two-dimensional depth integrated model or as a three-dimensional model. The model assumes hydrostatic pressures and includes the Boussinesq approximation to solve the Navier Stokes equations. The water elevation is the solution of the depth-integrated continuity equation in Generalized Wave-Continuity Equation form [16]. The velocity is obtained from the solution of the 2D or 3D momentum equations. These equations are discretized in space using the finite element method (FEM) and in time using the finite difference method (FDM). This model can be run in Cartesian or spherical coordinate system. ADCIRC boundary conditions include water elevation, discharge, slip conditions for velocity, external and internal barrier overflow, surface stress (wind/wave radiation stress), atmospheric pressure and Sommerfield conditions. It can be run in parallel computers to enhance the operative efficiency of the simulations.

  ADCIRC enables the use two types of grids, depending on the discrete approach used to reach the solution. If a structured (cell-based) grid is used, the solution is reached by means of the finite difference method. The solution is obtained by approximating the derivatives in the governing equations. The structured grid is generally efficient and easy to implement, but it is difficult to fit arbitrary geometries and to refine critical regions. However, it is also possible to implement an unstructured grid. In this case, the solution is approached by the finite element method, this is, approximating the unknowns over discrete elements and minimizing the global error of the solution. This type of grid enables variable resolution and flexibility, what leads to accuracy in the solution, but is computationally more expensive.

  ADCIRC has been validated for very different hydraulic phenomena, including storm surge due to hurricanes [1]. ADCIRC can be coupled to SWAN (Simulating WAves Nearshore) in order to include wind waves in the surge simulation.

- **MIKE21 Flexible Mesh**: MIKE21 FM also solves the Navier Stokes equations to calculate the water elevation and the flow velocity. However, this model uses the finite volume method (FVM) to reach the solution. This method applies the conservation of mass law to obtain the value of the variable of interest. In MIKE21 FM, it is possible to use structured grids (simple rectilinear grids), multiple rectilinear nested grids that enable to focus the grid resolution in specific locations, and unstructured (flexible) grids, which gives flexibility to adapt the grid resolution to the model domain. As ADCIRC, MIKE21 can be run in multiple cores to reduce the computational time of the simulations. The advantage of MIKE21 with respect to ADCIRC is that it is modular. This modular nature enable the coupling of several phenomena in one simulation, within the own software. Among others, it is possible to couple modules to simulate hydrodynamic phenomena, transport of substances, sediment transport or waves.

- **Delft3D Flexible Mesh**: Delft3D FM is a multi-dimensional (1D, 2D and 3D) hydrodynamic simulation program that calculates non-steady flow and transport that results from tidal and meteorological forcing on structured and unstructured, boundary fitted grids [13]. The solution to the Navier-Stokes equations are obtained by means of the finite volume method (FVM). It is developed by Deltares, which is an independent institute for applied research in the field of water and subsurface [12]. As MIKE21 FM, Delft3D FM is a modular software in which different processes can be integrated, such as hydrodynamics,

waves, coastal morphology, transport of particles and sediment transport. These coupled models can be managed from a main interface called DeltaShell, from which the integrated models can be run. The model has been thoroughly validated for the simulation of storm surge [14].

- **SLOSH**: SLOSH stands for Sea, Lake and Overland Surge from Hurricanes. It is a model developed by the National Weather Services (NWS) to estimate in real-time storm surge heights and winds resulting from historical, hypothetical or predicted hurricanes. This model is simpler than ADCIRC, MIKE21 FM or Delft3D FM, since it does not incorporate advective terms in the shallow water equations. Several non-linear terms are also neglected. The hydraulic processes that it includes are simple, specially those related to flooding. Many of the physical parameters are just empirical and not physically justifiable. The accuracy in the calculation is reduced for the sake of the speed of calculation. The model accounts for astronomical tides by specifying an initial tidal level, but does not include rainfall amounts, riverflow or wind-driven waves.

2.2.2.3 Modeling storm surge with Delft3D Flexible Mesh

Delft3D FM has been tested and verified under tropical cyclone conditions to represent accurately storm surge and coastal flooding. This makes Delft3D FM a suitable software to model storm surge in this project. The DeltaShell interface makes possible the implementation of model inputs and the graphical visualization of the model. The model can be set up by clicking on the different tabs shown in the DeltaShell interface. The same actions can be done by giving the orders via scripting, thanks to the IronPython application included in the interface. The latest option enables the simulation of different scenarios by removing and adding input files to the model through the script, what automatizes the simulation process.

Delft3D FM solves the Navier-Stokes equations for an incompressible fluid under the shallow water and the Boussinesq assumptions, in two (depth-averaged) and three dimensions. The system of equations solved by the model are the momentum equations in horizontal direction and the continuity equation [13]. Delft3D FM includes mathematical formulations that represent many different physical processes, such as the effect of the Earth rotation (Coriolis force) and the effect of wind driven flows in the water level (including tropical cyclone winds), which are specially important for the modeling of storm surge. The model also solves an algorithm to simulate the drying and flooding of tidal flats that enables the simulation of coastal flooding.

The mathematical formulations that represent the physical phenomena take into consideration several assumptions. The most relevant one consists in assuming hydrostatic pressures in the vertical axis, which is justified by the fact that the depth in the model domain is much smaller than the horizontal length scale. This assumption is also commonly known as shallow water assumption, and implies that the vertical momentum equation is reduced to the hydrostatic pressure relation. Another consequence is that vertical accelerations are neglected since they are much smaller than the acceleration due to gravity. Further information about the assumptions taken in Delft3D FM is given in [13].

To model the storm surge caused by hurricanes, the following input is required:

- **Coordinate Reference System (CRS)**: all the input files should be written in the same CRS. The model CRS can be adjusted in the General Settings of DeltaShell.

- **Unstructured mesh**: It is possible to create unstructured meshes in Delft3D FM. This makes possible to couple regions of large resolutions with regions of small resolutions with much greater freedom, using triangles, pentagons and hexagons. Generally, smaller cell sizes are required in regions of shallow waters with large bathymetry gradients due to the influence that the bathymetry slope can have on the development of the storm surge. However, in deep waters the cell size can be larger due to the relatively low development of the surge in these regions. Therefore, a flexible mesh enables to optimize the computational time of the simulations, increasing the detail in shallow by means of smaller cells and increasing the size of the cells in deep waters. Unstructured meshes can be imported (format *_net.nc*) or created in the mesh generator of Delft3D FM (RGFGRID). To create an unstructured mesh, first several regular meshes with different resolutions are created, then the meshes are transformed to irregular meshes and finally they are connected by generating meshes among them.

- **Bathymetry**: The bathymetry is the depth of the water bodies. It is implemented by means of a raster in format *.xyz*. Once the bathymetry is imported in the model, it must be interpolated to the unstructured mesh. The bathymetry can have a different spatial resolution than the unstructured mesh. It is noted

that the bathymetry raster should be larger than the computational mesh, so as all the cells of the mesh get information about the water depth.

- **Initial and boundary conditions**: Delft3D FM solves numerically the shallow water equations, in order to calculate water levels and the velocities in the problem domain. The solution of the differential equations is the sum of a transient and a particular solution [86]:

$$\begin{pmatrix}\zeta\\u\end{pmatrix} = \begin{pmatrix}\zeta\\u\end{pmatrix}_T + \begin{pmatrix}\zeta\\u\end{pmatrix}_P$$

To solve these equations, it is necessary to implement boundary conditions and initial conditions.

  - **Initial conditions**: The initial conditions are necessary to start a time-dependent simulation and consist of a water level and a flow velocity:

$$\zeta(x,y,0) = \zeta_0, \quad [x,y] \in [0,L_x] \times [0,L_y] \tag{2.16}$$

$$u(x,y,0) = u_0, \quad [x,y] \in [0,L_x] \times [0,L_y] \tag{2.17}$$

    The transient solution is dissipated in a certain period, called spin-up time. In terms of physics, the transient solution represents waves with eigen frequencies of the model domain. The reflection of these waves on the boundaries can generate standing wave patterns. These waves might be dissipated by the bottom friction and viscosity terms or let them move outside the domain. The disappearance of these waves is the spin-up time. Generally, the consistency of the initial conditions with the boundary conditions is only relevant if the simulation period has a similar duration than the spin-up time. If the initial conditions imposed are close to the boundary conditions, the spin-up time is reduced. Therefore, to avoid the influence of the initial conditions in the particular solution, either the initial conditions should be sufficiently accurate or the simulation must start earlier in order to dissipate the transient solution before the effects of the surge wave become relevant.

  - **Boundary conditions**: The model reaches an equilibrium state after the dissipation of the initial condition effect. At this stage, the solution reaches a steady state, only governed by the forcing imposed by the boundary conditions. Therefore, the particular solution of the shallow water equations only depends on the boundary conditions:

$$\lim_{t\to\infty} \begin{pmatrix}\zeta\\u\end{pmatrix} = \begin{pmatrix}\zeta\\u\end{pmatrix}_P$$

Since the interest lies on identifying the effect of the boundary conditions in the domain, the starting time of the simulation should be set so as the steady state is reached several days before the hurricane makes landfall.

Initial conditions on the water level are imposed. These can be obtained from a previous run, in whose case it is considered that the simulation has a hot start, or from a user-prescribed (space varying or uniform) input fields, in whose case it is considered that the simulation has a cold start. Delft3D FM enables the implementation of a smoothing period parameter that enables the gradual adjustment of the boundary conditions, reducing the spin-up time of the simulations. Spatially varying initial conditions can be imported in the model in format *.csv*, while a constant initial condition can be prescribed directly in DeltaShell.

The imposition of flow boundary conditions on the model is made in two steps. First, the geometry of the boundaries of the model is created. This can be done by drawing polylines in DeltaShell, whose vertices correspond to boundary support points. In this project, water levels are imposed in the open sea boundaries, by prescribing the amplitude and the phase of the astronomical constituents of the tide. However, it is also possible to impose water level time-series and also Q-h relations in the case of water level boundary conditions. Other flow boundary conditions that Delft3D FM supports are discharges, flow velocities, water level gradients and Sommerfeld conditions on reflective boundaries. The boundary conditions are imposed at each of the support points, except for the discharge boundary conditions, which

are imposed along the boundary lines. Apart from flow initial and boundary conditions, in case of surge modelling due to hurricanes it is also required to impose atmospheric initial and boundary conditions, given by air pressure constant values. The format of the geometry of the boundary conditions is *.pli* and the format of the files containing all the information about the boundary conditions is *.bnd*.

- **Physical parameters**: The physical parameters of the model are the roughness, the viscosity and the diffusivity. They can be specified as a uniform value or as a spatially varying field (raster in format *.xyz*). In case the latter is used, the rasters should be interpolated to the unstructured mesh.
  - **Roughness**: For 2D depth-averaged flow, the shear-stress at the bed induced by a turbulent flow (τ_b) is assumed to be given by a quadratic friction law:

$$\tau_b = \frac{\rho_w g U|U|}{C^2} \tag{2.18}$$

    where ρ_w is the water density (1025 kg/m^3), g is the acceleration due to gravity (9.81 m/s^2), U is the depth-averaged horizontal velocity and C is the Chézy coefficient. C can be related to the Manning number (n) according to the Manning equation:

$$C = \frac{R^{1/6}}{n} \tag{2.19}$$

    In this project, the Manning number is used. However, there are other friction formulations available in Delft3D FM, such as the White-Colebrook and the Z_0 formulations. The values of the Manning number depend on the type of soil and the land use (in the case of overland flooding).
  - **Viscosity and diffusivity**: In Delft3D FM the 3D turbulent eddies are bounded by the water depth. The vertical eddy viscosity and diffusivity coefficients determine their contribution to the vertical exchange of horizontal momentum and mass. For 3D shallow water flow the stress tensor is anisotropic, and the horizontal viscosity and diffusivity coefficients are much larger than the vertical coefficients. The horizontal eddy viscosity and diffusivity combine the effect of the 3D turbulent eddies and the horizontal motions that cannot be resolved by the horizontal grid [13].
- **Wind**: Wind forces can induce variations in the flow field. The wind force is coupled to the Delft3D FM flow equations as a shear stress, represented by the quadratic expression:

$$\tau_w = \rho_a C_d U_{10}^2 \tag{2.20}$$

  where ρ_a is the air density (1.205 kg/m^3), C_d is the wind drag coefficient (dependent on U_{10}) and U_{10} is the wind speed at 10 meters above the free surface (time and space dependent).

  When hurricanes are considered, U_{10} is given by a 2D wind field in spiderweb format (Figure 2.8). The location of each point of the spiderweb is given in geographical coordinates. Each point includes the information of three variables: wind speed at 10 meters above the free surface, wind direction and the pressure drop at MSL. The 2D wind field is imported in Delft3D FM in spiderweb format (*.spw*). The spiderweb is generated by means of the Holland model, according to the equations described in Chapter 2.2.1.2. The wind field is given on a polar grid with the center (eye) of the hurricane being the origin of the polar coordinate system. Since the hurricane progresses with time, one spiderweb is given per time step.

  Recent research suggests that the sea conditions, fetch shoaling, wave breaking and sea spray may also have an influence on C_d [3]. Many formulations simplify these influences by proposing relationships between C_d and U_{10}. The simplest manner to impose C_d is assuming a constant drag value. A more detailed description of C_d is given by [73], [8] and [66].

  Smith and Banke (1975) represented the drag coefficient as a linearly varying or piecewise linearly varying function (Figure 2.13). When only A is defined the relationship is considered constant. When A and B are given, the relationship is linearly varying. When A, B and C are defined, the relationship is piecewise linearly varying. The breaking points vary for the different wind models.

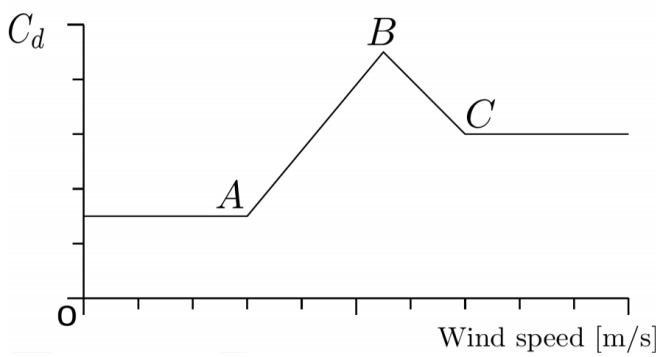

Figure 2.13: Dependence of the drag coefficient on the wind speed according to [73] [13].

The drag coefficient remains constant until wind speed reaches the value at the point A. From this value, the drag starts to increase until reaching a maximum value at point B. The physical meaning of this increase in the drag is that the resistance increases when the wind speed increases, due to the contact of the wind with more water particles. For higher speeds, the resistance levels off or decreases due to the effect of sea-spray droplets in suspension generated by breaking waves [47]. From approximately 50 m/s, the entire sea surface is covered by a foam layer and the drag coefficient remains constant (point C).

The [8] formulation is also widely applied when modelling the wind drag. It is based on the assumption that the wind flow over the water surface is a fully developed turbulent boundary layer. In this formulation the friction velocity, wind speed (at 10 meters above the water surface), and friction of the water surface are needed as input. [8] assumes a logaritmic wind speed profile:

$$\frac{U_{10}}{u_*} = \frac{1}{\kappa} \ln\left(\frac{z_{10}}{z_0}\right) \tag{2.21}$$

with κ de Von Kárman constant (0.4), z_{10} the distance to the water surface (10 meters) and u_* the friction velocity. The drag coefficient is defined as:

$$C_d = \frac{u_*^2}{U_{10}^2} \tag{2.22}$$

[8] proposed to represent the friction of the water surface as z_0 according to:

$$z_0 = \frac{bu_*^2}{g} \tag{2.23}$$

where b is a specific constant (0.025). Since the above expression is implicit for u_*, the system is solved iteratively.

In Figure 2.14, it is shown the relationship between C_d and U_{10} according to [8] and [47] (solid lines). The approximation of these models can be done in Delft3D FM by means of the model proposed by [73] (dashed lines).

[66] investigated the azimuthal dependence of the wind drag coefficient during hurricanes, determined from mean GPS sonde wind speed profiles. Based on his research, the storms can be separated into three regions. The first region is the left front of the storm, where the swell travels across the wind, the second region is the right front where the swell and the wind coincides and the third region is the left rear, where the sea is more confused and at times has winds going against the waves. In Figure 2.15, it is shown a real example of application of this wind model.

The results of the research were not clear to affirm that azimuthal drag dependence exists for near coastal ares. However, deep water wind profiles showed that C_d increases in sectors where the wind blows across

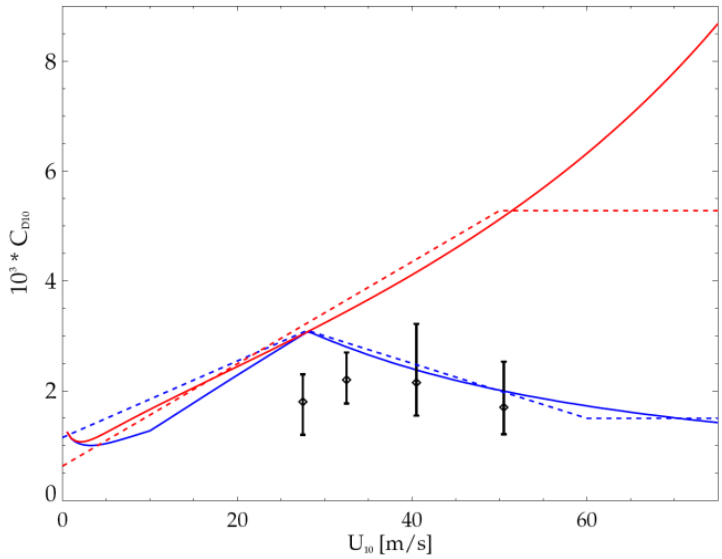

Figure 2.14: C_d as a function of U_{10} according to Charnock's relation using the Charnock's constant value equal to 0.025 (solid, red) and the new parameterization following [47] (solid, blue). The dashed lines represent the approximations used in Delft3D FM. Observational data by [65] are indicated by diamonds. Figure from [80].

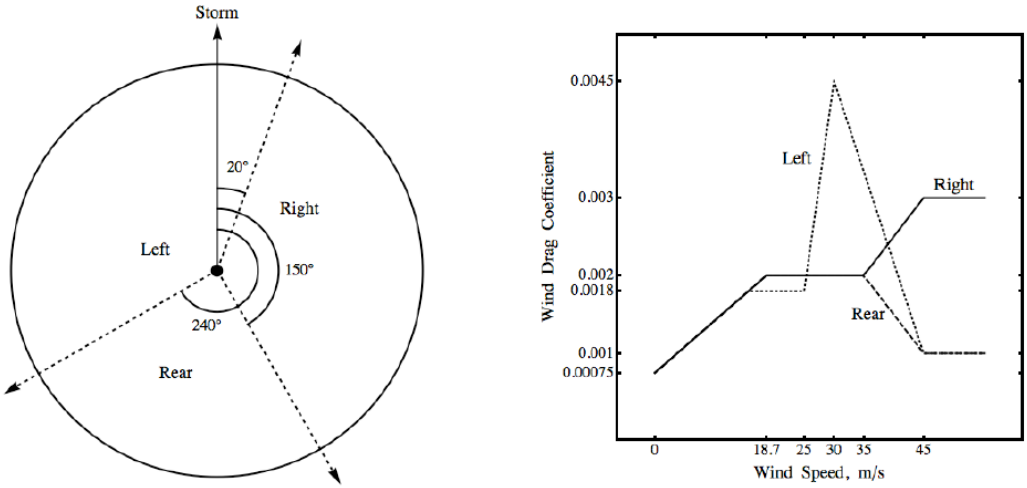

Figure 2.15: Schematization of the azimuthal wind drag, showing the relationship between C_d and U_{10} according to the azimuthal sector relative to the direction of the storm [66].

or in opposite direction of the waves. This explains the larger values reached on the front left region of the storm than on the right front and the rear region of the storm for wind speeds between 25 m/s and 33 m/s. When the storm reaches the hurricane category, the strength of the wind exceeds the effect that the waves can cause in the drag coefficient, and the right sector (in the Northern Hemisphere) reaches larger values of C_d than in the other two sectors.

- **Time frame and time step**: To run the model, it is necessary to specify a reference date, a start date and a stop date of simulation. The reference date should correspond to a date before the starting date of the simulation. The start time should coincide with the first time step of the spiderweb representing the 2D wind field. The user time step is the time step of the wind field imposed in the model. Delft3D FM applies linear interpolation to implement the spiderweb values in the model, in case the user time step does not coincide with the time interval of the spiderweb. Delft3D FM uses an explicit advection scheme to compute the numerical solution of the problem. Therefore, to achieve a stable numerical computation,

the time step of the simulation is automatically limited based on the Courant-Friedrichs-Levy (CFL) condition, which is necessary (but not sufficient) to guarantee the stability of the computation:

$$C \geq \frac{u\Delta t}{\Delta x} \tag{2.24}$$

It is advised to use a Courant number of 0.7 or lower to compute the time step size from the CFL criterion, in order to ensure the stability of the numerical solution of the hydraulic problem. This time step is computed automatically by Delft3D FM, by solving Eq. (2.24).

2.2.3 Skill metrics for the model validation

The model is validated by quantifying the goodness of fit of the simulation in Delft3D FM. The following skill metrics where used to this end: Coefficient of Determination (R^2, which describes how well a regression line fits a set of data, with an ideal value of one), Slope of the best fit line (m, with an ideal value of one), Mean Normalized Bias ($Bias$, which is a measure of the model's magnitude of overprediction or underprediction normalized to the observed value, with an ideal value of zero) and the Scatter Index (SI, which is the standard deviation normalized by the mean observed value, with an ideal value of equaling zero). If O is the observed value, E is the error in terms of modeled minus observed, and N is the number of data points, the equation for Mean Normalized Bias is:

$$Bias = \frac{\frac{1}{N}\sum_{i=1}^{N} E_i}{\frac{1}{N}\sum_{i=1}^{N} |O_i|} \tag{2.25}$$

and the equation for the Scatter Index (SI) is:

$$SI = \frac{\sqrt{\frac{1}{N}\sum_{i=1}^{N}(E_i - \hat{E})^2}}{\frac{1}{N}\sum_{i=1}^{N} |O_i|} \tag{2.26}$$

2.2.4 Probabilistic modeling

The implementation of machine learning and artificial intelligence techniques in the hydraulic engineering field has enabled the reduction of the computational time required to run traditional hydraulic models. Two of the most developed methods to predict water levels are the Artificial Neuronal Networks (ANN) and the Bayesian Networks (BN). [36] proved that storm surge can also be estimated accurately by means of Surge Response Functions (SRF). These functions are scaling laws derived from high-resolution numerical simulations. By means of these functions, it is possible to make fast estimations of the probabilistic maximum surge due to hurricanes.

In the last decade, BN and ANN have been used to solve a wide range of coastal engineering problems. BN have been applied to estimate coastal flood hazard due to waves on coral reef-lined coasts [64], the coastal vulnerability due to sea level rise [28] and the modeling of hydraulic boundary conditions for hurricane flood risk analysis [71]. ANN have been used to evaluate the response of a harbour to long waves [46], rubble-mound breakwater stability [6], the estimation of swell conditions in coastal regions [2] or wave run-up and overtopping at coastal structures [82] and also in storm surge estimation due to hurricane [83].

BNs allow to represent the dependencies among hurricane variables graphically. This feature facilitates the understanding of the physical processes that rule storm surge. Apart from enabling the estimation of surge, it is possible to infer values in the BN in a certain number of variables of the network to generate synthetic data. For instance, it is possible to estimate hurricane wind speeds by inferring surge values in a BN. Given these characteristics, it is considered adequate to approach this project by means of BNs.

2.2.4.1 Bayesian Networks (BN)

BN are graphical models that allow for the representation of a probability distribution over more than one variable [53]. BN consist of nodes, which represent random variables, and arcs of connection among the nodes, which indicate the dependence between the variables (Figure 2.16). The lack of connection between nodes shows the independence between two variables. The joint distribution of several variables can be represented by Directed Acyclic Graphs (DAG). These graphs will determine the causal relationships between variables and the sampling order. Therefore, the DAG shows the variables from which we need information first in order

to obtain information about another variable that succeeds them. The direct predecessors and successors of a variable are called parents and children, respectively.

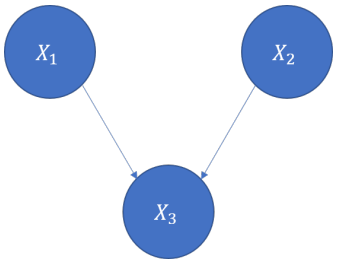

Figure 2.16: Basic structure of a BN.

The joint probability density of the children can be computed as the product of the conditional probabilities on the parents:

$$f(x_1, ..., x_n) = \prod_{i=1}^{n} f(x_i | x_{Pa(X_i)}) \tag{2.27}$$

where $x_{Pa(X_i)}$ is the set of parent nodes of X_i, with $i = 1, ..., n$. The marginal probability density is used for the nodes without parents.

Depending on the nature of the variables (discrete or continuous), discrete and non-parametric Bayesian Netorks (NPBN) are distinguished. Since in this project it is dealt exclusively with continuous variables, only the features of NPBN are reviewed in this chapter. Typically, the dependence between continuous variables in a NPBN can be quantified by means of copulas or multivariate distributions. Copula models differ from multivariate distributions in the fact that in the case of copulas the marginal distributions of each individual variable does not characterize the behavior of the joint distribution [23]. Since in many occasions the marginal distributions of the variables involved in the Bayesian Network are not known, it is advisable to use copulas instead of multivariate distributions in order to avoid the influence of the marginal distributions chosen in the final relationship between variables.

2.2.4.1.1 Copula fitting

Copulas are functions that represent the joint distribution of several variables, whose marginal distributions have been transformed to uniform ranked distributions. The use of rank correlations coefficients to assess the dependence among variables measures monotone dependence, rather than just linear (as is the case when using marginal distributions when using the Pearson correlation coefficients). Moreover, due to this transformation process, the copula model is independent of the marginal distribution of the individual variables. The joint cumulative distribution function $H(x, y)$ of any pair of continuous random variables (X, Y) can be written as [23]:

$$H(x, y) = C(F(x), G(y)), \quad x, y \in \text{Re} \tag{2.28}$$

where $F(x)$ and $G(y)$ are the marginal distributions and $C \in [0, 1] \times [0, 1]$ is the copula function.

The fitting process of a copula model to a data set is made in four main steps:

1. **Transformation of the marginal distributions to uniform on [0,1]**: To build the empirical copula, first the marginal distributions should be transformed to uniform ranked distributions. Therefore, the sample is transformed as follows:

$$(X_1, Y_1), ..., (X_n, Y_n) \rightarrow (R_1, S_1), ..., (R_n, S_n) \tag{2.29}$$

where X, Y represent the values of the sample of study, R, S are the ranked values of the variables of study and n the length of the sample.

2. **Construction of the empirical copula**: The empirical formula (C_n) is constructed as follows:

$$C_n(u,v) = \frac{1}{n}\sum_{i=1}^{n} 1\left(\frac{R_i}{n+1} \leq u, \frac{S_i}{n+1} \leq v\right) \tag{2.30}$$

The empirical copula can be seen as a square matrix of dimension j, where j is the number of equidistant points between 0 and 1 that represent the domain of u and v. This number of points is arbitrary. The value of every component of this matrix corresponds to the number of pairs of ranked variables R_i, S_i that after being normalized by $n+1$ are smaller or equal than u and v, respectively. The copula model is expected to be more statistically significant for larger samples, but the significance of the model is not influenced by the number of equidistant points chosen between 0 and 1, this is, the dimension of the matrix that corresponds to the theoretical copula.

3. **Fit specific copula models to the empirical copula**: The existing copula models can be grouped in three main families: Archimedian copulas, extreme value copulas and meta-elliptical copulas. Apart from these families, there are other copula models that cannot be classified under the previous families, but are out of the scope of this research. In this project, the goodness of fit of Gaussian (meta-elliptical), Clayton (Archimedian) and Gumbel (Archimedian) copulas will be tested, due to their common use in Hydraulic Engineering applications.

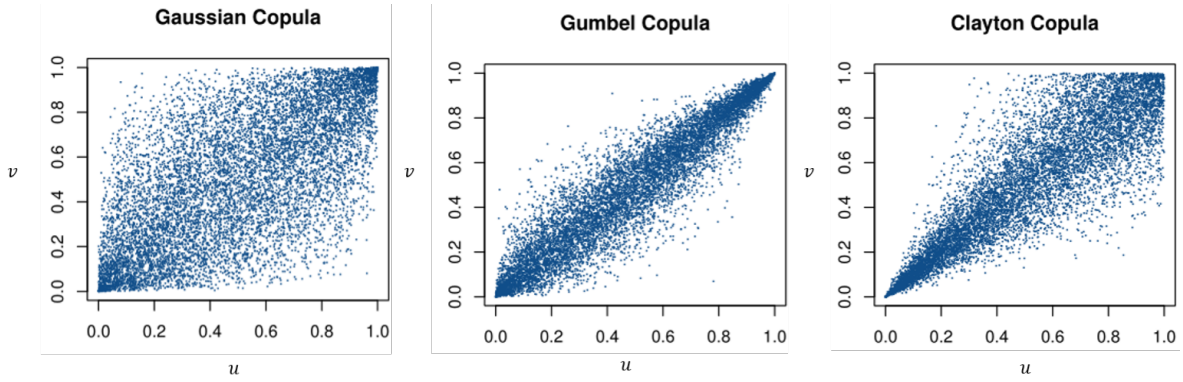

Figure 2.17: Example of randomly generated samples of Gaussian, Gumbel and Clayton copulae.

The functions representing these theoretical copula models are shown below. The Gaussian copula is:

$$C_\rho^{Gaussian} = \Phi_\rho\big(\phi^{-1}(u), \phi^{-1}(v)\big) \tag{2.31}$$

where:

$$\Phi_\rho(x_1,x_2) = \int_{-\infty}^{x_2}\int_{-\infty}^{x_1} \frac{1}{2\pi\sigma_1\sigma_2\sqrt{1-\rho^2}} \exp\Big(-\frac{\big(\frac{s_1-\mu_1}{\sigma_1}\big)^2 + \big(\frac{s_2-\mu_2}{\sigma_2}\big)^2 - \frac{2\rho(s_1-\mu_1)(s_2-\mu_2)}{\sigma_1\sigma_2}}{2(1-\rho^2)}\Big) ds_1 ds_2 \tag{2.32}$$

where $x_1, x_2 \in \mathbb{R}$, μ_i and σ_i are the mean and the standard deviation of x_i and ρ is the parameter of the Gaussian copula. As mentioned before, u, v are in $[0,1]^2$. The Gumbel copula has the following expression:

$$C_\theta^{Gumbel}(u,v) = \exp\big(-(-\ln u)^\theta + (-\ln v)^\theta\big)^{1/\theta} \tag{2.33}$$

where $\theta \in [1,\infty)$. θ is the parameter of the Gumbel copula. The expression of the Clayton copula is writen as follows:

$$C_\beta^{Clayton}(u,v) = (u^{-\beta} + v^{-\beta} - 1)^{-1/\beta} \tag{2.34}$$

where $\theta \in [-1,\infty) - \{0\}$. β is the parameter of the Clayton copula.

The difference among the Gaussian, the Clayton and the Gumbel copula models is on the tail dependence (Figure 2.17). A distribution shows tail dependence when the correlation grows when approaching the extremes of the distribution. While Gaussian copulas do not show tail dependence and are symmetric, Gumbel copulas present larger dependence among high values of the variables (upper right corner of the plots in Figure 2.17) than among the low values of the variables (down left corner of the plots in Figure 2.17). In contrast, Clayton copulas presents larger dependence among low values of the variables.

The copula models explained are defined by one parameter, by which the theoretical copulas are fitted to the empirical copula. The value of this parameter can be estimated by different methods. Examples of these methods are the estimation based on the Kendall tau, based on the Spearman rho or based on the maximum pseudolikelihood. If θ is real, one of the methods to obtain the rank-based estimator of the copula parameter is by means of the Kendall tau, which measures the dependence between pairs of variables based on ranks. The empirical value of the Kendall tau is (τ_n):

$$\tau_n = \frac{P_n - Q_n}{\binom{n}{2}} = \frac{4}{n(n-1)} P_n - 1 \tag{2.35}$$

where P_n and Q_n are the number of concordant and discordant pairs, respectively. Two pairs (X_i, Y_i), (X_j, Y_j) are said to be concordant when $(X_i - X_j) \cdot (Y_i - Y_j) > 0$, and discordant when $(X_i - X_j) \cdot (Y_i - Y_j) < 0$. Ties do not represent a problem, since the borderline case $(X_i - X_j) \cdot (Y_i - Y_j) = 0$ occurs with probability zero under the assumption that X and Y are continuous. Therefore, τ_n is a function of the ranks of the observations only, since $(X_i - X_j) \cdot (Y_i - Y_j) > 0$ if and only if $(R_i - R_j) \cdot (S_i - S_j) > 0$.

If $\theta = g(\tau)$, for some smooth function g (being θ a population value), then $\hat{\theta} = g(\tau_n)$ may be referred as the Kendall estimator of θ. A small adaptation of Proposition 3.1 of [24] implies that:

$$\sqrt{n} \frac{\tau_n - \tau}{4S} \approx N(0, 1) \tag{2.36}$$

being n the size of the sample, τ_n the estimator of the population value of the Kendall tau τ and S the sample standard deviation:

$$S^2 = \frac{1}{n} \sum_{i=1}^{n} (W_i + \hat{W}_i - 2\overline{W})^2 \tag{2.37}$$

with:

$$W_i = C_n \left(\frac{R_i}{n+1}, \frac{S_i}{n+1} \right) \tag{2.38}$$

$$\hat{W}_i = \frac{1}{n} \sum_{j=1}^{n} I_{ji} = \frac{1}{n} \#j : X_i \leq X_j, Y_i \leq Y_j \tag{2.39}$$

$$\overline{W} = \frac{1}{n} \sum_{j=1}^{n} W_i \tag{2.40}$$

Applying the Slutsky's theorem (also referred as *Delta method*) implies that as $n \to \infty$:

$$\hat{\theta}_n \approx N \left(\theta, \frac{1}{n} 4S g'(\tau_n)^2 \right) \tag{2.41}$$

being g' the first derivative on θ of the function g. The $100 \times (1 - \alpha)\%$ confidence interval for θ is given by:

$$\hat{\theta}_n \pm z_{\alpha/2} \frac{1}{\sqrt{n}} 4S \left| g'(\tau_n)^2 \right| \tag{2.42}$$

where $z_{\alpha/2}$ is the value of the inverse standard normal distribution for a probability of $1 - \alpha/2$, being alpha an arbitrary value.

4. **Assessment of the goodness of fit of the copula models to the data**: The fit of the copula models is assessed using semi-correlation and Cramer-von-Mises tests [71]:

   - **Semi-correlations**: This metric is used to test how well a chosen copula fits the tails of a data set. To do so, the overall correlation (ρ) for the normal transform of the original data (Z_λ) is compared to the semi-correlation in the tail quadrants. Generally, if the absolute value of the semi-correlation is larger than the overall correlation, then the data is considered to be tail dependent.

     The semi-correlations are calculated according to the following expressions:

     $$\begin{cases} \rho_{NE} = \rho\big((Z_i, Z_j)|[Z_i > 0 \wedge Z_j > 0]\big) \\ \rho_{NW} = \rho\big((Z_i, Z_j)|[Z_i < 0 \wedge Z_j > 0]\big) \\ \rho_{SW} = \rho\big((Z_i, Z_j)|[Z_i < 0 \wedge Z_j < 0]\big) \\ \rho_{SE} = \rho\big((Z_i, Z_j)|[Z_i > 0 \wedge Z_j < 0]\big) \end{cases} \tag{2.43}$$

     where (Z_i, Z_j) are the standard normal transforms of X_i and X_j.

   - **Cramer-von-Mises statistic (CM)**: The CM statistic is the sum of the squared differences between the empirical copula and the fitted copula model (Gaussian, Gumbel, Clayton) for a given number of samples. Generally, the copula with the lowest CM statistic is the best estimate for the data set. The CM statistic is computed as follows:

     $$CM_n(u) = \sum_{|u|} C_{\hat{\theta}_n}(u) - B(u)^2, \quad \in [0,1]^2 \tag{2.44}$$

     where $B(u) = \sum 1(U_i \leq u)$ is the empirical copula and $C_{\hat{\theta}_n}(u)$ is a copula model with parameter $\hat{\theta}_n$ fitted to the data. Based on the assessment of the goodness of fit, it is selected the copula model that better represents the joint probability distribution of the variables of interest.

2.2.4.1.2 Construction and validation of the Bayesian Network

The NPBN is built by adding arcs between variables only if their rank correlation is larger than a threshold value, which is application dependent and imposed by the user. The result of introducing arcs to capture causal or temporal relationships is called a skeletal NPBN. The constructed NPBN should overcome two validation steps: the first tests validates that the normal copula adequately represents the data set used and the second tests verifies that the NPBN is an adequate model of the saturated graph, this is, that the assumed conditional independencies are valid for the data set given. For the first validation there are distinguished two determinants. DER is the determinant of the empirical rank correlation matrix. DNR is the determinant of the empirical normal rank correlation matrix, which is the rank correlation matrix obtained by transforming the marginals to standard normals, and then transforming the product moment correlations to rank correlations. A statistical test for the suitability of DNR for representing DER is to obtain the sampling distribution of DNR and check whether DER is within the 90% central confidence band of DNR. [30] proposes the following procedure to do so:

1. Compute DER by first transforming marginals to uniforms and then calculating the product moment correlation of the transformed variables.

2. Construct the normal version of each variable using the marginal distributions and the standard normal distribution ($Z_i = \phi^{-1}(F_{X_i}(X_i))$) and calculate the product moment correlation matrix.

3. Compute DNR using the relationship between the rank correlation and the product moment correlation given by Pearson's transformation:

   $$r(X_i, X_j) = \frac{6}{\pi} \sin^{-1}\left(\frac{\rho(X_i, X_j)}{2}\right) \tag{2.45}$$

4. Re-sample the *normal* data to obtain the empirical distribution of DNR and extract the 5th and the 95th quantiles of this distribution.

5. Compare DER with the quantities from step 4. If DER is within these bounds, do not reject the joint normal copula, otherwise reject this hypothesis.

It should be noted that for small data sets, the normal copula assumption is rarely rejected on the basis of this test. This occurs also when assuming other copulas as well. By contrast, this test is quite severe for large data sets. Even when it is not a perfect fit, normal copulas present important advantages with respect to other copula models and therefore even when rejected in the case of large data sets, they can represent well multivariate data, but this is only true for applications where tail dependence is not expected.

For the second validation step, it is introduced the determinant of the rank correlation matrix of a NPBN using the normal copula (DBN). The procedure to validate the NPBN structure is similar to the first validation step:

1. Construct a skeletal NPBN.
2. Re-sample to obtain the distribution of DBN.
3. If DNR is within the 90% central confidence band of DBN, then stop, else continue with the following steps.
4. Find the pair of variables such that the arc between them is not in the DAG and their rank correlation is greater (in absolute value) than the rank correlation of any other pair not in the DAG. Add an arc between them and recompute DBN together with its 90% central confidence band.
5. If DNR is within the 90 % central confidence band of DBN, then stop, else repeat step 4.

The data mining scheme to generate DER, DNR and DBN is shown in Figure 2.18.

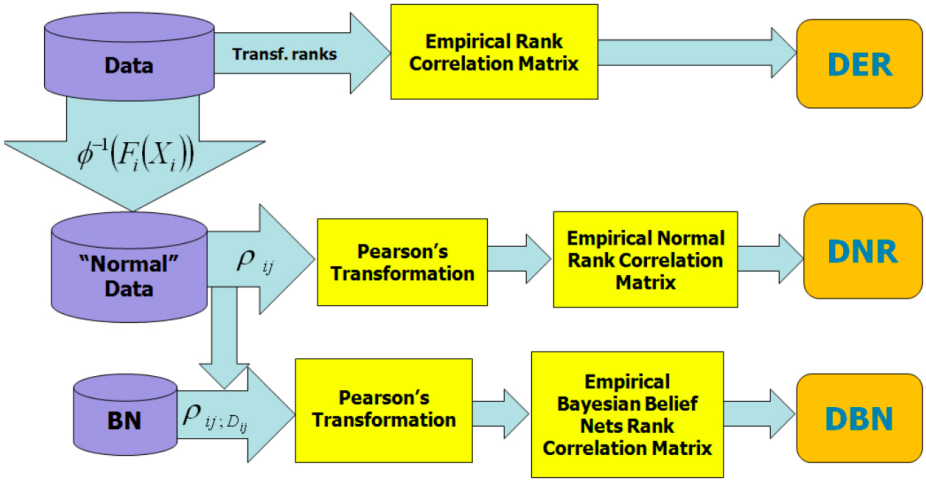

Figure 2.18: Data mining scheme followed to compute DER, DNR and DBN to validate the NPBN [29].

In the present research, it is used a standalone uncertainty analysis software package called UniNet [78], which facilitates the manipulation of NPBN. UniNet assumes that the joint probability between the variables of the BN can be represented by normal copulas. This is the fastest way of performing inference in a NPBN. Since joint normal distributions are used exclusively, any conditional distribution will also be normal, what allows to perform inference analytically. If arbitrary copulas are used, sampling or similar methods must be used to perform inference. In such case, the inference process can become computationally expensive, specially whether the BN includes undirected cycles, since multiple integrals should be solved for each sample and for any conditionalization [53].

CHAPTER 3

Methodology

This Chapter describes the research approach followed to satisfy the objectives of the MSc Thesis described in Chapter 1.

3.1 Theoretical framework

The objective of this project is to develop a stochastic model capable of estimating surge at the coast of Mississippi. To do so, a Bayesian Network needs to be trained and validated by means of a hurricane data set consisting of a finite number of hurricanes. Each hurricane of the data set is described by five variables: forward speed (FS) and forward direction (FD) of the hurricane, wind speed (WS), distance from landfall to a specific recording station (LF) and maximum surge at this recording station (SS). The values of the first three variables mentioned correspond to the values at landfall. FS, FD, WS and LF are obtained from the hurricane best tracks. However, the value of the storm surge at a specific tidal elevation station is not available. To get the storm surge values, each of the hurricanes of the data set is simulated in Delft3D FM and the surge is recorded at an observation station.

The stochastic model needs to be trained by means of hurricane data, including surge levels. This information must be generated beforehand, by simulating a limited number of hurricanes with an hydrodynamic model. In this project, the hydrodynamic model Delft3D Flexible Mesh is used for this purpose. The approach followed to build the stochastic model is based on three main steps. The first step consists of setting up and validating the hydrodynamic model in Delft3D FM. Hurricane Katrina (2005) is simulated to calibrate the input parameters of the model, by comparing the maximum simulated water levels at a finite number of locations stations along the shoreline of Mississippi to the high water marks observed at the same locations during the event. Tide, surge and wave setup have been considered in the validation. The inputs of the model are the unstructured mesh, the bathymetry and topography, the hydraulic roughness, the hurricane forcing, the wind drag coefficient and the boundary conditions. For the latter, an astronomical tide has been imposed. A maximum wave setup has been assumed.

The second step in the construction of the stochastic model is the generation of a historical hurricane data base. The hurricane best tracks are retrieved from the HURDAT2 data base. The variables considered are the forward speed and the forward direction of the hurricane at landfall, the wind speed at landfall, the distance from landfall location to a reference point (Galveston Bay) and the maximum storm surge during the hurricane. In this case, only the hurricane forcing is considered as external action. The storm surge is recorded at Gulfport Harbour (central coast of Mississippi). The values of the surge are obtained by using the validated model to simulate the historical hurricanes making landfall in a specific domain surrounding Gulfport Harbour. Due to the scarce number of hurricanes making landfall in this region, the tracks of the hurricanes making landfall in the North of the Gulf of Mexico but outside the rectangular domain are shifted inside the domain, in order to generate a sufficiently large data base to train the stochastic model. A data base with a finite number of hurricanes is built, from which the 85% is used for the training of the stochastic model and the other 15% have been used for the validation of the stochastic model.

The final step is the setup and validation of the stochastic model, by comparing the storm surge obtained

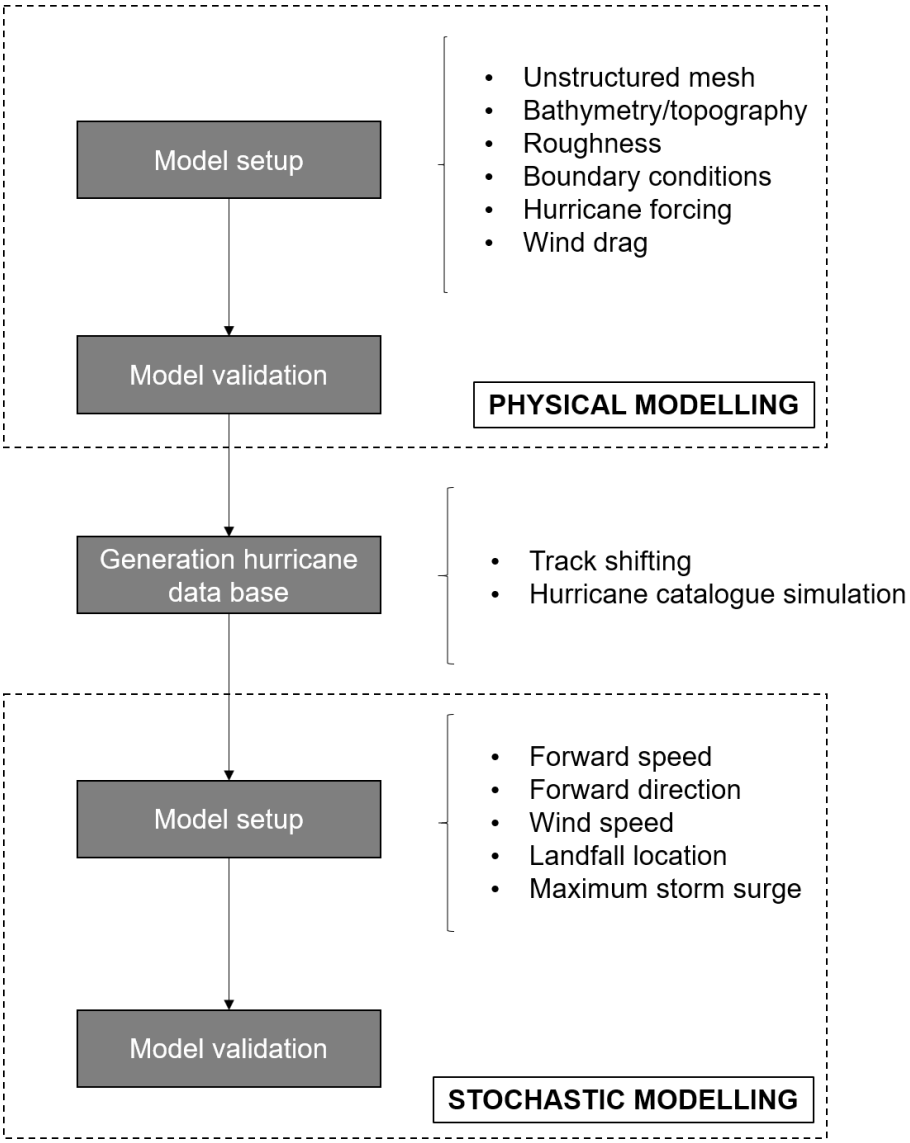

Figure 3.1: Workflow of the project.

from the stochastic model to the surge obtained from the hydrodynamic simulations. The stochastic model used to estimate storm surge has been a Bayesian Network that assumes normal copulas to represent the joint distribution between nodes of the network. The Bayesian Network provides the uncertainty of the estimation by giving a normal distribution of the surge.

CHAPTER 4

Physical model setup and validation

Delft3D FM is an hydrodynamic model that has been validated for a wide range of physical conditions, including storm surge, according to the quality assessment guidelines included in [11]. However, the quality of the simulation results depends on the adequacy of the available data, the suitability of the model chosen by the end user and the designated model parameters. As stated in [14], in order to obtain useful and accurate results for a particular application, the use of high-quality modeling tools is necessary but not sufficient. For this reason, to guarantee the goodness of the database generated to train the stochastic model, it is essential to ensure that the model to generate storm surge is adequately calibrated.

The objective of using Delft3D FM is to generate a catalogue of high-fidelity storm surge levels, given the best tracks of a list of historical hurricane events. The quality of Delft3D FM output will condition the accuracy of the stochastic model for storm surge prediction, since the probabilistic model will be trained with the database generated with the physical model. The purpose of this chapter is to set up the surge model and validate it. To do so, it is simulated an historical event in Delft3D FM and the resulting storm surge is compared to observed data recorded during the real event. Hurricane Katrina (2005) has been chosen to do the validation.

4.1 Historical hurricane used for validation: Hurricane Katrina (2005)

4.1.1 Description of the event

Hurricane Katrina was one of the strongest storms to impact the coast of the United States during the last 100 years. According to the [56], the storm began as tropical depression over the southeastern Bahamas on August 23, 2005. On August 24, the cyclone became tropical storm, receiving the name *Katrina*. It is estimated that Katrina reached hurricane status on August 25, 2005. Katrina made its first landfall very close to Miami as a Category 1 hurricane on the Saffir-Simpson Hurricane Scale, with maximum sustained winds of 70 knots (130 km/h). At that moment, the hurricane headed the southwest. It spent only 6 hours over land and weakened to a tropical storm with maximum sustained winds of 60 knots (111 km/h) as it emerged into the Gulf of Mexico. Katrina continued northward over the Gulf of Mexico, quickly regaining hurricane status and strengthening to a Category 5 hurricane on the morning of August 28, 2005. Katrina attained its peak intensity of 150 knots (278 km/h) about 275 km southeast of the mouth of the Mississippi River. Katrina remained a significantly large, sustained storm and impacted a broad area of the Gulf Coast. By the morning of August 29, Katrina weakened to a Category 3 storm, making landfall near Buras (Louisiana), with estimated maximum sustained winds of 110 knots (177 km/h). Heading northward, Katrina downgraded to a tropical depression in the state of Tennessee and dissipated on August 31 in southeastern Canada. The Hurricane Katrina storm track is shown in Figure 4.1.

The measurement of the storm surge produced by Hurricane Katrina along the states of Louisiana and Mississippi was complicated, mainly because the majority of the tidal gauges available failed during the event. The data recorded by the tidal gauges that resisted was complemented with the high watermarks (HWM) obtained by visual inspection in several structures located in flooded areas. The HWM collection campaign was organized by the Federal Emergency Management Agency (FEMA) and the US Army Corps of Engineers (USACE), and tables that include this data can be found in [56]. The HWM records show that the storm surge was about 7.5 to

Figure 4.1: Hurricane Katrina track (2005).

8.5 meters along the Mississippi coast with respect to the vertical datum NAVD88, in the vicinity of Bay Saint Louis. At this location, the difference between the NAVD88 and the Mean Sea Level (MSL) is 6 centimeters [57]. The maximum observed HWM was located at Pass Christian, where the surge reached 8.5 meters. From Gulfport to Pascagoula, in the east coast of Mississippi state, the surge reached from 5 to 7 meters. In terms of extension, the surge spread at least 10 kilometers inland in many locations of coastal Mississippi and up to 20 kilometers inland in bays and rivers. The records also show that the surge crossed the Interstate 10 highway in several locations [56].

The exceptional flood extent provoked by Hurricane Katrina is mainly attributed to the great hurricane horizontal size, being the water level additionally enhanced by the waves generated when the hurricane reached category 5 the day before making landfall. Additionally, 200 to 250 mm of rainfall were reported in southwest Mississippi during landfall. In inland locations of the Mississippi state, lower levels of precipitation were observed, ranging from 100 to 200 mm.

4.2 Model setup

The Delft3D FM model aims to represent the storm surge provoked by hurricanes as close as possible. Reaching a high accuracy in the simulation comes at a price of a large computational time, since the resolution of the mesh should be small enough to capture the bathymetry and topography gradients and the time step small enough to capture the progress of the surge. Due to time limitations, it is key to find a tradeoff between the accuracy and the computational time, since it is desired to simulate enough hurricanes to generate a stochastic model that is sufficiently trained.

The model calibration process is iterative. During this process, it is evaluated what is the accuracy of the simulation output and what is the sensitivity of the model to variations in the input. It is also assessed what is the computational time and the variation of the results for different time steps. In the following paragraphs, the input archives used to set up the model and the output format is described.

4.2.1 Model input

The mesh used in Delft3D FM is known as ULtralite-Levee-Removed mesh (ULLR), which is formed by 417,642 nodes and 826,866 triangular elements (Figure 4.2). This mesh has been widely used in ADCIRC models for storm surge and flood modelling. The domain of the mesh is restricted to the Gulf of Mexico, with open sea

boundaries at the Strait of Florida and the Yucatan Channel. These boundaries are intersected by Cuba. This mesh has a resolution of 8-30 km in the deep waters of the Gulf of Mexico, 2-8 km in the continental shelf, reaches a resolution of approximately 500 m in the floodplains and 100 m in the rivers Mississippi and Atchafalaya. This mesh can be used to evaluate storm surge and overland flooding. The refined mesh has 460,296 nodes. The mesh has been refined to reach 200 meters of resolution in the shoreline. The ULLR mesh has been converted from the ADCIRC format (*fort.14*) to the Delft3D FM format by means of an Open Earth Tool developed by Deltares that is called *adcirc2dflowfm*. The bathymetry used in the Delft3D FM model is extracted from the General Bathymetric Chart of Oceans [22] and it has a uniform resolution of 15 arc-second (cell size of roughly 460 meters by 460 meters) (Figure 4.3).

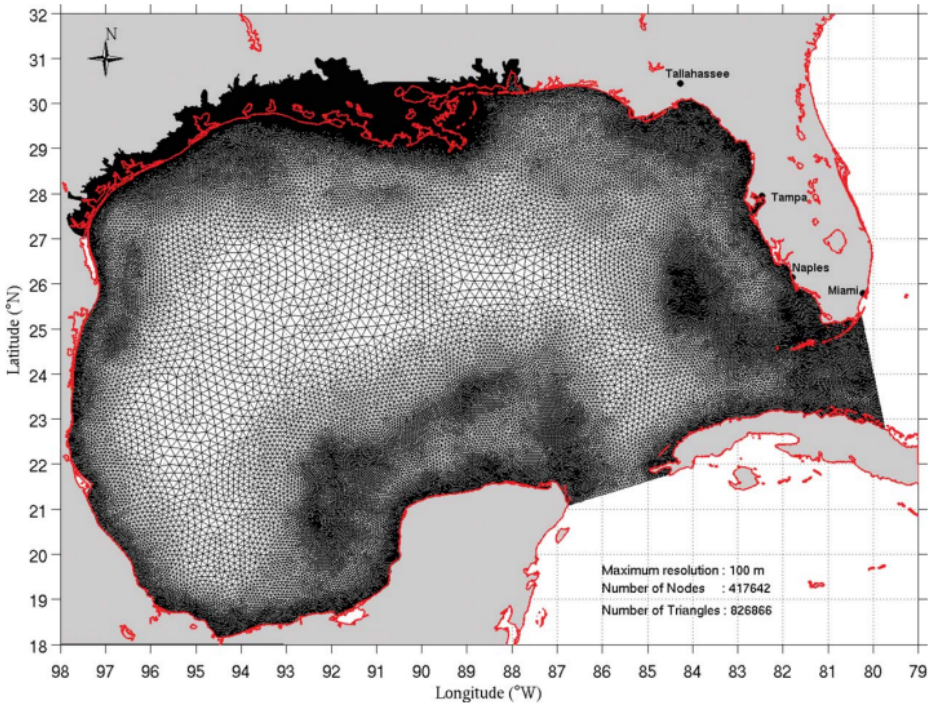

Figure 4.2: Unstructured mesh ULLR, as represented by [35]. The easternmost open sea boundary is the Strait of Florida and the southernmost boundary is the Yucatan Channel.

The model is forced at the open sea boundaries located at the Strait of Florida (segment connecting the coordinates $79.3930°W$ $22.7721°N$ and $80.2665°W$ $25.3130°N$) and the Yucatan Channel (segment connecting the coordinates $86.7685°W$ $21.0826°N$ and $84.5170°W$ $21.7772°N$) by imposing tidal potential functions. The Eastcoast2001 tidal database is used [54] to determine the amplitude and phases of the tidal constituents at these boundaries. The Eastcoast2001 was derived from a 90-day simulation run with the K_1, O_1, Q_1 diurnal and the M_2, S_2, N_2, K_2 semidiurnal astronomical tidal constituents forced on the open ocean boundary ($60°W$ meridian). Eastcoast2001 was validated by comparing the simulation results to the tidal constituents obtained from an harmonic decomposition at 101 tidal elevation stations along the entire model domain. In Appendix B.1, it is shown the comparison between the modelled and the Eastcoast2001 predicted amplitude and phase of the 7 tidal constituents, at the Gulfport Harbour tidal elevation station ($89.0817°W$ $30.3600°N$), at the central coast of Mississippi. The error falls within the 10% for almost all components.

The astronomical tidal constituents considered in the Delft3D model are K_1, O_1, Q_1 (diurnal) and the M_2, S_2, N_2, K_2 (semidiurnal). The amplitude and the phase angle of the constituents are very site specific. By means of a Fortran program developed by [76], it is possible to calculate the amplitude and phase of the tidal constituents at any location covered by the Eastcoast2001 database. In Table 4.1, these characteristics are specified for the Florida Strait and the Yucatan Channel. The time-series of the tide during the time of the arrival of Hurricane Katrina at the middle point of the Florida Strait and the Yucatan Channel are shown in Figure 4.4.

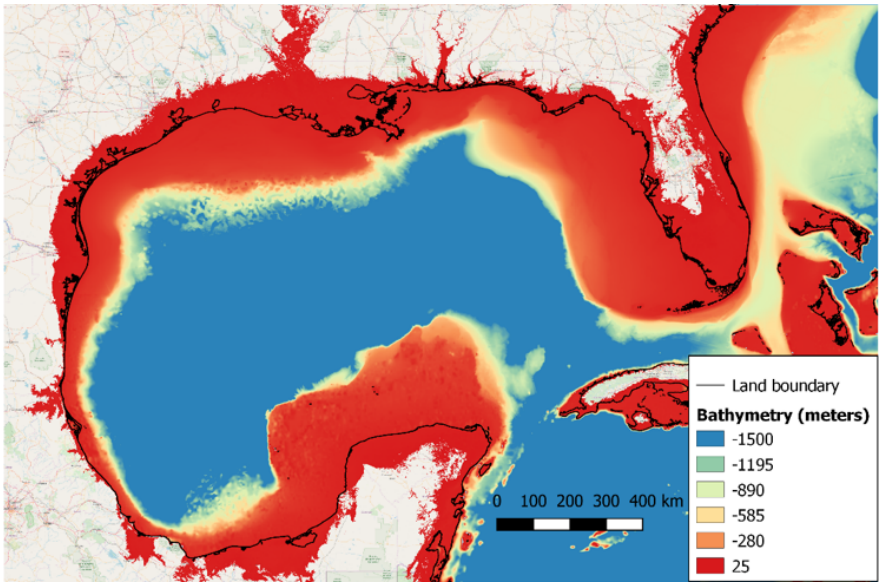

Figure 4.3: Bathymetry and topography of the Gulf of Mexico up to 25 meters above the MSL. Data extracted from GEBCO (2019).

	Yucatan Channel						**Florida Strait**					
	West point		**Middle point**		**East point**		**North point**		**Middle point**		**South point**	
	a (m)	$\phi(°)$	**a (m)**	$\phi(°)$	**a (m)**	$\phi(°)$	**a (m)**	$\phi(°)$	**a (m)**	$\phi(°)$	**a (m)**	$\phi(°)$
Q1	0.0092	19.86	0.0121	5.04	0.0105	346.80	0.0079	308.58	0.0100	359.79	0.0111	9.74
O1	0.0323	40.27	0.0470	19.46	0.0405	354.40	0.0344	311.43	0.0404	13.43	0.0450	22.37
K1	0.0120	51.13	0.0298	10.42	0.0301	322.40	0.0293	278.72	0.0287	9.72	0.0333	18.02
N2	0.0128	91.27	0.0126	5.64	0.0138	91.89	0.0706	4.07	0.0532	2.92	0.0544	17.45
M2	0.0509	100.66	0.0525	89.20	0.0559	96.17	0.3203	21.53	0.2493	22.06	0.2647	33.66
S2	0.0269	45.88	0.0287	95.13	0.0329	52.04	0.0696	47.01	0.0625	52.91	0.0676	70.29
K2	0.0069	11.27	0.0070	52.68	0.0083	25.18	0.0165	51.79	0.0154	56.28	0.0170	74.63

Table 4.1: Amplitude (a) and phase (ϕ) of the seven tidal constituents considered at the open sea boundaries of the model.

A good approximation of the wind drag coefficient consists of using different linear piecewise expressions in function of the velocity, as shown in the parametrization of [47] (Figure 2.14). Explanations on the model of [47] are given in the review of wind drag model included in Chapter 2.2.2.3. An approximation with the linear piecewise function of three points proposed by [73] is used to represent C_d in Delft3D FM (Figure 4.5).

The 2D windfield for Hurricane Katrina is generated by running the Holland model in Matlab. The modified Holland model proposed by [81] is used [34] to generate the 2D wind and pressure fields in Matlab. The hurricane forcing consists of a 2D field that includes three variables: wind speed (W_x, W_y), wind direction (θ) and air pressure at MSL (p). The windfield is given on a polar grid with the center (eye) of the hurricane being the origin of the polar coordinate system. The position of the eye and the associated wind field (spiderweb) varies in time. The shape of the spiderweb is given in Figure 2.8. The grid has a radial resolution of 1 km, and the domain of the radius covers from 1 m to 3,000 km away from the origin. The angular resolution of the spiderweb is $\frac{\pi}{12}$ radians (15 degrees), and the domain of the angle covers from 0 to 2π radians. Note that the reference of the angle heads the north direction on the horizontal plane. Therefore, using (2.4) and Eq. (2.6), the pressure and the wind speed can be computed (Eq. (2.4) and Eq. (2.6)):

$$\begin{cases} W = f(R, \theta) \\ p = f(R, \theta) \end{cases} \tag{4.1}$$

where $[R, \theta] \in [1, 3 \cdot 10^6] \times [0, 2\pi)$. The units of R, θ, W and p are meters, radians, meters per second and

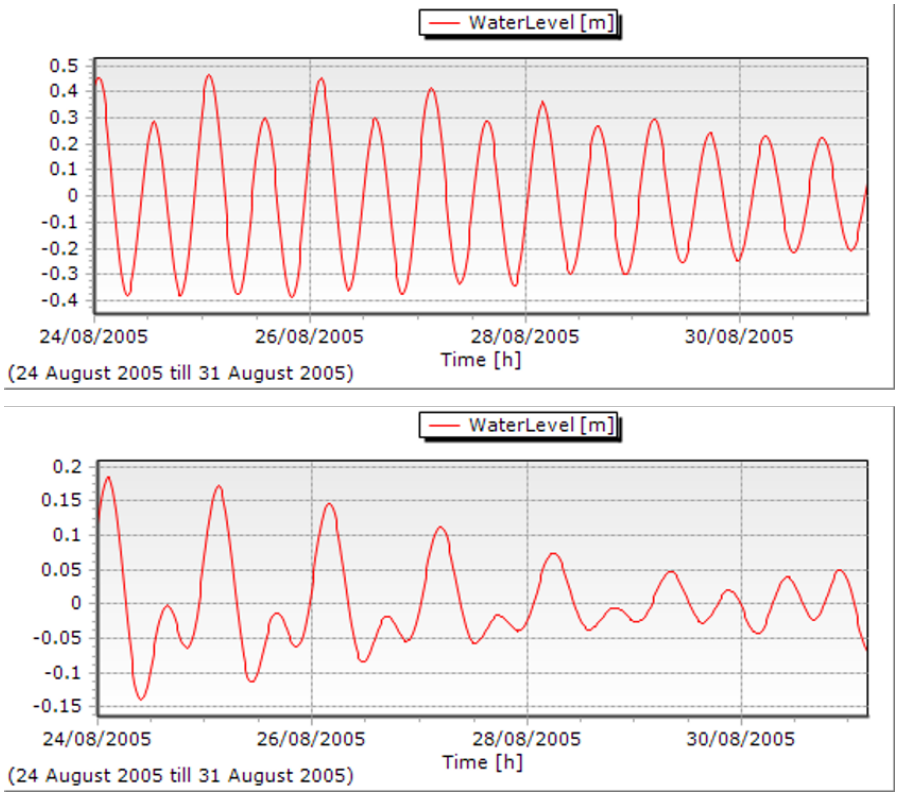

Figure 4.4: Time-series of the tide during the arrival of Hurricane Katrina to the coast of Mississippi (24th to 31st August 2005) at the middle point of the Florida Strait (top) and the Yucatan Channel (bottom), as read by Delft3D FM.

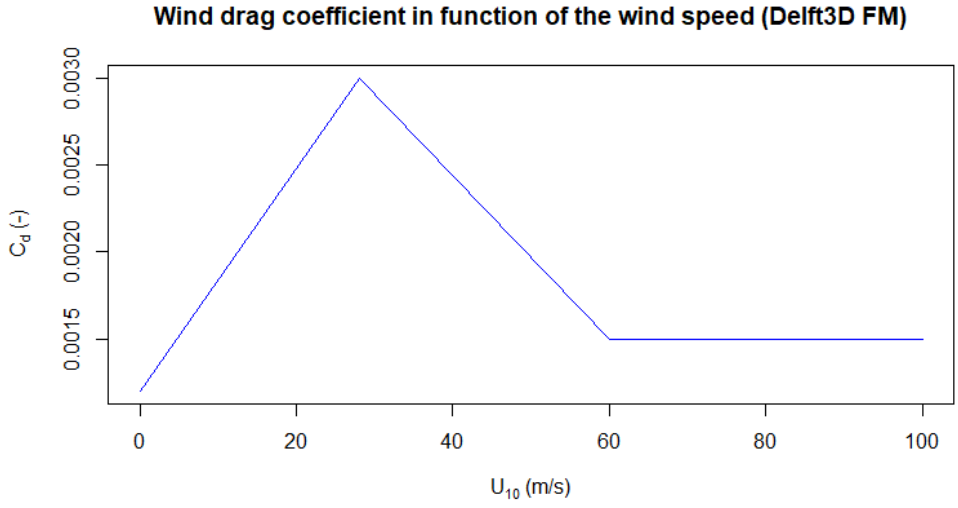

Figure 4.5: Approximation of the wind drag coefficient in Delft3D FM, based on [47].

Pascals, respectively. W can be decomposed in components (x-component heading the east and y-component heading the north in the plane) (Figure 4.6):

$$\begin{cases} W_x = W \sin(\theta) \\ W_y = W \cos(\theta) \end{cases} \tag{4.2}$$

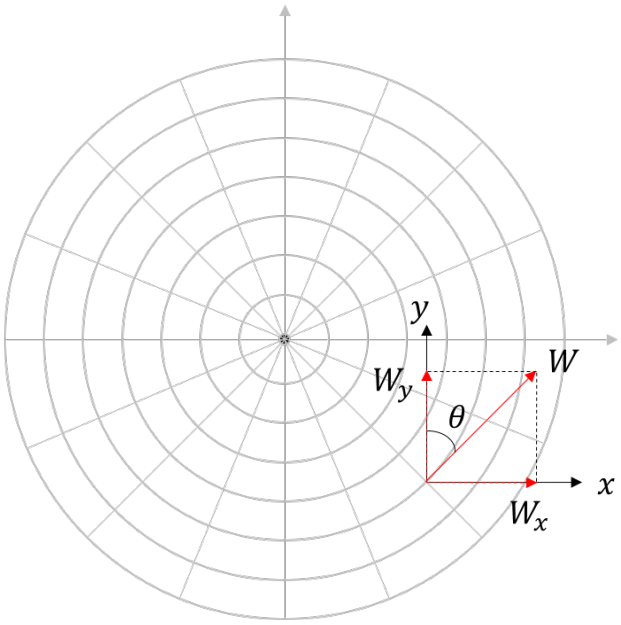

Figure 4.6: Separation of the wind velocity (W) in components in x-direction and y-direction (W_x, W_y) for an arbitrary point of the spiderweb.

The 2D wind and pressure fields for Hurricane Katrina some hours before landfall (29th August of 2005 at 14.45 h) as read by Delft3D FM are shown in Figure 4.7.

The sea bed and topography friction is computed by using the Manning formulation, which applies spatially variable coefficients based on land cover databases [5]. These values have been extracted from the Mississippi Gap Analysis Program (Appendix C). The Manning coefficient varies from 0.025 at the sea to 0.2 in dense forest areas.

4.2.2 Running the model

After defining the input for the hydrodynamic simulation in Delft3D FM for each of the hurricanes of the catalogue, the computation can be executed either using DeltaShell (on Windows) or using batch scripts (on Linux and Windows). If DeltaShell is used, the status of the computation and messages on the execution of the model are visible on a message window. If batch scripts are used, all the messages are written in the diagnostics file (*.dia*). It is possible to run a work in the DeltaShell while running a simulation if batch scripts are used to run the model.

In this project, both approaches have been used. DeltaShell includes an interface for Python Scripting, by which it is possible to set up and execute Delft3D FM models. This tool has been used to run several scenarios in series. On the other hand, batch scripts have been used on Linux to execute works. In this case, the High Performance Computing 11 (HPC11) cluster from the Delft University of Technology has been used to run simulations in 1 node (in series) and 2 nodes (in parallel and in series). This cluster uses the server CentOS7 and has a total of 20 nodes and 400 CPUs. The name of the commandline executable for the model in Linux is *dflowfm*. These executables call libraries that are included in the program files of Delft3D FM to execute the simulations.

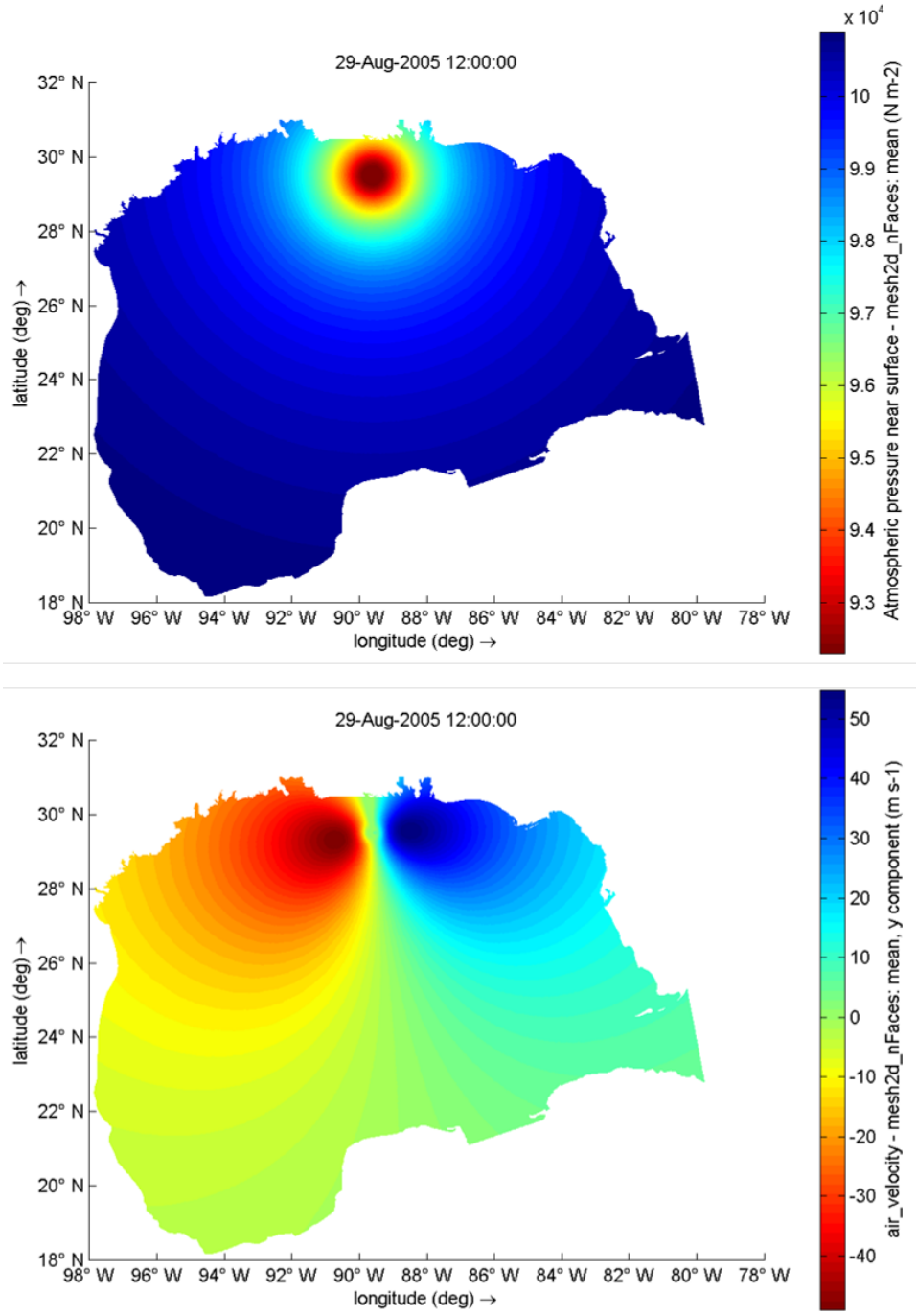

Figure 4.7: 2D visualization of the air pressure (top) and the wind velocities in y-direction (bottom) close when Hurricane Katrina is reaching the coast of Mississippi and Louisiana. Pressures are in Pascals and wind velocities are in meters per second.

4.2.3 Model output

Delft3D FM enables the possibility to write two types of output files: history files and map files. History files include time-series of the different variables at specific locations that can be specified beforehand by implementing *observation points* (manually or by importing a *.csv* file) and map files include time-series of the different

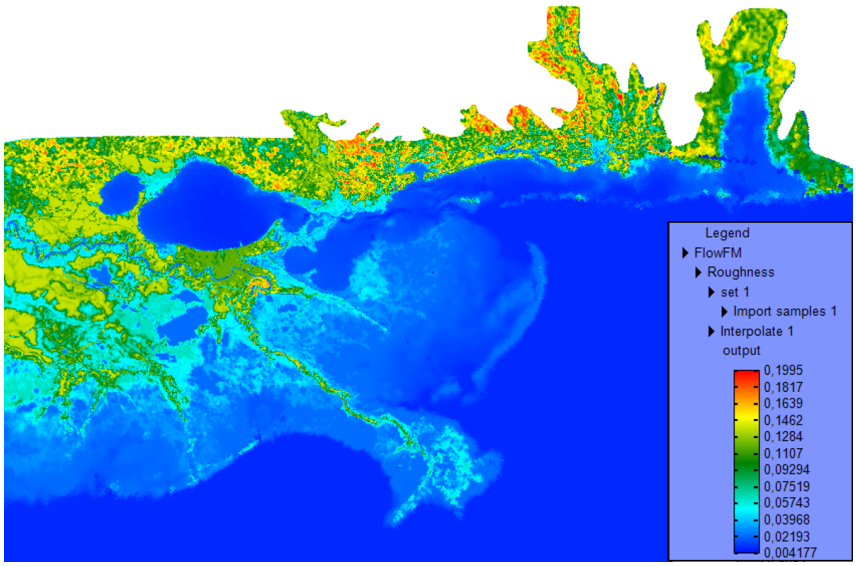

Figure 4.8: Values of the Manning coefficient in the sea and overland domain of Mississippi.

variables for each cell of the unstructured grid. These files are created in *.nc* format, and therefore they can be manipulated with external programming interfaces. In this project, the *.nc* files were treated with R language. The writing time step of the results in history and map files should be proportional to the user time step of the 2D wind field.

For the sake of the computational efficiency, map files are written at a lower frequency than history files (2 hours and 15 minutes, respectively), since they will only used for general visual verification of the results. The development of the 2D fields of water levels and wind can be visualized by means of QUICKPLOT, which is a useful tool that can be opened in Delft3D FM. It is also possible to check the results in the canvas of the DeltaShell, by selecting the desired variable and activating the Time Navigator or in R.

4.3 Wave setup

The water level also rises due to the contribution of waves, which transmit momentum to the water column when they break. During Hurricane Katrina, Mississippi coast experienced relatively small wave breaking induced setup (approximately 0.3 meters, Figure 4.9). The Mississippi coast is located far from the edge of the continental shelf and the bed slope is gentle, what leads to dissipate the energy of the breaking waves before reaching the shoreline.

The barrier islands reduced the wave energy of the offshore waves and dissipated up to 85% of their energy. Behind the barrier islands, there were generated fetch and depth-limited waves that barely reached heights between 2.5 and 3.8 meters along the coast of Mississippi [72]. Therefore, using the plot of Figure 2.5, the wave setup might be between 10% and 14% of this wave height, which is approximately the assumed value of 0.3 meters. This contribution is added to the water levels caused by surge and tide.

The influence of waves can be quantified with hydraulic models such as Delft3D FM or the coupled model SWAN+ADCIRC, as applied in [15], which may require large computational times. Due to the relatively small influence of the waves on the total water levels, it is considered practical to assume a maximum wave setup of 0.3 meters along the coast of Mississippi.

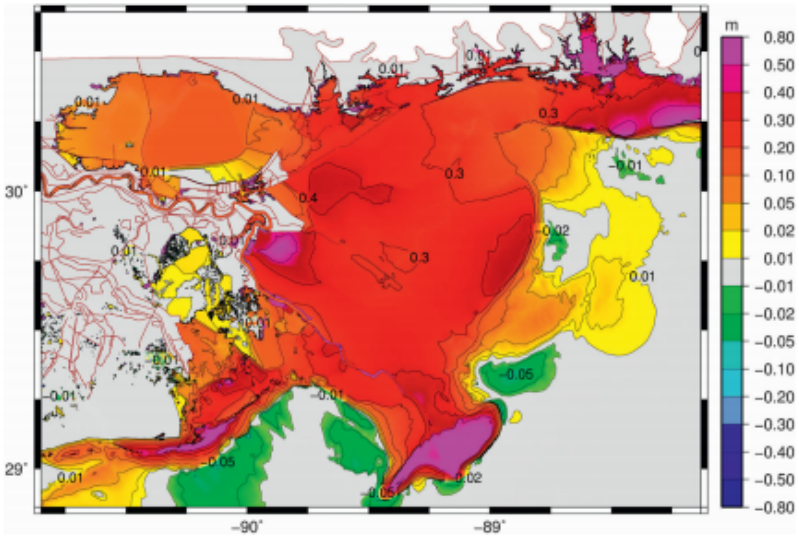

FIG. 16. Effect of waves on the maximum water levels (m) during Hurricane Katrina.

Figure 4.9: Effect of waves on the maximum water levels (m) during Hurricane Katrina [4].

4.4 Validation of the tide

A 37-day tide simulation has been run for a time step of 1 second, by imposing the tidal constituents shown in Table 4.1 at the Yucatan Channel and the Florida Strait. The period of simulation was from the 24th July to the 31st August 2005. The water levels have been recorded at three NOAA tidal elevation stations, for which the predicted tides for the period of Hurricane Katrina are available: Waveland (ID: 8747766; 89.3667°W, 30.2817°N), Gulfport Harbour (ID: 8745557; 89.0817°W, 30.3600°N) and Pascagoula Point (ID: 8741196; 88.5333°W, 30.3400°N). These stations have been chosen for the validation because they are at the western border, the middle and the eastern border of the coast of the Mississippi state, in order to represent the adequate modeling of the tides along the study area. The SI and the Bias of the results at each station are calculated according to Eq. (2.26) and Eq. (2.25) and summarized in Table 4.2.

	Waveland	**Gulfport Harbour**	**Pascagoula**	**Average**
SI	0.389	0.190	0.303	0.294
Bias	-0.246	-0.342	-0.008	-0.199

Table 4.2: SI and Bias of the water levels obtained from the simulation of the tide at Waveland, Gulfport Harbour and Pascagoula.

The low values of the SI (0.19 to 0.39) and the Bias (-0.01 to -0.34) show the good performance of the model to represent the tides at the coast of Mississippi. The slight underestimation of the tide shown by the negative values of the Bias (particularly in Waveland) might be explained by the difficulty to capture fine-scale details of the bathymetry with the 200-meter resolution mesh and the 460-meter resolution bathymetry.

4.5 Validation of the storm tide

The strong wind and high surge that hit the coast of Mississippi during Hurricane Katrina damaged all the NOAA tidal stations present in Mississippi that record the water levels. Consequently, there are not available continuous time-series of the water levels in the coast of Mississippi. However, FEMA and USACE gathered HWMs from buildings, trees and other sites in order record the overland water depths and the flood extent. The HWMs are used to do the validation of the Delft3D FM model.

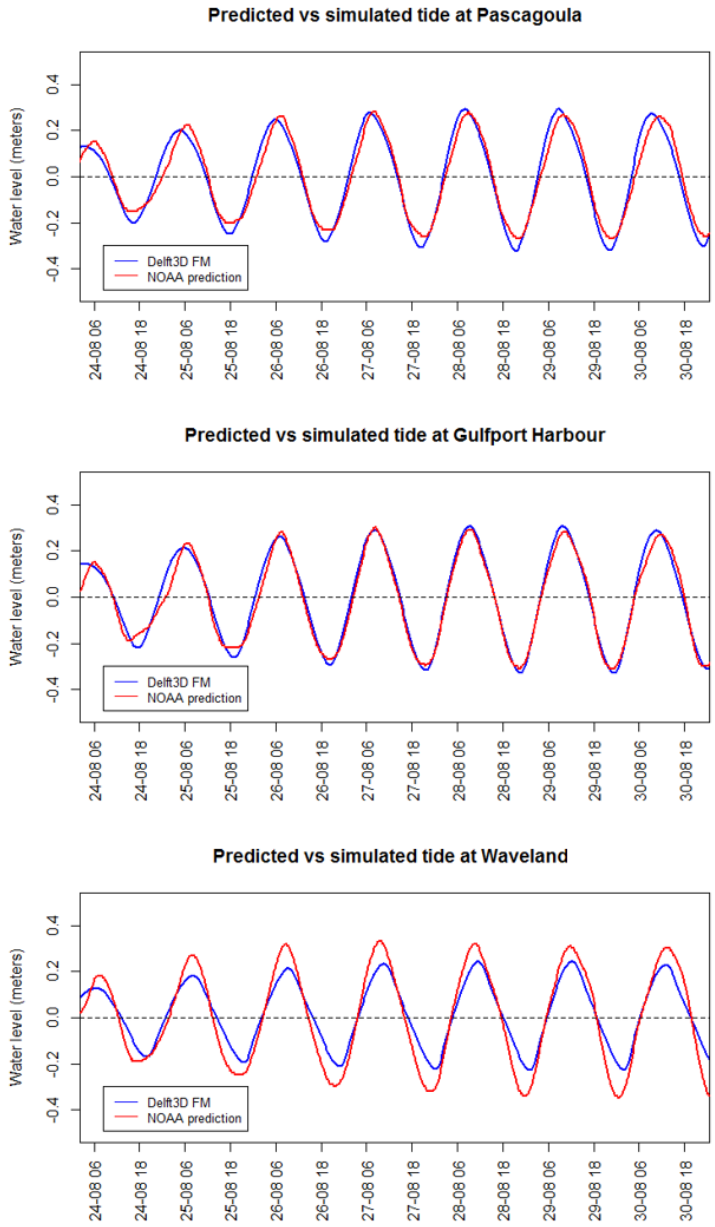

Figure 4.10: Comparison of the predicted tides by NOAA and the simulated tides in Delft3D FM at Pascagoula Point, Gulfport Harbour and Waveland tidal elevation stations, in the coast of Mississippi.

The total water levels achieved during Hurricane Katrina include the surge, the tide and the wave setup. The surge and the tide are simulated together in Delft3D FM, by implementing the input explained in Chapter 4.2.1. The maximum water level of each cell is extracted from the water level time series of every cell, and the wave setup is added to the maximum values. These values, which can be considered simulated HWMs, are compared to the HWMs recorded by FEMA for the coastal areas of the state of Mississippi [79]. The unstructured mesh used for the simulation is too coarse to capture the presence of road levees, such as the Interstate 10 highway. Consequently, only HWMs that are immediately close to the water are considered. A total of 41 HWMs from FEMA have been used for the validation. Figure 4.11 (top) shows a scatter plot comparing the measured and the computed HWMs at the 41 stations and Figure 4.11 (bottom) displays the absolute error for each of the 41 stations considered along the coast of Mississippi.

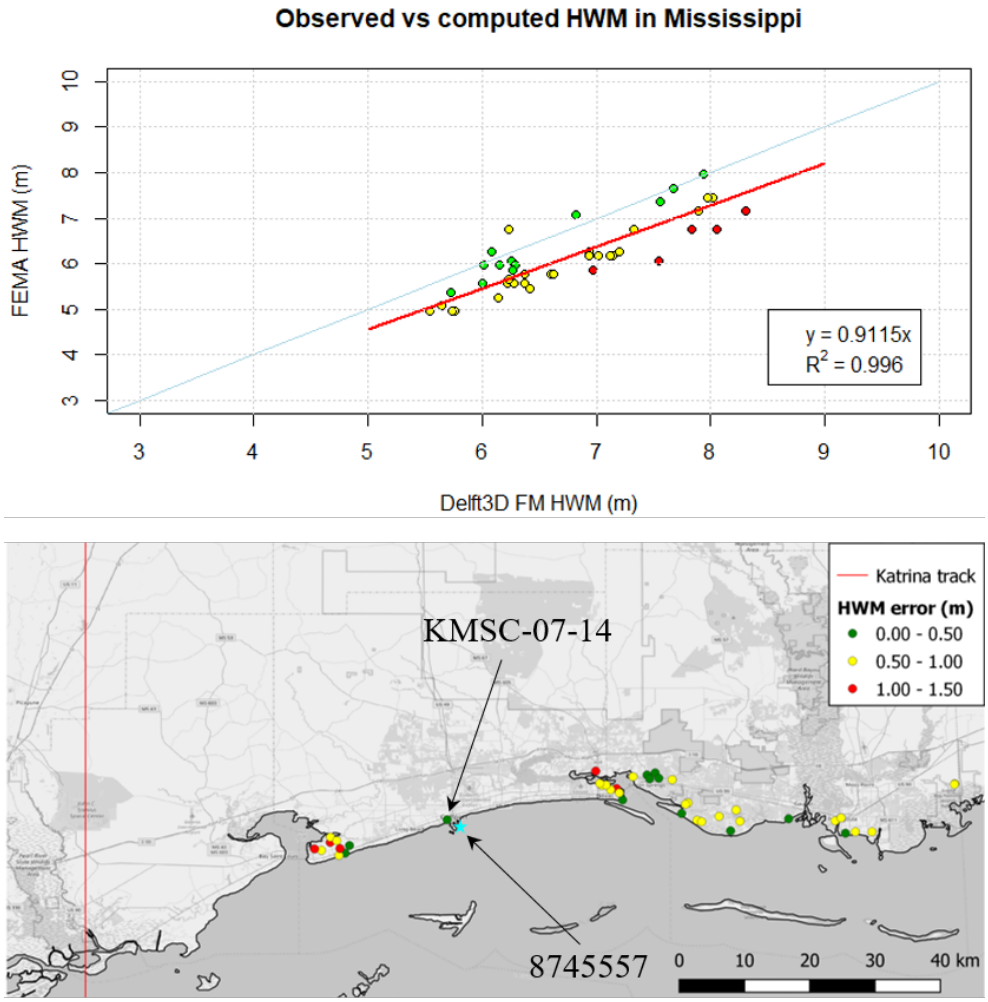

Figure 4.11: Top: Scatter plot showing the comparison between computed and measured HWMs at the 41 FEMA locations. The green circles show a difference between the simulated and the measured water levels lower than 0.5 meters, white circles show differences between 0.5 and 1 meter and red circles show differences of more than 1 meter. Bottom: Error of the simulation at the 41 HWM locations provided by FEMA along the coast of Mississippi. The green circles show a difference between the simulated and the measured water levels lower than 0.5 meters, white circles show differences between 0.5 and 1 meter and red circles show differences of more than 1 meter. The maximum error is 1.48 meters.

The value of the R^2 for a fitted line that passes through the origin is 0.995 and the best fit for the slope is 0.912. The average absolute error is 0.64 meters, which represents an average relative error of 9.5%. These values confirm the reasonably good representation of the phenomena that induces storm tide. The absence of coastal protection structures in the areas where the water levels are recorded facilitates the modelling of nearshore overland flood. The breach of dikes and other structures induce vertical turbulence and other phenomena that adds complexity to the modelling.

Despite the limited error in the estimation of the HWMs, in Figure 4.11 it is observed that the majority of the HWMs obtained in Delft3D FM reach higher values than the HWMs recorded by FEMA. In particular, 28 out of 29 points that have an error larger than 0.5 are overestimating the flood levels. This has an influence on the slope of the fitted line, whose value is smaller than 1.

The main point of interest for this validation is located at the Gulfport Harbour NOAA station (ID: 8745557; $89.0817°W$, $30.3600°N$), since this location will be used to record the surge obtained from the simulations of

the historical hurricane catalogue. These data will be used to feed the Bayesian Network. In Figure 4.12 (top), the values of the simulated storm surge reached at the Gulfport Harbour, the coastal flooding simulated at the station KMSC-07-14 from the FEMA and the HWMs recorded by FEMA at the same station are compared. At the bottom of Figure 4.12, the simulated wind speeds in x and y-directions and the air pressure at MSL at station KMSC-07-14 are represented.

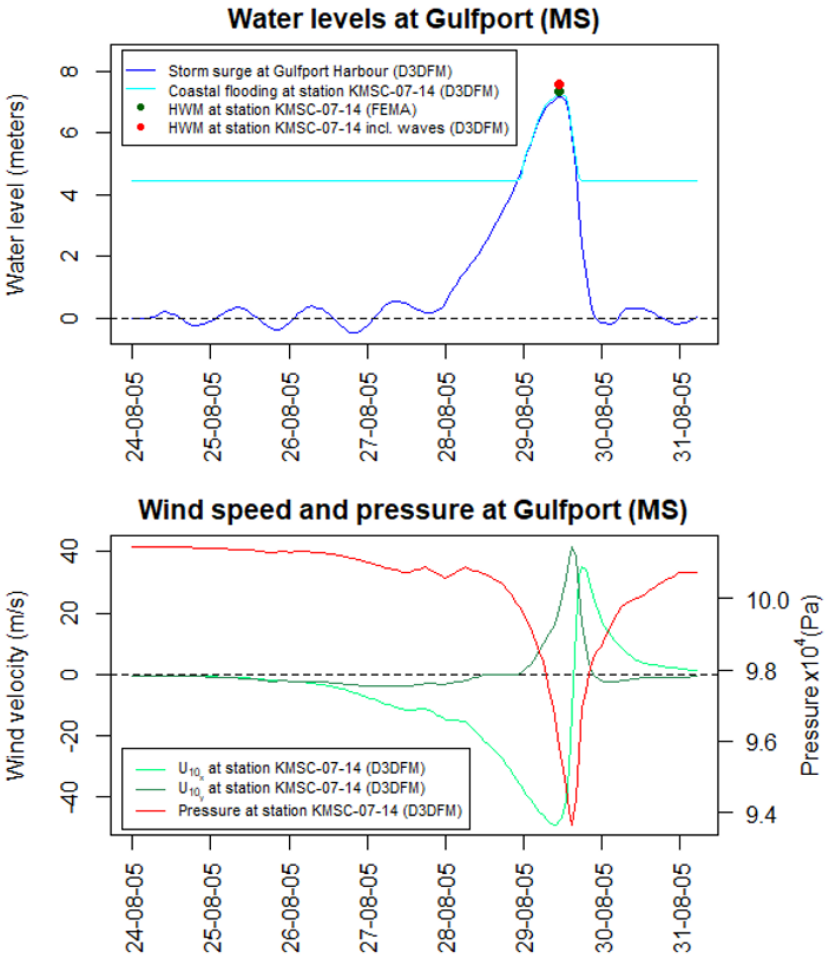

Figure 4.12: Top: Time-series of the variation of the water level during Hurricane Katrina, as simulated in Delft3D FM. Bottom: Time-series of the wind speed in x and y-direction and the air pressure at MSL during Hurricane Katrina, as simulated in Delft3D FM.

The oscillations on the simulated water level (dark blue) shown at the top plot on Figure 4.12 represent the astronomical tide that arrives to the Gulfport Harbour station, before the hurricane makes landfall. When the hurricane approaches the shoreline at the West of Mississippi, the water level increases to a maximum of 7.16 meters + MSL. Adding up the 0.3 meters of wave setup, the maximum water surge level reaches 7.46 meters + MSL. According to the simulation, the station KMSC-07-14 is dry until approximately the moment of landfall. The water level then increases to 7.26 meters + MSL (cyan). The contribution of waves increases this flood level to 7.56 meters + MSL (red dot). As could be expected beforehand, the increase in the Manning roughness when the surge wave passes from the sea to overland leads to a slight increase in the overland water level, due to the transformation of kinetic energy of the wave into potential energy. The HWM recorded by FEMA reaches 7.37 meters + MSL at the KMSC-07-14 station (green dot), which is only 19 centimeters less than the simulated HWM at the same station (relative error of barely 2.5%). Therefore, it is considered that the model that has been set up is skilled to do suitable estimations of water levels in Gulfport Harbour.

CHAPTER 5

Generation of the hurricane data base

The validation of the model guarantees the capability of the model to simulate hurricane events in the region of study and generate accurate storm surge data. The next step in the project is the generation of a storm surge catalogue, by simulating a catalogue of historical hurricanes in Delft3D FM. Ideally, the storm surge catalogue would be extensive, in order to have a long data set to provide the stochastic model with an optimal training. However, there are several challenges that arise at this point. First, the historical catalogue of hurricanes contain a limited number of events that occurred in the domain of study. Second, the computational time required to generate the model input (i.e. the spiderweb) or to run the simulation can be a limiting factor in the number of events considered, due to the time limitation of the project. The purpose of this chapter is to explain the strategies followed to elaborate efficiently a storm surge database by means of a physical model.

5.1 Hurricane selection

The 2D wind and pressure fields can be generated by applying the Holland model to the hurricane best tracks retrieved from the HURDAT2 database, as done for Hurricane Katrina. The HURDAT2 database includes best tracks for 1864 historical events developing in the Atlantic (and Gulf of Mexico) basin of the United States, for the period 1851-2018. Two conditions must be satisfied by the events of the HURDAT2 data base to be selected for the hurricane catalogue of this project:

1. **Hurricane category**: The hurricane must have reached at least Category 1 in the Saffir-Simpson scale at some point of its track. This means that tropical depressions and tropical storms are left out from the catalogue (wind events with maximum speeds lower than 33 m/s). The reason to leave these events out is that they might cause negligible surge, what can introduce noise in the stochastic model.

2. **Number of hurricane best track points**: Only hurricanes that have more than 15 best track points in the HURDAT2 database are considered for the catalogue. In case this number is lower, it is considered that the information of the best track is not sufficiently complete to achieve the desired accuracy in the storm surge simulation.

An observation station has been located in Gulfport Harbour ($89.0817°W$, $30.3600°N$) in order to record the surge caused by each of the hurricanes of the catalogue. This location has been chosen due to its centered position in the coast of Mississippi. Initially, only hurricanes making landfall in a radius of 120 kilometers around Gulfport Habour were considered. This criterion was established considering the average swath of hurricane intensities in hurricane events, which is 240 kilometers according to [39]. From the 1864 historical events in the HURDAT2 database, only 371 reach the category of hurricane. From this amount, 356 have at least 15 hurricane best track points. Out of the 356, only 22 hurricanes made landfall in the mentioned 240-kilometer alongshore region. In Appendix E, the landfall domain and the hurricane tracks of the 22 hurricanes that fall in the region are shown.

A sample of 22 hurricanes is small to train a stochastic model. As a result, the sample should be increased. A new bounding box of 600 kilometers alongshore (300 kilometers at each side of Gulfport Harbour) was considered. The domain of the new bounding box is (Eq. (5.1)):

$$\begin{cases} long \in [-91.795, -86.405] \\ lat \in [28.500, 31.000] \end{cases} \tag{5.1}$$

There are 48 hurricanes falling in the new bounding box, which is still a low number of hurricanes for the training of a stochastic model. To increase further the number of hurricanes of the catalogue, the tracks of the hurricanes satisfying a condition imposed on the angle (forward direction of the hurricane) at landfall in the Gulf of Mexico are shifted inside the bounding box. The range of angles of the hurricanes making landfall in the bounding box varies from 201.84° to 349.30°, considering an axis pointing to the East as reference and the increase of the angle in clockwise direction. Hence, the hurricanes that make landfall outside the bounding box but whose angle at landfall is within the specified domain are shifted inside the bounding box. There are 92 hurricanes satisfying the condition on the angle at landfall. This elevates the number of hurricanes for the catalogue to 140 events, which is already an acceptable number to train the Bayesian Network.

To shift the tracks of the hurricanes making landfall outside the bounding box it is followed a specific procedure. To start, it is generated a simplified coastline that represents the coastline within the bounding box. To do so, it is created a shapefile of lines in QGIS, which is divided into segments of 500 meters (*v.split* using the GRASS toolbox). The vertices of the segments of the line are extracted, generating a shapefile of points. Subsequently, it is assigned to each hurricane a random point from the extracted vertices in which the simplified coastline is divided (in this case, the total number of points was 1146), considering that landfall locations to the west and to the east of Gulfport Harbour are assigned alternatively, in order to have the same number of hurricanes making landfall at both sides of the observation station (this is applied only to the shifted hurricanes). The coordinates of each point can be extracted by using the raster calculator in QGIS. Subsequently, it is assigned one random point of the simplified shoreline to each of the 140 hurricanes. Moreover, the landfall coordinates of each hurricane are known, since they are given in the best track. Consequently, if the hurricane must make landfall in the point assigned, all the points of the historical hurricane must be shifted a distance (in degrees):

$$\begin{cases} \Delta x = lon_{point} - lon_{hur,real} \\ \Delta y = lat_{point} - lat_{hur,real} \end{cases} \tag{5.2}$$

where lon_{point} and lat_{point} are the longitude and the latitude of the random point assigned to a historical hurricane at the simplified coastline, and $lon_{hur,real}$ and $lat_{hur,real}$ are the longitude and the latitude of the landfall location of the hurricane. In Figure 5.1, there are shown the original tracks of the hurricanes of the HURDAT2 database (top) and the tracks of the hurricanes after being shifted to the specified bounding box (bottom).

As mentioned in Chapter 2.2.1.2, the minimum pressure in the hurricane eye (p_c) is only available since 1979. p_c is needed to generate the wind and pressure spiderwebs by means of the Holland model. For the hurricanes occurring prior to 1979, p_c can be calculated in function of the maximum sustained wind at 10 meters above the MSL (Eq. (2.11)), which is equal to the cyclostrophic wind. It is recalled that in the radius of maximum winds the Coriollis force is small with respect to the pressure gradient and the centrifugal forces and the air is in cyclostrophic balance (the geostrophic component of the wind is negligible). After applying this expression, the Holland model can be used to generate the spiderwebs for each of the hurricanes. In order to gain efficiency in the spiderweb generation, it is developed a Matlab script that can run the Holland model for n iterations. It is noted that Delft3D FM do not read spiderwebs dated prior to 1900. To solve this issue, 200 years have been added to the hurricanes occurring before 1900 before running the Holland model to generate the spiderwebs of each hurricane.

5.2 Simulation of the selected hurricanes

Since the interest lies strictly on estimating storm surge, neither wave setup nor tides are included in the simulation of the hurricane catalogue. As mentioned before, tides and wave setup were included in Katrina just for the sake of validation. Therefore, the initial and boundary conditions on water levels are 0 for all the simulated hurricanes (the boundary and initial conditions do not change from hurricane to hurricane). This is specified by imposing an astronomic tide with just the constant tidal constituent $A_0 = 0$ at the open sea boundaries of the model. The rest of the parameters of the model that have been calibrated in the validation remain the same for all the simulated hurricanes, except for the spiderweb, which is different for each hurricane. The reference time, the start time and the end time of the simulation also change for the simulation of each historical hurricane.

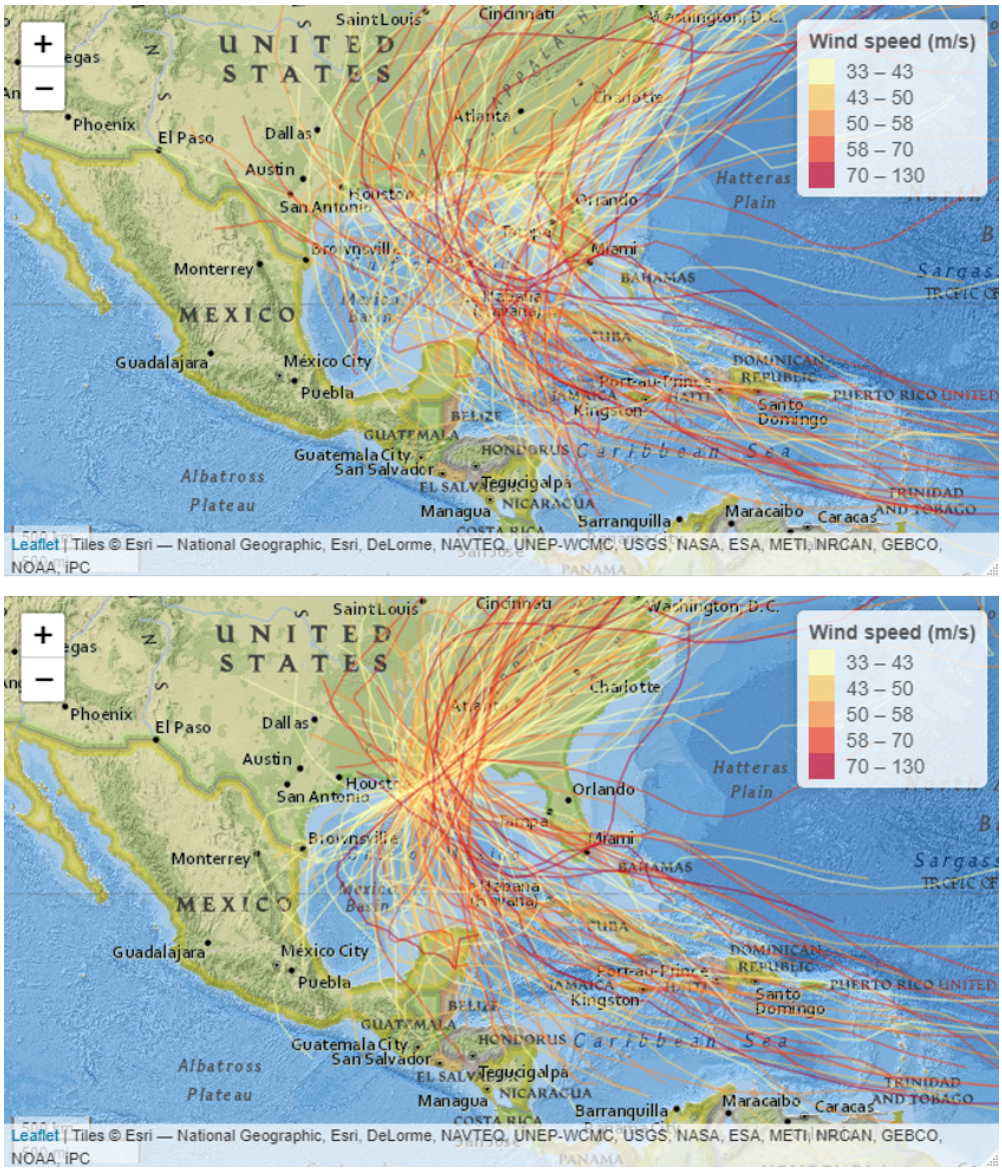

Figure 5.1: Original tracks of the hurricanes of the HURDAT2 database (top) and tracks of the hurricanes after being shifted to the location of study (bottom). The color of the tracks indicate the intensity reached along the lifetime of each hurricane.

The spiderweb file (*.spw*) is called by means of the external forcing file (*.ext*), which in turn is called by the Flow FM model file (*.mdu*). The information regarding the dates is included in the *.mdu*. When running the hurricane catalogue in batch, the *.ext* and the *.mdu* files have been generated in R beforehand, together with the *.sh*, which are the Linux shell executable files to run each hurricane simulation. When using the Python Scripting tool in the DeltaShell interface, the *.mdu* and *.ext* files are overwritten at each iteration with the information of the hurricane entering the loop.

5.3 Analysis of the results of the simulations

To check that the results of the simulations are reasonable, it is plotted the storm surge, the wind speed and the pressure drop recorded at the location of the tidal station in function of time. In the following paragraphs, the results for two random simulated hurricanes are analyzed.

- **Hurricane Cindy (AL032005, 2005)**: Hurricane Cindy approached the shoreline of Louisiana in a slight oblique direction to the coast, passing over the Mississippi Delta before making landfall in the Mississippi State. The maximum value of the simulated surge during Hurricane Cindy is 2.53 meters (Figure 5.2, top). This is approximately the value that was reached in reality which was 5.5 feet above the normal tidal level [74]. Considering a tide normal tide of 1 feet and wave setup of 1 feet (as seen in the validation)), the actual value of the water level might have reached 8 feet (2.44 meter). As seen in Figure 5.2 (top), the track of the hurricane (red) passed by the East of the recording station (yellow). In Figure 5.2 (bottom), the plot shows a pressure drop of approximately 18 hPa with respect to the normal atmospheric pressure (1015 hPa) that practically coincides in time with the maximum surge.

  The x and y-components of the wind speed are 0 at the start of the simulation because the only wind-field in the domain of study considered in the simulation is the spiderweb. For the same reason, both components also converge to 0 when the hurricane moves away from the observation point (Figure 5.2, bottom). The x-component of the wind speed is negative when the hurricane approaches the coast, but it becomes positive when the hurricane progresses further from the longitude of the observation station. Due to the Coriollis force, the swirling winds rotate in counterclockwise direction in the Northern hemisphere. Accordingly, when the hurricane is heading the North and right before making landfall, a station located to the North with respect to the hurricane eye feels strong winds with x-component heading the West. Similarly, right after the eye of the hurricane passes through the location of the station, the x-component of the wind recorded at the station will head the East.

  The counterclockwise direction of the swirling wind due to the Coriollis force also explains the behavior of the y-component of the windspeed. In this case, the hurricane passes by the West side of the observation station and then moves obliquely to the East. Because of this movement, initially the y-component of the wind becomes positive, but once it leaves the station behind, it becomes negative. This negative wind speed in y-direction pushes the water offshore, causing slightly negative water levels after the hurricane passes through the observation point (Figure 5.2, bottom).

- **Hurricane AL021950 (1950)**: This case is differentiated from the Hurricane Cindy in the behavior of the y-component of the wind speed (Figure 5.3, bottom). Due to the perpendicular approach of the hurricane to the coastline, the hurricane arrives to the shore and moves away from eat by the same side of the observation station. Consequently, the sign of the y-component of the wind speed does not vary. Since the hurricane is moving to the East of the observation station, the station undergoes North-South winds along the whole duration of the event, this is, the sign of the y-component of the wind speed is negative. Due to the fact that the hurricane made landfall to the East of the observation point, the storm surge recorded at the observation station and the regions of West Mississippi and Louisiana was lower than at the coast of Alabama and Florida.

5.4 Data set for the training and validation of the Bayesian Network

Five hurricane variables are considered in the Bayesian Network: forward speed and forward direction of the hurricane (Eq. (2.1) and Eq. (2.2), denoted as FS and FD respectively), maximum sustained wind speed (WS), distance from landfall location to a reference point located at the Galveston Bay (LF) and maximum storm surge level (SS). The values of the first three variables are taken at landfall. FD and FS are calculated when generating the spiderwebs, by using the difference in position and time between consecutive best track points 6 hours before landfall. WS is given directly in the hurricane best track data. The maximum storm surge for each hurricane at Gulfport Harbour is obtained from the simulations in Delft3D FM. It is noted that the radius of the hurricane is not used in the stochastic model due to the reduced number of hurricanes in the catalogue including this variable (this variable is only included in the best tracks since 2004).

To calculate the distance between the landfall location and Galveston Bay (LF), it is used the simplified coastline created beforehandto assign random landfall locations to hurricanes that originally made landfall outside the defined bounding box. Since the random points of the simplified coastline were already assigned to shift the historical hurricanes, the landfall position of each hurricane is known. The ID of the points of the simplified coastline are in ascending order along the line (from West to East) and the segments between points measure 500 meters. Hence, it is possible to calculate the distance between each point and Galveston Bay by calculating the distance along the lines in QGIS or R (Figure 5.4).

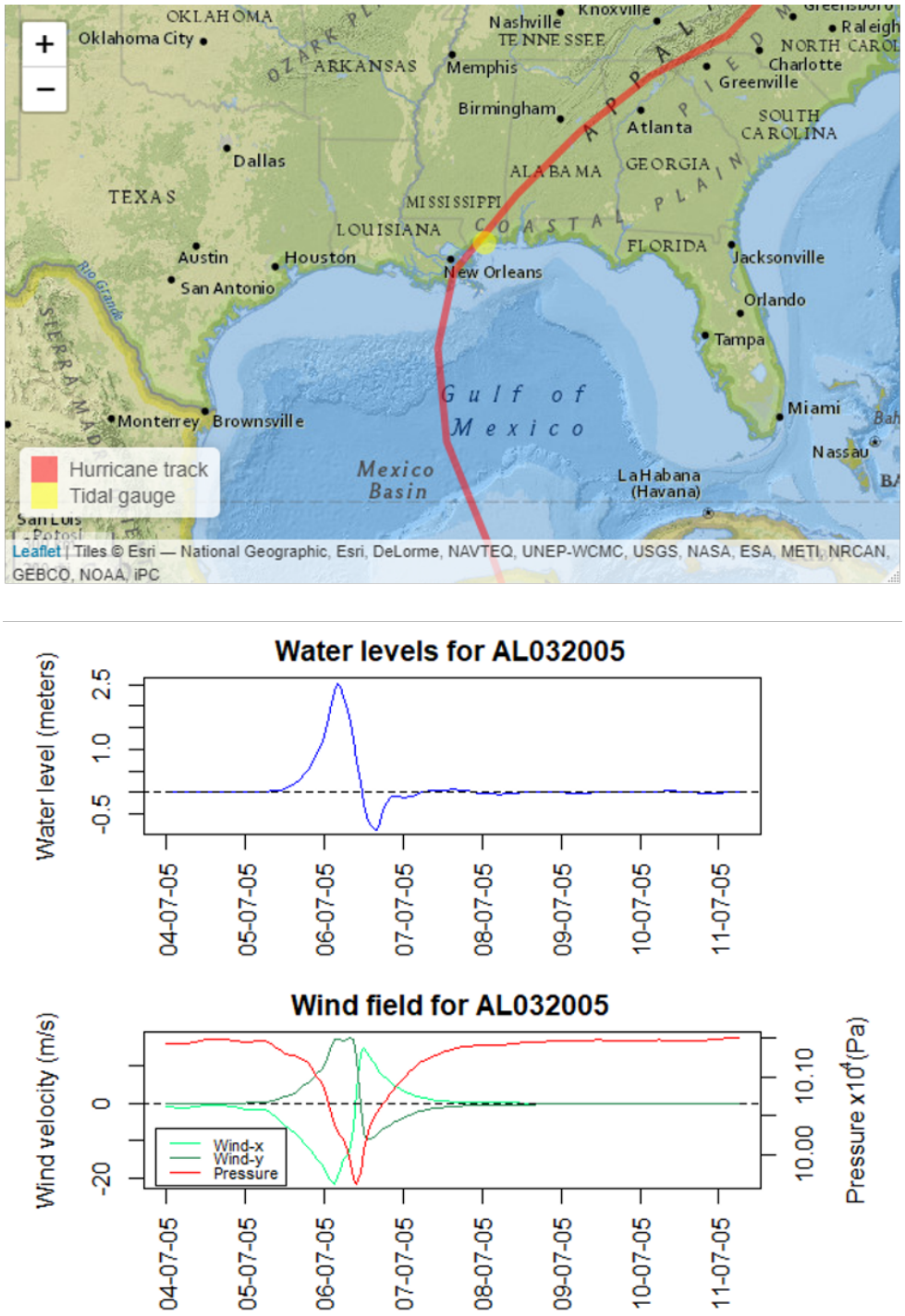

Figure 5.2: Top: Track of the Hurricane Cindy (2005) and observation point (in yellow) at Gulfport Harbour, where surge, wind speed and pressure is recorded during the simulation. Bottom: Storm surge, wind speed in x-direction, wind speed in y-direction and air pressure registered in Gulfport Harbour during the simulation of Hurricane Cindy (2005).

The data set generated consists of 140 hurricanes, each of them characterized by the 5 hurricane variables: WS, FD, FS, LF and SS. In Figure 5.5, it is shown the histogram of each of the variables of interest mentioned. Table 5.1 gives the range of values, the mean and the standard deviation of the hurricane variables.

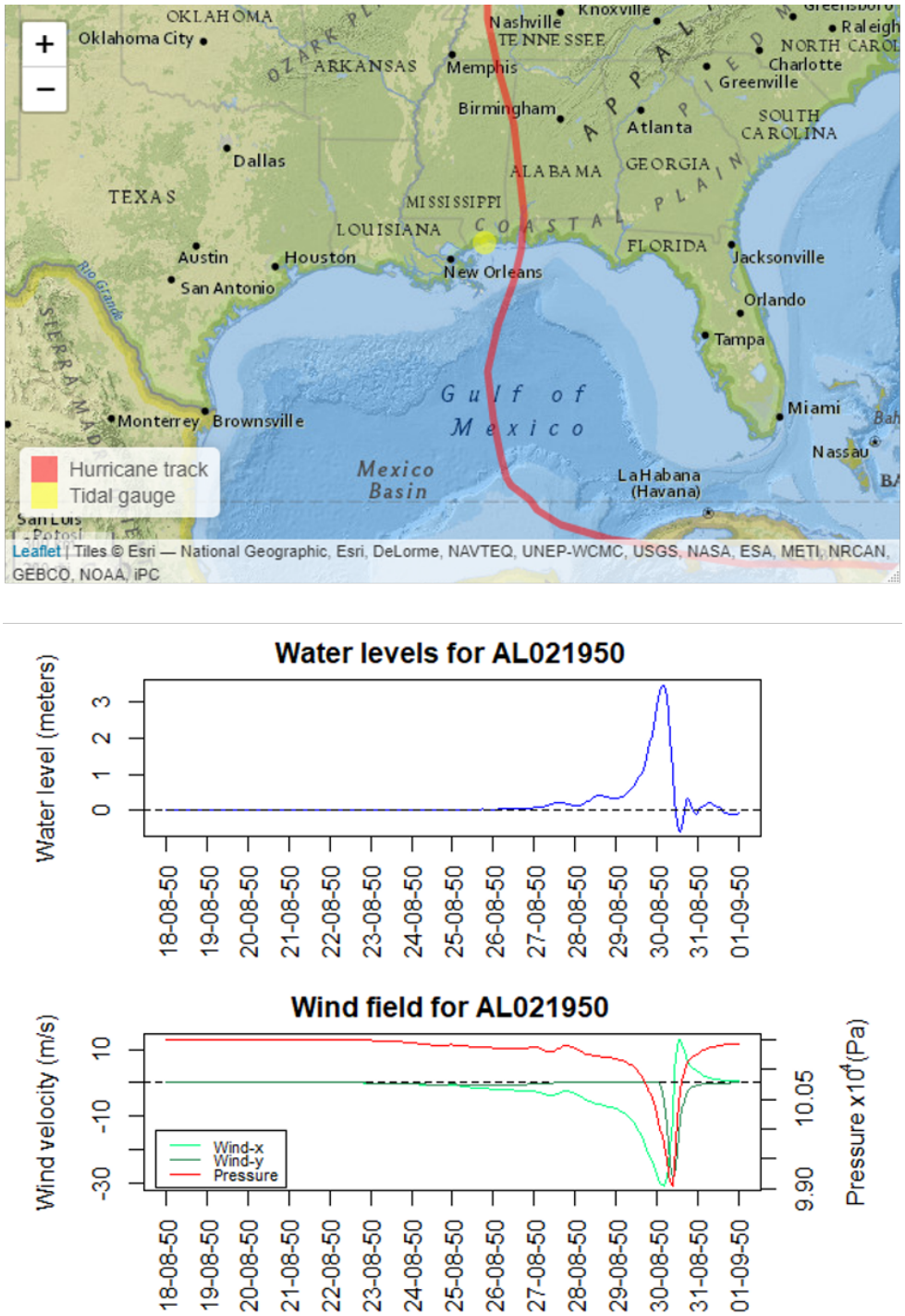

Figure 5.3: Top: Track of the Hurricane AL0121950 (1950) and observation point (in yellow) at Gulfport Harbour. Bottom: Storm surge, wind speed in x-direction, wind speed in y-direction and air pressure registered in Gulfport Harbour during the simulation of Hurricane AL021950 (1950).

The range of values observed for all the variables are reasonable. The values for the wind speed start from 65 km/h, which is the case for hurricanes which achieved higher intensities in deep waters and weakened when they approached the coast. The maximum values on the data base reach approximately 280 km/h, which correspond

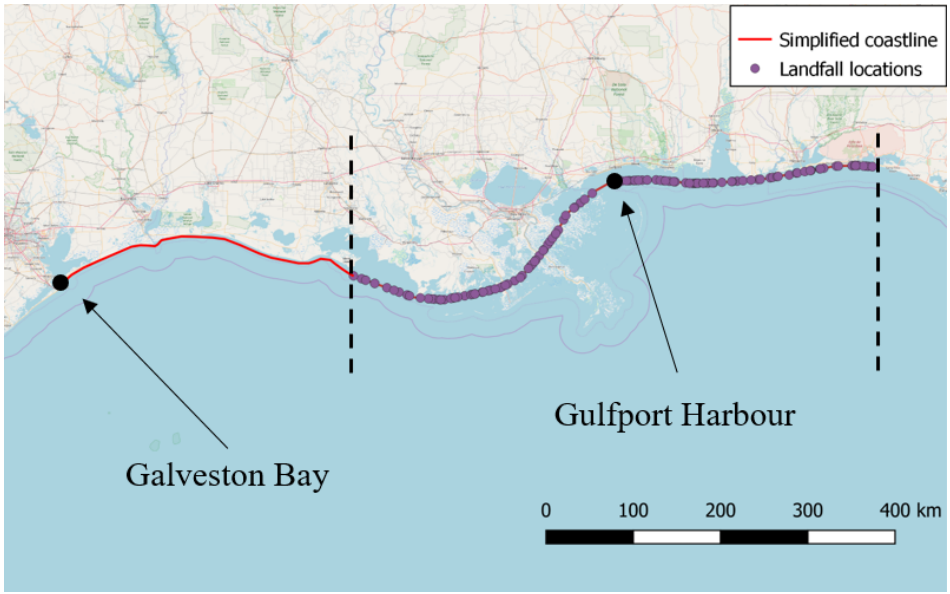

Figure 5.4: Representation of the simplified coastline and landfall location of the hurricanes of the catalogue. The dashed lines represent the western and eastern edges of the bounding box.

	Units	Range	Mean	Standard deviation
Wind Speed (WS)	[km/h]	64.76-277.56	147.11	39.57
Forward Direction (FD)	[degrees]	201.80-348.69	280.17	40.32
Forward Speed (FS)	[km/h]	7.87-61.42	24.86	12.08
Landfall Distance (LF)	[km]	347.46-915.46	635.86	164.64
Maximum Surge (SS)	[m]	0.03-7.52	3.11	1.62

Table 5.1: Range, mean and standard deviations of the hurricane variables used in the stochastic model.

to Category 5 hurricanes in the Saffir-Simpson scale. The histogram shown in Figure 5.5 shows that the majority of the hurricanes reach maximum wind speeds up to 200 km/h, meaning that the Hurricanes up to Category 3 are the most common in the data base.

The restriction in the angle of landfall impose a condition to the values of the forward direction of the hurricane at landfall beforehand, being this angle in the range 202° to 349°. The histogram of the FD (Figure 5.5) shows that the most repeated values are around 300° although the average value is 280°.

The Hurricane Research Division from [59] analyzed the forward speed of the hurricanes of the HURDAT database based on the latitude. The average forward speed for latitudes between 25° and 30° was 20.1 km/h and between 30° and 35° was 27.1 km/h. The average forward speed of the hurricanes of the data base for this project is 24.86 km/h (Table 5.1), which falls in the range of the values obtained in the NOAA analysis. The histogram shown in Figure 5.5 shows that the most common values for FS are in the range from 10 km/h to 30 km/h.

Due to the alternative assignment of landfall locations to the shifted hurricanes to each side of the Gulfport Harbour, the distribution of the landfall location shown in Figure 5.5 is quite uniform between 350 km and 950 kilometers. The average value of the landfall location is 636 kilometers from the Galveston Bay, which is close to the center of the bounding box (669 kilometers from Galveston Bay, along the simplified coastline).

Finally, the storm surge values that result from the simulations in Delft3D FM present an average in 3.11 meters + MSL (Table 5.1), which is a reasonable value considering that only those events that reached the category of hurricane were considered in the simulations.

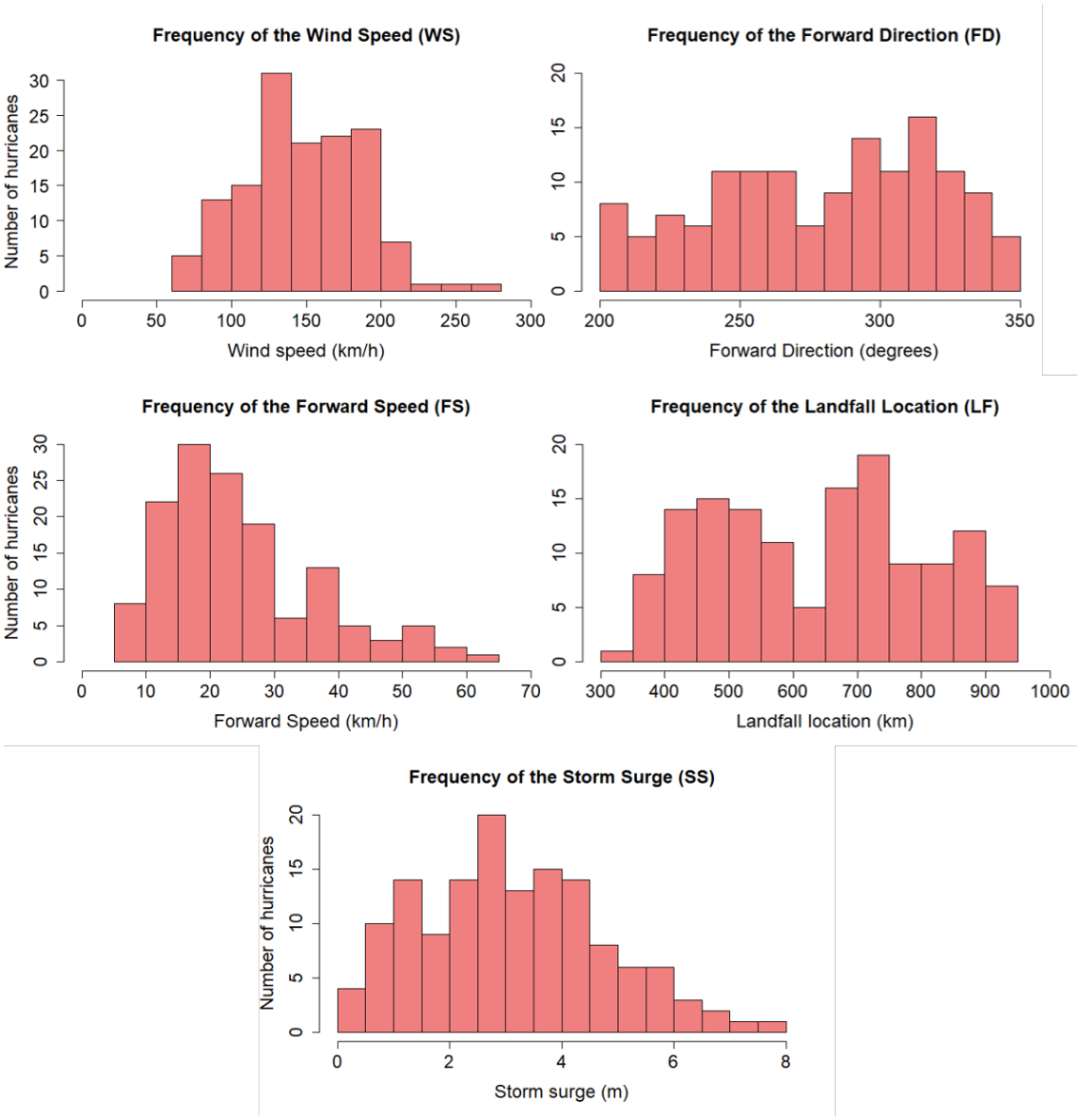

Figure 5.5: Histograms of the variables of interest considered in the stochastic model.

CHAPTER 6

Stochastic model setup and validation

In recent times, stochastic models have been under extensive research to solve hydraulic engineering problems, especially due to the fast speed of computation of these models compared to computational modelling. Moreover, the statistics skip any complex process that might be behind a physical phenomenon, since the solution can be approached by just analyzing data and recognizing the dependencies between variables and the patterns that the data sets follow. However, as in the current case, a physical model is necessary to generate part of the data set to train the stochastic model, since part of the data might not be available.

The identification of the dependencies among the different hurricane variables has two main interests. On the one hand, it enables the fast prediction of the hurricane parameters in a span of seconds. The immediacy in the forecast enables the application of emergency measures in case a hurricane approaches a specific area. On the other hand, it enables the generation of a synthetic hurricane catalogue linked to probabilities of occurrence, by inferring different combinations of hurricane parameters.

In this chapter, it is analyzed the dependence among the hurricane parameters discussed in the previous chapter, which are the wind speed, the forward speed and the forward direction of the hurricane, the landfall location and the maximum storm surge. With the information of 140 hurricanes, it is built a Bayesian Network based on the model of [71] to estimate hurricane variables in Mississippi. These results are validated, by inferring the hurricane variables of several events and comparing the results to the Delft3D FM output. To do so, the hurricane data set is divided into a training data set comprising 85% of the data (119 storms) and a testing data set comprising 15% of the data (21 storms). The storms that take part of the training and the testing data set have been selected randomly.

6.1 Bayesian Network developed by [71] to estimate storm surge levels

The assessment of the dependencies among hurricane variables can be done by pairs. In this project, bivariate copulas are used to model the dependence between pairs of variables. This mathematical entity enables the calculation of the joint probability of two variables. However, it might occur that more variables are involved in the dependence relationships. In such a case, the probability of one variable might be conditioned on one or more other variables and those, in turn, being conditioned by other variables. This increase in the degree of complexity of the structure leads to the construction of larger entities. One of the methods to solve this type of problems are the Bayesian Networks (BN). BN are used to calculate the conditional probability of one parameter by applying the Bayes Theorem on a predefined network, which is formed by nodes that are interrelated by arcs. For further information about the principles of a BN, it is referred to Section 2.2.4.1.

The BN constructed by [71] is used as a reference in this project (Figure 6.1), given the similarity of the case. In [71], a BN based on Gaussian copulas is applied to calculate the boundary conditions for hurricane flood risk analysis in the Galveston Bay (Texas, US). The variables considered in the BN are the wind speed, the forward speed and the forward direction of the hurricane, the radius of maximum winds, the landfall location, the precipitation and the storm surge. It is noted that in the present project the precipitation and the radius to

maximum winds of the hurricane are not considered in the BN. The reason for not considering precipitation is that in this project it is desired to assess exclusively storm surge. The radius of the hurricane is not considered because no data is available before 2004 regarding the hurricane size, what makes this variable poorly defined, given the short number of events occurring after 2004 in the hurricane database.

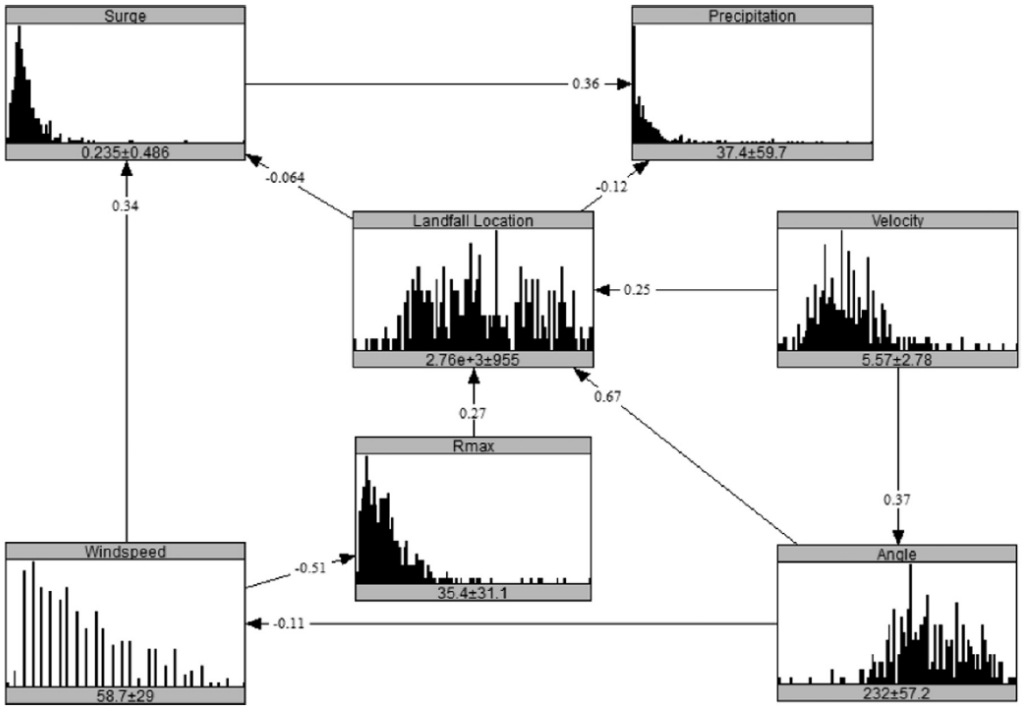

Figure 6.1: BN built by [71] used for the modeling of the hydraulic boundary conditions for hurricane flood risk analysis at the Galveston Bay (Gulf of Mexico).

The construction of the model shown in Figure 6.1 followed a process of optimization and validation. First, it was created a database of hurricanes and their features for the region of the Gulf of Mexico. The hurricanes that made landfall in the coast of the Gulf of Mexico were selected from the IBTrACS database. Then, it was found the intersection between the tracks and a simplified coastline in order to determine a landfall location. The tracks of the hurricane included information relative to the wind speed, the radius of maximum winds and the coordinates of every track point. The forward direction and the forward speed were calculated with the coordinates of the track for each time step. Every cyclone had assigned these variables for typically six hours before the landfall.

It is noted that the axis pointing to the east is taken as reference to calculate the forward direction of the hurricane, which is the angle between the eastwards axis and the vector of the forward speed of the hurricane. The reference to calculate the distance to landfall is Cancun (Mexico). The distance to landfall is calculated as the distance between Cancun and the landfall location, following a generated simplified coastline.

The storm surge levels were obtained from tidal gauges located at the entrance of the Galveston Bay, which had available predicted water levels at an hourly frequency. The maximum water level per day was calculated by subtracting from the result the sea level rise. For each of the storms making landfall at the coast of the Gulf of Mexico, the maximum water level at +/- 48 hours surrounding landfall was taken for the data set.

The third step in the process was the calculation of the average daily precipitation, for which six rainfall gauges from the National Climatic Data Center (NCDC) surrounding the Clear Creek Watershed (Galveston Bay) were used. To do so, it was used the Thiessen polygon method to spatially average the rainfall over the Galveston area. The precipitation for each of the events was quantified as the five-day cumulative precipitation surrounding the date of the hurricane landfall. The decision on a five-day accumulation of precipitation is because in

previous studies it was determined that the 90% of the total cumulative rainfall occurs during the first 72 hours after landfall, when analyzed over a 10-day period.

Subsequently, the dependencies among hurricane variables were analyzed by means of copulas and a non-parametric BN was built and validated. Given the advantages in computational efficiency offered by Gaussian copulas, it was queried the use of these type of copulas by comparing the goodness of fit to the data to Gaussian, Gumbel and Clayton copulas. To do this comparison, the semicorrelations among hurricane variables and the Cramer-von-Mises statistic for the Gaussian, Clayton and Gumbel copula were calculated (Table 6.1). The conclusion that followed was that the Gaussian copula can represent an acceptable approximation of the dependencies among the variables of the BN, because of the relatively low value of the Cramer-von-Mises statistic and the similar semicorrelation values for many of the variable combinations.

		ρ	$\rho_{\mathbf{SW}}$	$\rho_{\mathbf{NE}}$	$\rho_{\mathbf{SE}}$	$\rho_{\mathbf{NW}}$	$\mathbf{CM_{Gauss}}$	$\mathbf{CM_{Clayton}}$	$\mathbf{CM_{Gumbel}}$
WS	**FD**	**-0.11**	-0.06	-0.35	**0.14**	**0.16**	**0.31**	0.43	0.44
WS	**SS**	**0.36**	**-0.07**	**0.31**	0.12	0.28	0.41	0.91	**0.40**
FD	**FS**	**0.39**	**0.29**	**0.38**	0.10	-0.21	0.21	0.46	**0.18**
FD	**LF**	**0.71**	**0.55**	**0.32**	0.35	-0.26	**0.24**	0.86	0.44
FS	**LF**	**0.26**	**0.00**	**0.44**	0.06	-0.12	0.33	0.66	**0.25**
LF	**SS**	**-0.09**	**0.11**	**-0.09**	0.54	-0.09	1.99	2.26	1.82

Table 6.1: Semicorrelations of the four quadrants for the hurricane variables of interest and values of the Cramer-von-Mises statistic for the Gaussian, the Clayton and the Gumbel copulas [71].

After validating the normal copula assumption, it was created a Non-Parametric Bayesian Network by means of the software package UniNet. To maximize the number of samples used to build the network, the NPBN was built using the empirical distribution and the joint data for six variables: wind speed, forward speed, forward direction, precipitation, landfall location and storm surge. The radius of maximum winds was added as a user-defined random variable (log-normal distribution) due to the incompleteness of the data (only available since 2004). Initially, was generated a saturated graph in order to obtain all the possible combinations in the BN. Subsequently, the rank correlation coefficients were calculated. The arcs having a correlation coefficient lower than 0.1 were eliminated, since it was assumed that two variables are practically independent if this value is not reached. This process resulted in the BN showed in Figure 6.1.

To make sure that the Gaussian copula assumption is valid for the data base used, it was checked that the DER is within the central 90% confidence interval of the DNR. The validity of the NPBN structure was also inspected by checking that the DNR falls in the central 90% confidence band of the DBN. The DBN, the DNR and the DER were calculated as described in 2.2.4.1. The two validation tests were satisfactory. In the next two sections, the results of the model described are compared with the BN built for the present project.

6.2 Analysis of the dependence among hurricane parameters: bivariate copulas

Leaving the radius to maximum winds (R_{max}) and the precipitation apart from the BN proposed by [71], five hurricane variables are linked as shown in Figure 5.1. A total of six pairs of variables representing the links are analyzed. To find the copula that fits a data set, several steps should be followed. The first step in the process is the transformation of the data set to a uniform ranked data set and the construction of the empirical copulas. This is done using Eq. (2.30). The second step is fitting several theoretical copulas to the empirical copula. In this case, the Gaussian, the Gumbel and the Clayton copula models are tested. Finally, it is assessed the goodness of fit of each of the copulas to the empirical copula by means of the calculation of the semi-correlations and the Cramer von Mises statistic. The expressions of the Gaussian, Gumbel and Clayton copulas are given in Eq. (2.31), Eq. (2.33) and Eq. (2.34). Following the same reference systems for the variables than the ones used in [71], the correlation, semi-correlations and Cramer von Mises coefficients are calculated for the hurricane catalogue of Mississippi (Table 6.2):

The correlations (ρ) summarized in Table 6.2 show that three out of six pairs of variables are positively correlated, meaning that the increase in the value of one variable is associated to the increase in the value of

		ρ	$\rho_{\mathbf{SW}}$	$\rho_{\mathbf{NE}}$	$\rho_{\mathbf{SE}}$	$\rho_{\mathbf{NW}}$	$\mathbf{CM_{Gauss}}$	$\mathbf{CM_{Clayton}}$	$\mathbf{CM_{Gumbel}}$
WS	**FD**	**-0.25**	0.18	-0.21	**-0.29**	**-0.10**	**3.64**	10.93	10.93
WS	**SS**	**0.65**	**0.55**	**0.68**	-0.62	-0.12	4.14	7.88	**3.50**
FD	**FS**	**0.31**	**0.17**	**0.54**	0.25	0.20	4.26	7.99	**2.87**
FD	**LF**	**0.18**	**-0.06**	**0.00**	-0.56	0.41	2.31	3.13	**2.08**
FS	**LF**	**-0.13**	-0.34	0.18	**-0.28**	**0.24**	**3.93**	4.95	4.95
LF	**SS**	**-0.21**	0.14	0.00	**-0.09**	**0.33**	**5.39**	11.35	11.35

Table 6.2: Calculated semicorrelations of the four quadrants for the hurricane variables of interest and values of the Cramer-von-Mises statistic for the Gaussian, the Clayton and the Gumbel copulas.

the other variable of the pair. The other three pairs of variables are negatively correlated. WS-SS present a strong positive correlation ($\rho = 0.65$), while FD-FS and FD-LF show positive dependence but in a lower grade ($\rho = 0.31$ and $\rho = 0.18$, respectively). It is observed negative dependence on the pair LF-SS, due to the backward push of the water when the hurricane makes landfall to the East of the observation station, and therefore lower surge levels for larger distances from Galveston Bay ($\rho = -0.21$). The pairs WS-FD and FS-LF also show negative dependence ($\rho = -0.25$ and $\rho = -0.13$). The pairs showing negative correlation can be represented by means of the Clayton and Gumbel copulas by taking the complementary value of either U or V, and keeping the original value of the other variable. This means that the points $(U, 1 - V)$ or $(U - 1, V)$ should be plotted instead of the original set of points (U, V) to represent negative correlations by means of these copula models.

The small differences among the semicorrelations on the quadrants of interest (bolded values in Table 6.2) and the low values of the Cramer-von-Mises statistic (calculated with Eq. (2.43) and Eq. 2.44, respectively) for the approximation by Gaussian copula indicate that the use of the Gaussian copula to represent the relationships among the pairs of variables is acceptable. In four out of six pairs, the semicorrelations show similar values for the diagonal quadrants in the standard normalized space of the ranks, with the same sign. According to the Cramer-von-Mises values, despite the better performance of the Gumbel copula (lower values for positively correlated pairs of variables), the values of the statistic obtained with the Gaussian copula are close enough to take the Gaussian copula assumption as valid. The comparison among Cramer-von-Mises values for the model of [71] and the current BN cannot be done in absolute terms, because the values obtained depend on the number of points plotted. If more values are used when evaluating the copula, the CM values are larger, since more error is accumulated. In this project, 14161 values were used to compare the empirical copula and the fitted copula models.

As explained in Chapter 2.2.4.1, the use of Gaussian copulas in BN is very interesting from the computational point of view, since there is no need to solve numerically a large number of integrals as a consequence of sampling processes, what does happen when using other theoretical copulas.

6.3 Application of the Gaussian copula assumption to a Bayesian Network (BN) in UniNet

The acceptance of the Gaussian copula assumption enables the construction of the BN in UniNet, which is a package that facilitates the construction and edition of the BN structure, as well as the resolution of BN by using normal copulas to solve the joint distribution among the nodes of the network. With Uninet, it is also possible to validate the normal copula assumption or the BN structure. Values can be inferred in the network to do estimations of the variables of interest.

Taking as a reference the model of [71], and leaving out the radius of maximum winds and the precipitation, the model in UniNet looks as shown in Figure 6.4. The rank correlation coefficient is indicated in the arcs and the marginal distributions are visible in the nodes.

An interesting observation from the calculated correlations is that the absolute value of the correlation coefficient connecting the variables is larger than 0.1, which was the criterion that [71] established to assume conditional independence in the BN proposed. Therefore, the structure proposed by [71] seems to be adequate also for this project. This aspect is confirmed by performing a test in Uninet that evaluates the robustness of the BN

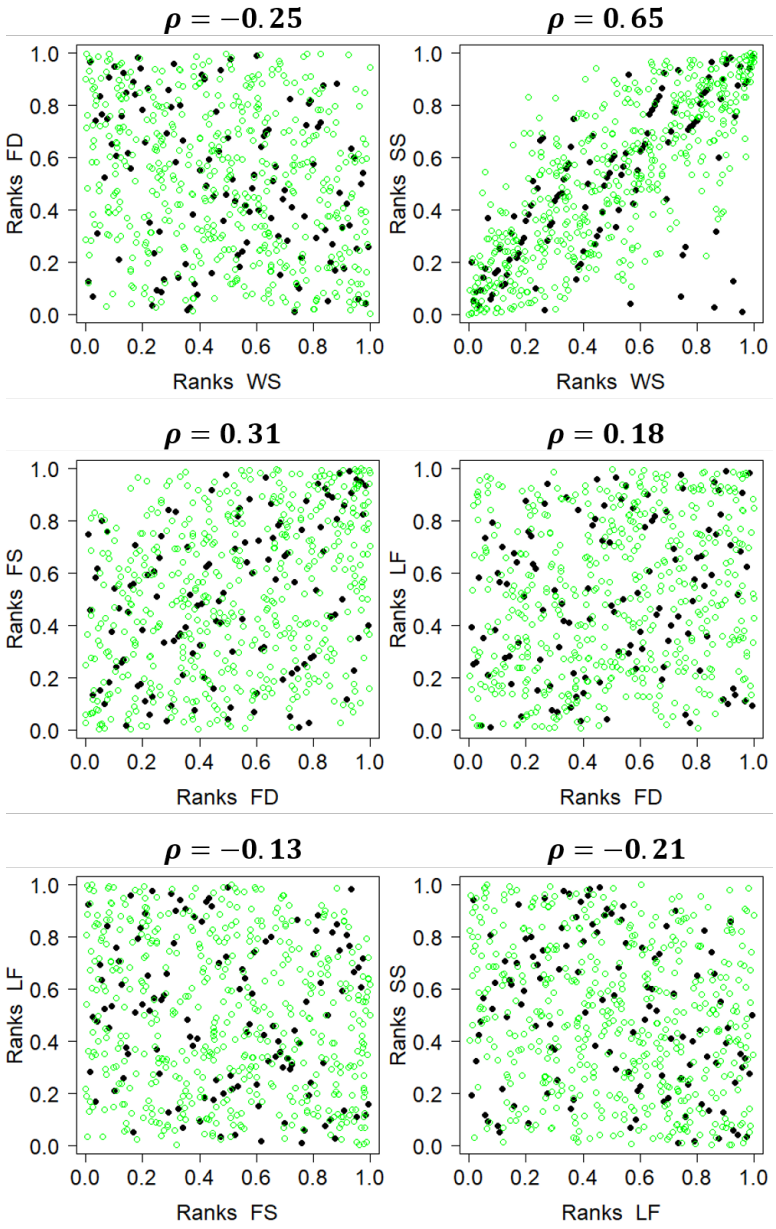

Figure 6.2: Representation of the fitted normal copulas (blue dots) to the empirical copula (black dots) by sampling.

structure. The use of Gaussian copulas to represent joint distributions between the variables of the network is also tested in Uninet. The two tests mentioned are described in Chapter 2.2.4.1.2. The results of the validation are successful, as shown in Figure 6.5, and therefore the assumptions made on Gaussian copula and the network structure are valid.

The rank correlation coefficients given by [71] and calculated for this project are compared in Table 6.3. These results show that the relationships found in both databases are similar, coinciding the sign of the correlation in five out of six cases. The rank correlation coefficients are similar in the case of WS-FD, FD-FS and LF-SS, with differences smaller than 0.15 in the rank correlation coefficients. The rank correlation between WS and FS shows a difference of 0.31, while in the case of FD-LF this ascends to 0.39. Finally, [71] finds a positive correlation between FS and LF, while in this project these variables seem to be negatively correlated.

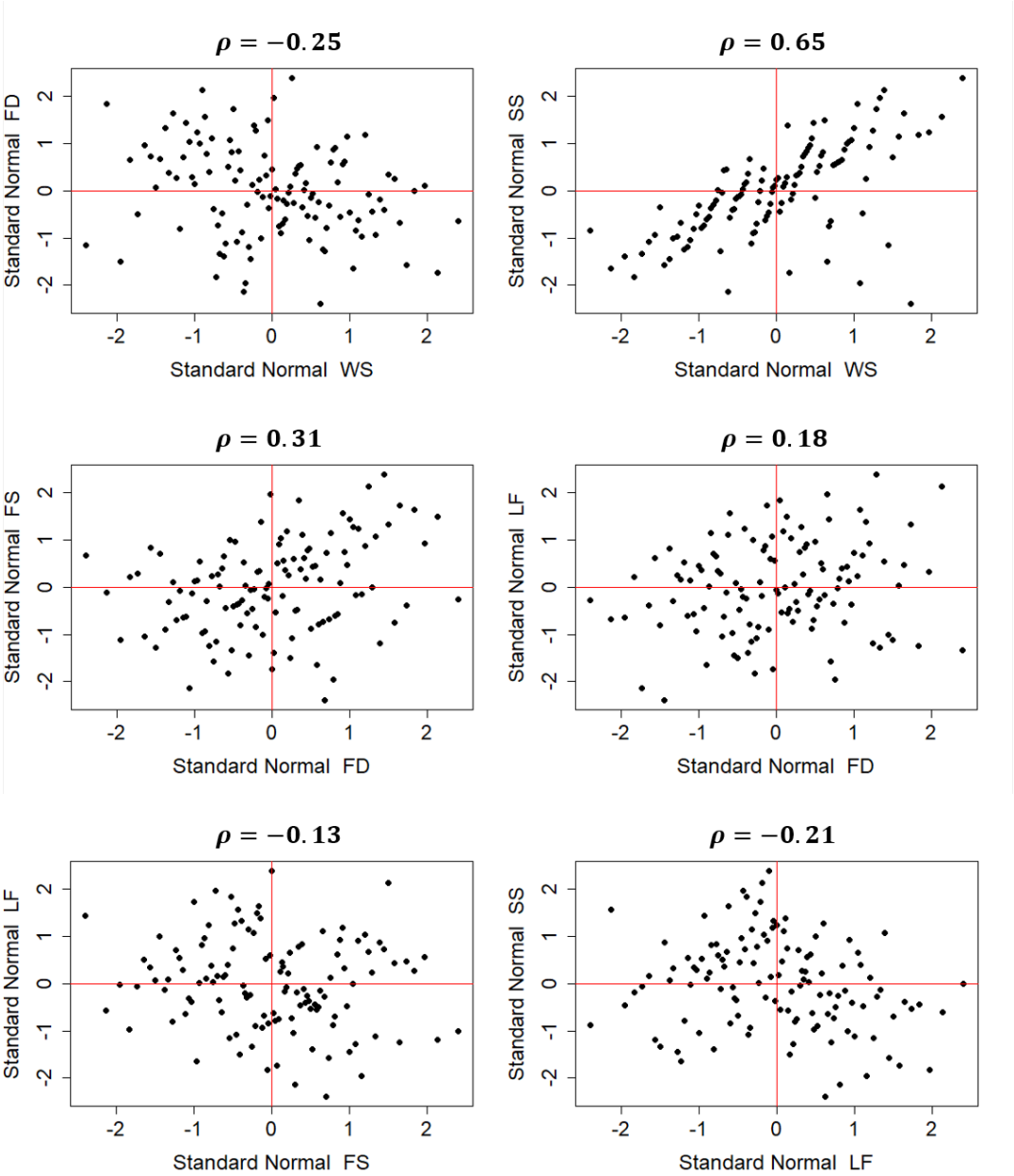

Figure 6.3: Representation of the relationships between the hurricane variables in the standard normal space.

		ρ **(Sebastian, 2017)**	ρ **(Prida, 2020)**
WS	**FD**	-0.11	-0.25
WS	**SS**	0.34	0.65
FD	**FS**	0.37	0.31
FD	**LF**	0.67	0.18
FS	**LF**	0.25	-0.13
LF	**SS**	-0.07	-0.21

Table 6.3: Comparison of the rank correlation coefficients for the BN proposed in [71] and the adapted BN for this project.

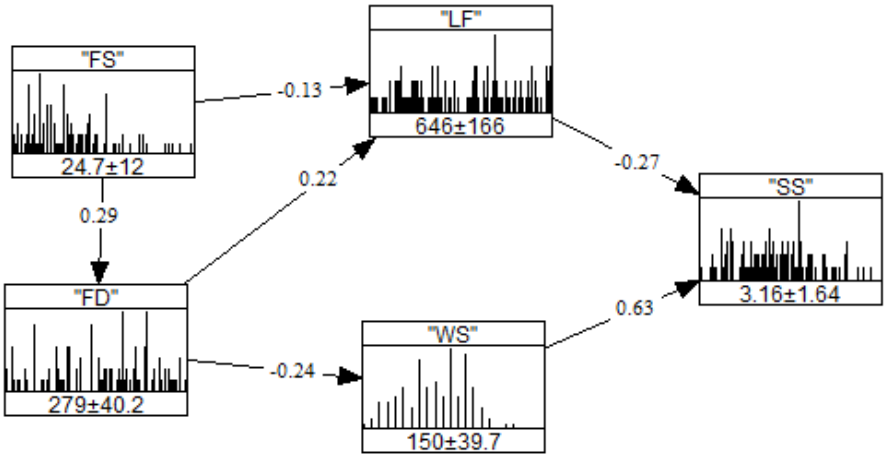

Figure 6.4: BN model relating hurricane variables at the coast of Mississippi.

6.4 Validation of the Bayesian Network

By means of Bayesain Networks it is possible to estimate values of specific nodes (i.e. variables) of the network by inferring values on other of nodes. This process is not unidirectional, meaning that the children of the BN (what we could call the output, which is the storm surge in this case) can be estimated by inferring values in one or more parent nodes, but parents can also be estimated by inferring values in the children nodes. The BN is easily and quickly updated in Uninet, providing new values for the variables interest after inferring values to specific nodes. Two applications of Bayesian Networks related to hurricanes and surge can be storm surge estimation (also in real time) or the generation of synthetic hurricanes for the application in other fields or projects.

To validate the accuracy in estimation of the BN, it is used a testing set that includes 19 storms of the data base. These storms have been selected randomly from the hurricane catalogue containing 140 storms. The values of the surge estimated by the BN are compared to the surge values obtained in Delft3D FM. The values of WS, FD, FS and LF are inferred in the BN for each event. Subsequently, the BN is updated and a normal distribution of the surge is estimated, being this defined by a mean and a standard deviation. Figure 6.6 shows an example of the inference and the updating of the BN for the storm AL252005. Figure 6.7 displays a scatter plot including the surge distributions for the 21 events considered in the validation.

The BN provides a normal distribution, with a mean and a standard deviation of the estimation. The results of the validation show that the mean of the normally distributed surge presents a best fit slope from the origin of 0.861 and an R^2 of 0.885. The average standard deviation is 1.16 meters.

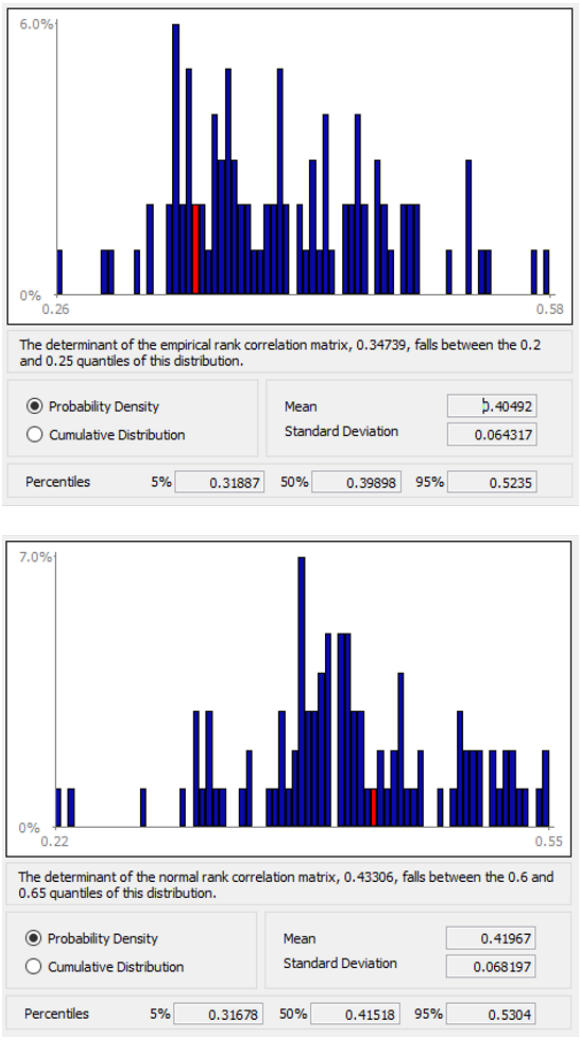

Figure 6.5: Probability density function of the DNR (top) and probability density function of the DBR (bottom). The DER falls inside the 90% central band of the distribution, and therefore the structure of the BN is robust to support the data. The DNR falls inside the 90% central band of the distribution, and therefore it is valid to assume Gaussian copulas in the BN proposed.

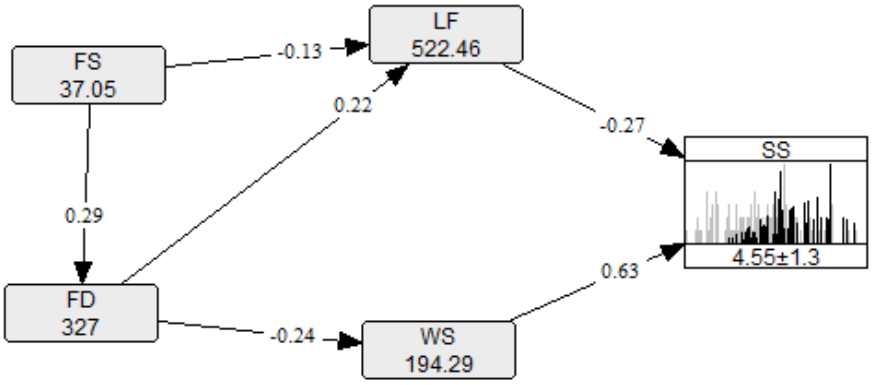

Figure 6.6: Estimation of the surge at Gulfport Harbour during the shifted storm AL252005, by means of inference of the wind speed, forward speed, forward direction and landfall location. The surge obtained from the simulation in Delft3D FM is 4.54 meters + MSL, while the BN estimates a surge with mean 4.55 meters + MSL and a standard deviation of 1.3 meters.

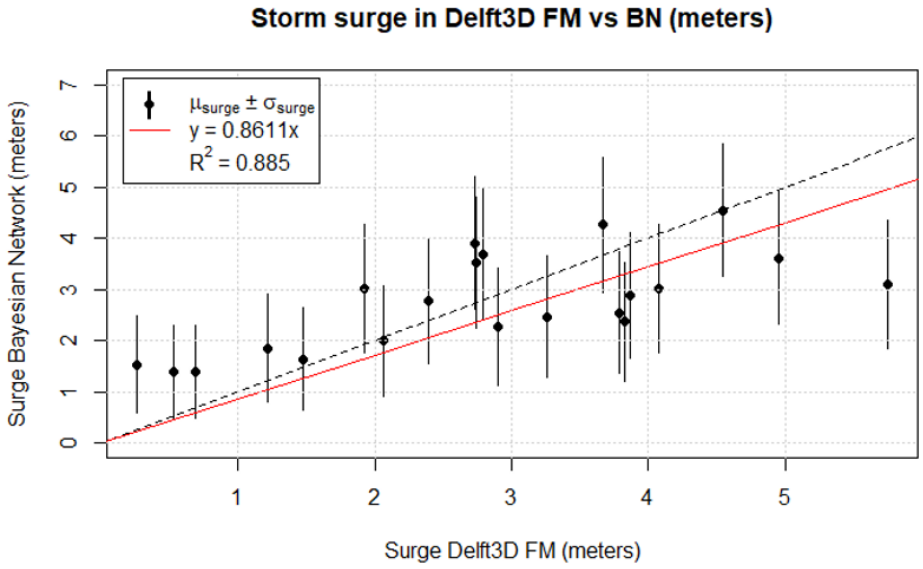

Figure 6.7: Comparison between the surge obtained from the simulation of 21 storms in Delft3D FM and the estimated surge by the Bayesian Network.

CHAPTER 7

Discussion

In modelling processes, the accuracy of the input data is critical to ensure the quality of the final outcome. This project includes two successive modelling processes, in which the second process uses the output from the first process. Therefore, it is necessary (but not sufficient) that the accuracy of the outcome of the first model is good enough in order to achieve reliable results from the second model. In this chapter, the strategies followed to build the physical and stochastic models and their limitations are discussed.

7.1 Physical modelling

The validation of the model based on HWMs did for Hurricane Katrina (2005) shows reasonably good results along the coast of Mississippi, with an average relative error of 9.5% for the HWMs, with a best fit slope for the HWM of 0.912 and an R^2 of 0.995. These results are particularly good for Gulfport, which is the area at which the surge for the generation of the surge data base was recorded. At this location, the relative error drops to 2.5% (19 centimeters for a maximum water level of 7.56 meters + MSL. These results demonstrate an adequate calibration of the model input.

Along the calibration process, it has been observed a particular sensitivity of the modelled surge to the wind drag coefficient (C_d). Several models could be used in order to represent this parameter, among others the model of Powell (2006) and the model of Makin (2005). It has been observed that the linear piece-wise expression for the wind drag in function of the wind speed is able to represent better the surge than the model of Powell. The water levels obtained in Delft3D FM when applying the wind drag model of Powell (2006) for the front right sector of the hurricane and the model of Makin (2005) for Hurricane Katrina (2005) are compared in Figure 7.1.

Both models consider that for hurricane wind speeds the momentum flux between wind and water starts to saturate. Due to the breaking of the waves, a very stable boundary layer is formed close to the surface, formed by spray droplets. For Powell, this layer provokes that C_d remains constant for increasing hurricane wind speeds. However, field data revealed the decrease of C_d for increasing hurricane wind speeds [47]. The Charnock parametrization is valid up to 33 m/s, but the overestimation made by the model of Powell increases specially for high intensity hurricanes, due to the larger difference in C_d. For hurricane Katrina, the drag given by the Powell model reaches values that double the drag given by the Makin model. The modelled surge in Delft3D FM when using the Powell model is 9.55 meters at Gulfport Harbour, which is approximately 1.4 meters more than the validated surge (7.16 meters). This notorious difference in the modelled surge shows the importance of performing a good calibration of the wind drag coefficient.

The 2D wind and pressure fields generated by the modified Holland model play a central role in the estimation of surge. Therefore, a great influence in the adequate calibration of the model is related to this input. Based on the comparison of the simulation of Hurricane Katrina in Delft3D FM of the 2D wind fields (Figure 7.3, left) and the high fidelity model H*Wind (Figure 7.3, right), it is observed that the modified Holland model by Veltcheva is capable of representing the asymmetric structure of the hurricane.

The effect of the forward speed of the hurricane and its contribution to the asymmetry of the wind field has been

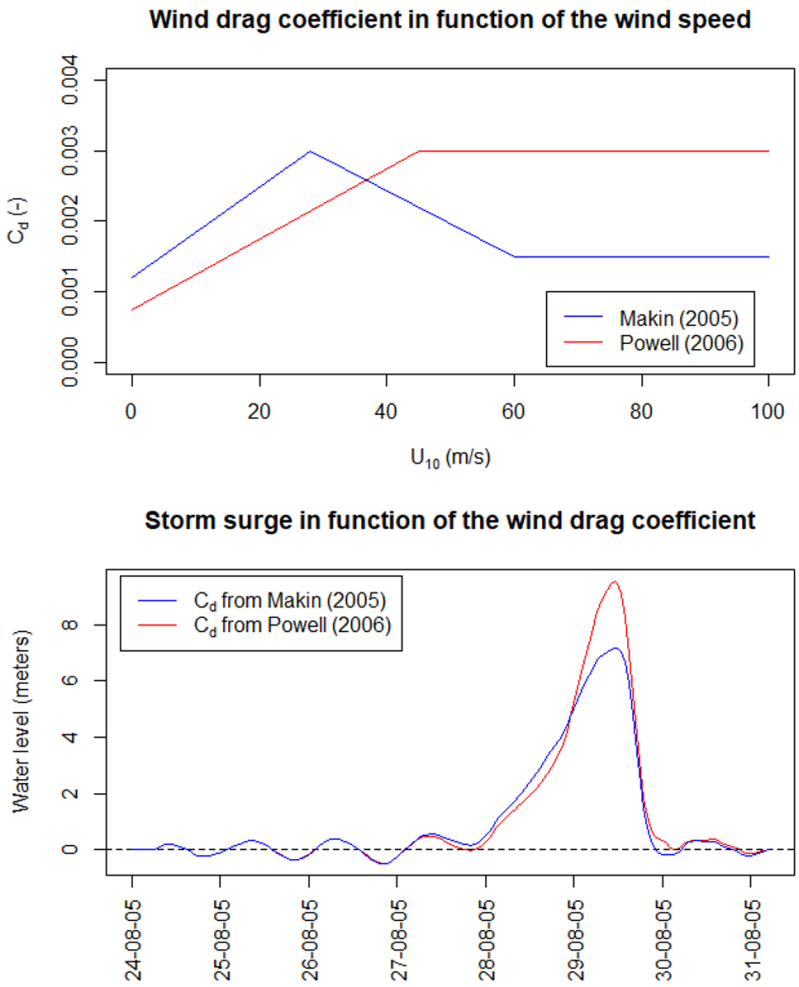

Figure 7.1: Comparison between the surge obtained when using the formulation of Makin (2005) and the formulation of Powell (2006).

observed by comparing the wind speed in function of the radius when applying the modified Holland model of [81] and the original Holland model (Figure 7.3, top) and the resulting surge when applying (Figure 7.3, bottom). For the wind comparison, it has been taken the section that includes the maximum wind speed within the radius of maximum winds. This value has been found for South-North winds (locations on a line that forms 90 degrees from the North, when counting in clockwise direction). The original Holland model do not consider the forward speed of the hurricane to calculate the wind velocity, and therefore it represents a symmetric wind field.

The maximum wind speed modelled for the asymmetric and the symmetric structure in the case of Katrina are 198.72 m/s and 190.08 m/s, respectively. This difference in the wind speed is barely 5%, which, which has led to a difference in surge between asymmetric and symmetric structure of just 10 centimeters at Gulfport Harbour. Therefore, in the validated case the asymmetry of the hurricane does not seem to have a relevant influence in the surge level. However, this is just a particular case. It is noted that the effect of the asymmetry can cause differences in water levels of up to 15% [85] and therefore the use of a parametric expressions (such as the model of Veltcheva) to model hurricane asymmetry is recommended.

Additionally, [81] proposed a formula to consider the asymmetry in the 2D pressure field. However, due to the relatively small effect that the pressure asymmetry induces in the water levels compared to the wind speed and the complexity of the expression proposed, the modified formulation of the pressure has not been considered.

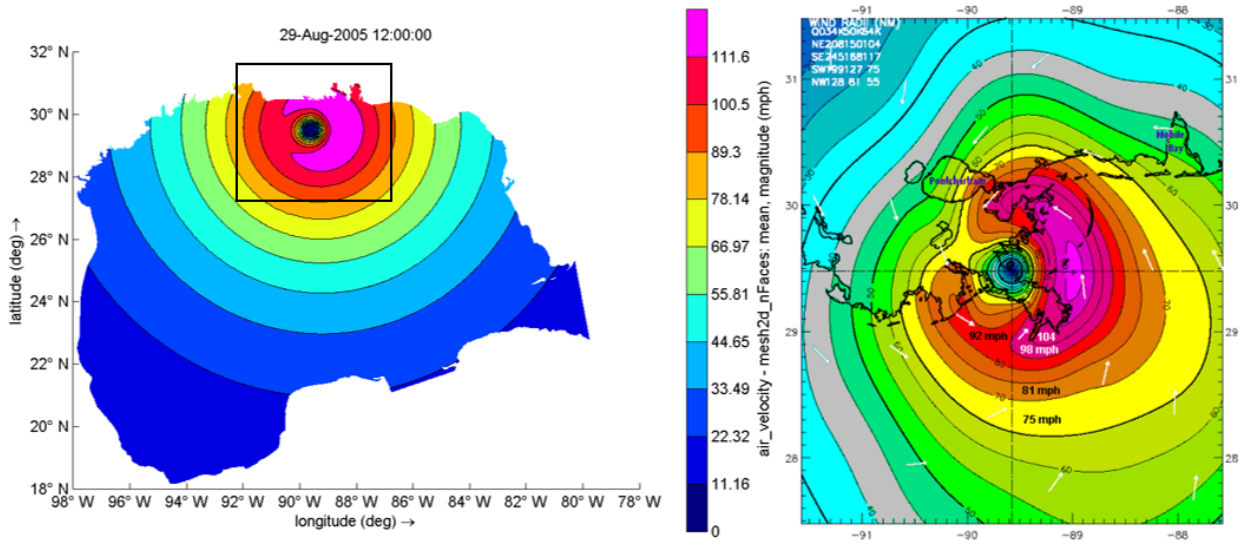

Figure 7.2: Comparison between the 2D wind field generated with the Holland model as read in Delft3D FM (top) and the 2D wind field as generated from post storm analysis data in H*Wind (bottom).

7.1.1 Limitations

The hydrodynamic model has been validated by comparing 41 observations of HWMs recorded after the event. Despite taking HWM locations that are close to the shoreline, they can be separated from the coastline by distances of the order of few kilometers. In inland regions, the topography becomes more complex than at the sea, and therefore, the level of detail of the topography must be much higher in order to capture those features that might alter the water flow.

The spatial resolution of the model is controlled by the resolution of the unstructured mesh, since any other input given in grid format is interpolated to it, adopting the resolution imposed by the mesh. The resolution of the unstructured mesh reaches a maximum of 200 meters in the shoreline. Moreover, the resolution of the bathymetry/topography and the hydraulic roughness is 500 meters. For storm surge, this resolution can be acceptable, as long as the bathymetry gradients are moderated. However, this resolution might be too coarse to achieve high accuracy in the simulation of overland flood, specially when coastal protection structures, highway and railway dikes, and other elevated infrastructure are present. The absence of dikes in the shoreline of Mississippi makes the surge validation at nearshore overland points acceptable.

7.2 Stochastic modelling

7.2.1 Observations

A previous step to the elaboration of the BN that is crucial in the process is the validation of the Gaussian copula assumption. Updating the BN in this conditions is matter of seconds, as has been observed during the validation of the surge estimations. This is due to the capability of the normal copula of performing inference analytically. Due to the unfeasibility of solving other copula families, the normal copula is seen as the unique copula capable of solving BNs in short times. This fact limits the accuracy in the modelling of tail dependencies in BNs. However, in this case the semicorrelations have shown acceptable values for the majority of the cases (4 out of 6) and the values of the Cramer-von-Mises for the normal copula have shown lower or very similar values to the values for the Gumbel copula. The relatively good fit of the copula has contributed to the reasonable fit of the estimated surge by the BN to the modelled surge in Delft3D FM, indicated by the slope of the best line fit of 0.861.

7.2.2 Limitations

The shifting strategy applied in Chapter 6 has led to increase the hurricane catalogue from 48 to 140 hurricanes. From those, 119 hurricanes have been used for the training of the Bayesian Network. This sample size has been

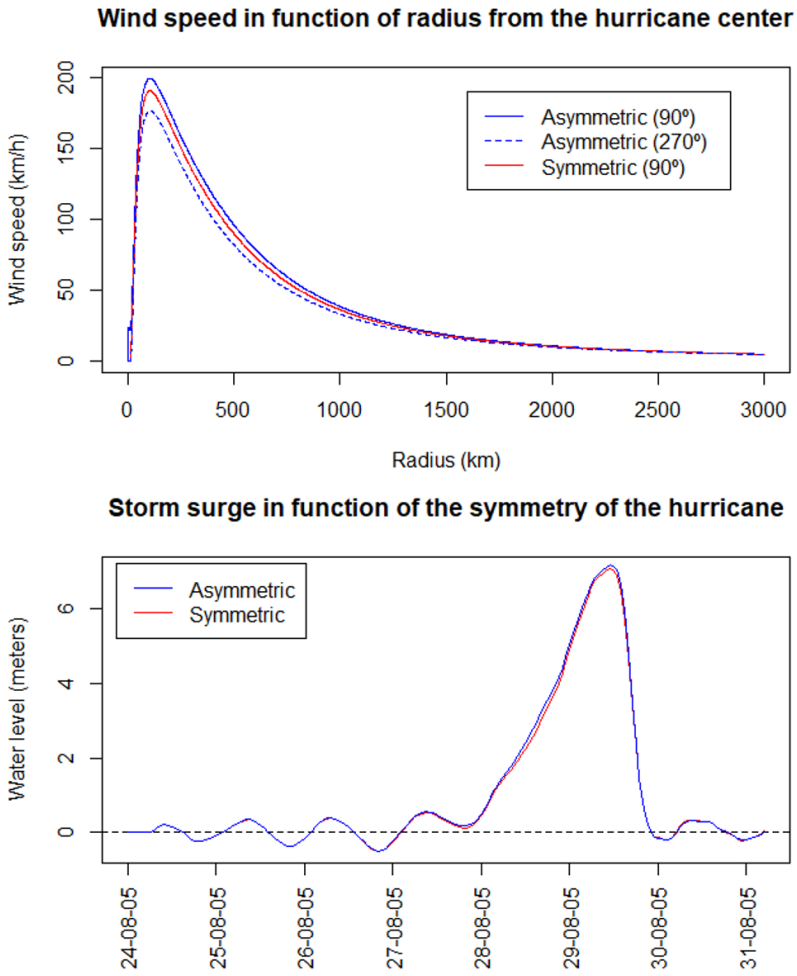

Figure 7.3: Comparison of the wind speed in function of the radius from the center of the hurricane, between a symmetric and an asymmetric structure. The degrees are counted from the North and in clockwise direction.

considered to be sufficient to train the stochastic model.

From the 6 pairs of hurricane variables considered, the combinations WS-FD, WS-SS, FD-FS are not affected by the shifting operation since the two values of the variables of the combination are not influenced by the landfall location. Despite the shifting, the correlation between LF-SS is not altered by the change of landfall location since the surge measurements are taken at a specific point.

However, the applicability of random shifting of tracks in the case of FS and LF should be further examined, since the values of FS and FD can be inherent to specific areas of the region examined (North of the Gulf of Mexico), due to the large extension of the area of study. In Figure 7.4 there are shown the original 140 tracks of the data base with the values of the FD (top) and FS (bottom) represented by a colour bar.

In the case of FD, it is observed that the hurricanes making landfall at the Eastern region of the Gulf of Mexico (e.g. Florida) generally have a larger angle of landfall than the hurricanes making landfall at the Western region of the Gulf of Mexico (e.g. Texas). However, in the case of FS this pattern is not as clear. In order to analyze further the relationship between angle and landfall location, the pairs FD-LF and FS-LF are plotted in the standard normal space and the correlations are calculated (Figure 7.5).

The results shown in Figure 7.5 prove that the landfall location is notably correlated to the forward speed and the forward direction of the hurricanes, with a correlation of 0.54 between FD and LF and a correlation of 0.23

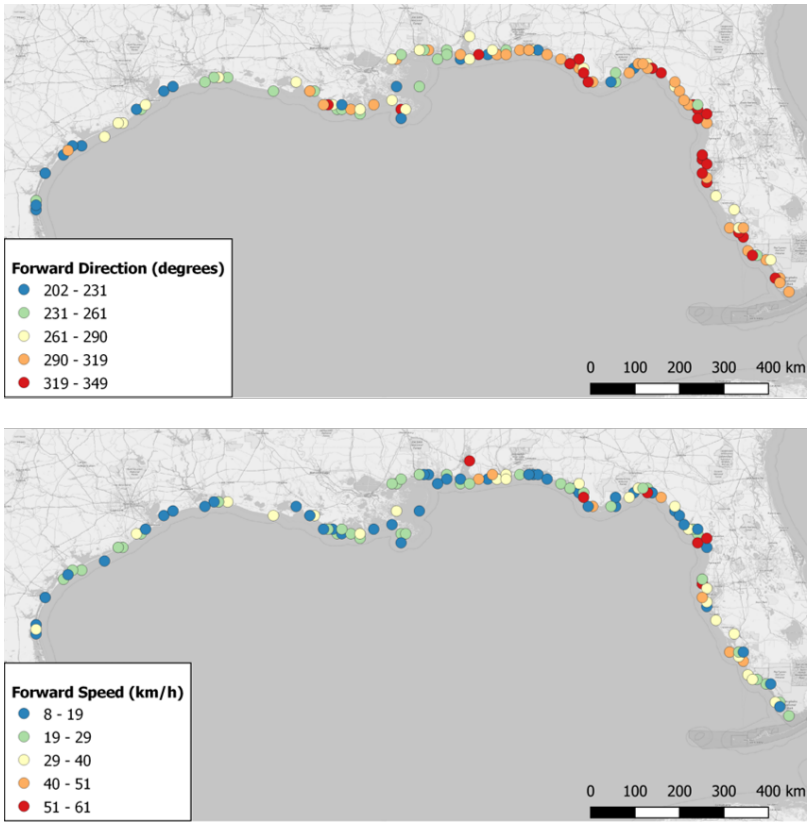

Figure 7.4: Original location of the landfall of the 140 hurricanes of the data set (before the shifting operation). The color of the points indicate the forward direction (top) and the forward speed (bottom) of the hurricanes at landfall.

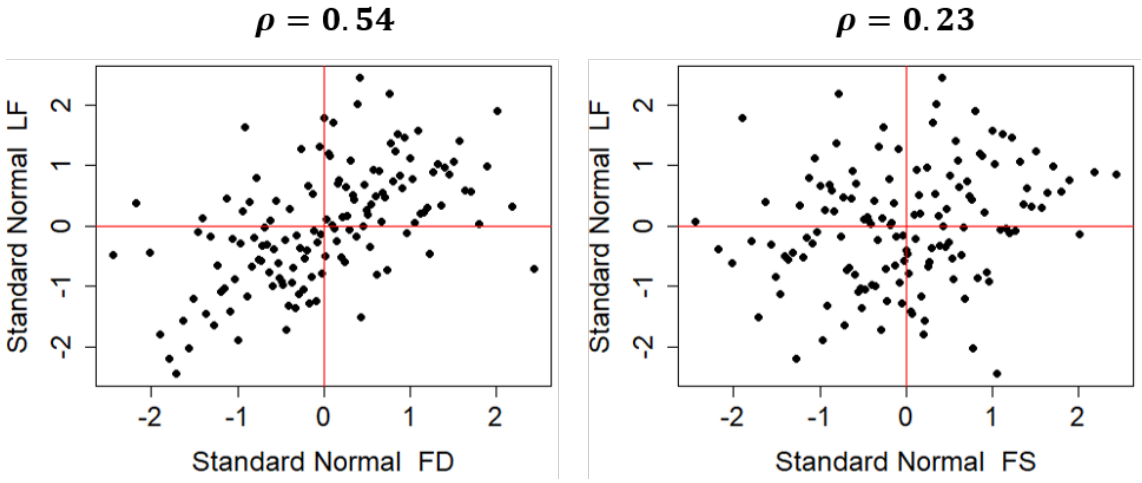

Figure 7.5: Correlation between FS-LF and FD-LF shown in the standard normal space.

between FS and LF. Indeed, these results are closer to the results obtained by [71] (correlation of 0.71 between FD and LF and correlation of 0.26 between FS-LF). In contrast, by assigning random landfall locations to the hurricanes the correlation coefficients obtained were considerably lower (0.18 for FD-LF and -0.13 for FS-LF). The shift of hurricanes to the defined bounding box without considering the correlations between FS-LF and FD-LF leads to the elaboration of a data set that is not fully representative for the area of study, what limits

the accuracy of the results of the BN.

CHAPTER 8

Conclusions

In this chapter, the key findings and recommendations for future research are given. The chapter has been divided into three sections, each of them giving an answer to each of the three research subquestions proposed in the introduction of the project (Chapter 1):

- How should the different input of the hydrodynamic model be calibrated to simulate surge at high fidelity?
- How should the hurricane data scarcity be tackled in order to generate a sufficiently large data set for the training of the stochastic model?
- What is the accuracy of the surge estimation and the time of computation of the stochastic model?

By answering the research subquestions, the main research question is answered:

Is it possible to estimate storm surge at reasonable accuracy and time in the coast of Mississippi by using a stochastic model?

The chapter ends proposing recommendations and potential research topics related to the project.

8.1 Key findings

8.1.1 Physical model setup and validation

In this project, a stochastic model has been developed with the objective to estimate storm surge at the coast of Mississippi (United States) at a reasonable accuracy without solving complex equations that represent physical processes. The approach followed to build the stochastic model has been based on three main steps. The first step has been the setup of the model, in which the input parameters of the model have been adequately calibrated, based on the comparison to real observations of the water levels in the coast of Mississippi. The second step has been the generation of a hurricane data base, in which the values of the surge have been obtained by simulating a finite number of hurricanes making landfall at the North of the Gulf of Mexico. The hurricane variables are recorded at Gulfport Harbour (central coast of Mississippi). The third and last step has been the setup and validation of the stochastic model, by comparing the the storm surge given obtained from the stochastic model with the surge obtained from the hydrodynamic simulations.

The Delft3D Flexible Mesh model has been used to hindcast the storm surge caused by hurricanes at the coast of Mississippi. The Ultra-Levee-Removed unstructured mesh has been adapted from ADCIRC to Delft3D FM format and has been refined at the area of study, obtaining a mesh of triangles (460,296 nodes) with maximum resolution of 200 meters at the shoreline and overland regions of Mississippi. The domain of the unstructured mesh comprises the entire Gulf of Mexico, taking as open sea boundaries the Yucatan Channel and the Florida Strait. A bathymetry and topography of 460 meters of resolution has been adopted. A variable hydraulic roughness has been applied based on the land cover, for which the Manning formulation has been used, A Manning coefficient of 0.025 has been used in open waters.

Hurricane Katrina (2005) has been simulated to calibrate and validate the model. Apart from the storm surge caused by the hurricane, the tide and the wave setup have also been considered, but only for validation purposes. An astronomical tide has been imposed at the open sea boundaries of the model, for which seven tidal constituents have been considered. The tide has been validated against tidal predictions made by NOAA for three tidal stations along the Mississippi coast, obtaining an average Scatter Index of 0.294 and an average Bias of -0.199, The sampling time of the simulation and the predicted tide was 15 minutes, being the total validation time seven days coinciding with the period of development and arrival to the Mississippi coast of Katrina (24 to 31 August 2005). The wind drag has been parametrized by means of the model of Makin [47], which expresses the wind drag coefficient in function of the sustained wind speed at 10 meters + MSL. The hurricane forcing has been obtained by applying the Holland model with the modifications of Veltcheva [81] to the best track data of Hurricane Katrina retrieved from the HURDAT2 database. Due to the reduced contribution of the wave setup compared to the storm surge and the important computational effort that modelling waves involve, a maximum wave setup of 0.3 meters has been assumed based on [4].

Hurricane Katrina has been simulated in Delft3D FM by implementing the explained inputs into the model. To validate the model, the simulated water levels have been compared to 41 high watermarks recorded by the Federal Emergency Management Agency (FEMA) of the United States that were located along the coast of Mississippi. The results of the validation show a best fit slope from the origin of 0.912 and an R^2 of 0.996. At Gulfport, the absolute error of the surge estimation is 19 centimeters, equivalent to a relative error of 2.5%. The absence of flood defences and the relative proximity of the validation stations to the shoreline (few kilometers at most) make possible to achieve a reasonable validation of the model for an unstructured mesh of 200 meters of resolution.

The model shows considerable sensitivity to the wind drag coefficient, which has been found to reach a maximum value of 0.003 for a wind speed of 33 m/s. The wind drag is reduced for increasing hurricane wind speeds due to the formation of a spray boundary layer generated from the wave breaking. The drag remains constant from a wind speed of 60 m/s at a value of 0.0015. The asymmetric structure of the hurricane is captured by the Holland model with the modifications of Veltcheva, which also considers the forward speed of the hurricane. The wind speeds obtained by the modified Holland model are compared to the original Holland model, which is axisymmetric and does not consider the influence of the forward speed of the hurricane on the wind speed. The results show that the maximum wind speed in the region of maximum winds is 9 m/s larger for the modified model compared to the original model. However, this difference does not seem to affect noticeably the surge at Gulfport Harbour (only 10 centimeters of difference between modified and original model).

8.1.2 Generation of the hurricane data base

The validated model has been used to simulate historical hurricanes (wind speed larger than 33 m/s at some instant during the lifetime of the hurricane) that made landfall in the North of the Gulf of Mexico, whose best tracks have been retrieved from the HURDAT2 database, which includes the best tracks of the historical hurricanes occurring in the Atlantic basin of the United States for the period 1851-2018. A landfall domain of 600 kilometers by 600 kilometers taking as center of the rectangle Gulfport Harbour has been delimited to select the historical hurricanes. However, due to the scarcity in the number of hurricanes making landfall in this region (48 hurricanes), hurricanes making landfall outside of the domain but in the Northern coast of the Gulf of Mexico have been shifted to the rectangular domain, conditioning their selection to have a forward direction at landfall that is within the range of angles of the hurricanes making landfall in the rectangular domain (201-349 degrees counting from the East and clockwise). A total of 140 hurricanes formed the data base, 92 of them being shifted to the rectangular domain. These 92 hurricanes have been randomly split into 2 groups of 45 and 46 hurricanes. The hurricanes from the first group and the second group have been shifted to a random location along a simplified coastline to the East and the West of Gulfport Harbour, respectively. The original landfall track point has been used to shift the hurricane tracks to the new location along the simplified coastline.

The hurricane catalogue has been simulated by means of Python scripts in the DeltaShell interface of Delft3D FM and running batch scripts on Linux. In the second case, the High Performance Computing 11 cluster from TU Delft has been used to run simulations in parallel by using two nodes. The average time of simulation of one hurricane has been approximately 45 minutes. Once the simulations have been completed, the data base has been elaborated. The hurricane variables considered in the stochastic model have been the forward speed and the forward direction of the hurricane, the wind speed, the distance from a reference point located

in Galveston Bay to the landfall location and the maximum storm surge recorded at the observation point of Gulfport Harbour. The values recorded at the moment of landfall have been considered for the forward speed, the forward direction and the wind speed.

8.1.3 Stochastic model setup and validation

The stochastic model used to estimate storm surge is a Bayesian Network that assumes normal copulas to represent the joint distribution between nodes of the network. From the 140 hurricanes of the data set, the 85% (119 hurricanes) have been used for the training of the Bayesian Network and 15% (21 hurricanes) have been used for the validation of the model. A similar network structure to the one proposed by [71] for the estimation of surge at Galveston Bay has been considered to do the estimation. The normal copula assumption has been validated by confirming that the determinant of the empirical normal rank correlation matrix (DNR) falls in the centered 90% interval of the determinant of the empirical Bayesian Network rank correlation matrix (DBN). On top of that, the semicorrelations of the transformed variables to ranks and to the standard normal space for four out of six pair of variables show similar values on the diagonals. The Cramer-von-Mises statistic shows a better performance than for the Gumbel and Clayton copulas for three out of six cases, while for the other three the value is slightly larger than for the Gumbel and Clayton copulas. The structure of the Bayesian Network has been validated by confirming that the determinant of the empirical rank correlation matrix (DER) falls in the centered 90% interval of the determinant of the empirical Bayesian Network rank correlation matrix (DBN).

The rank correlation coefficients for the Bayesian Network obtained for the developed hurricane data set have been compared to the values obtained by [71]. The results show that the correlation coefficients are similar, except for the the correlation between forward direction and landfall location (0.67 for [71] and 0.18 for the developed hurricane data base) and the correlation between forward speed and landfall location (0.25 for [71] and -0.13 for the developed hurricane data base). By analyzing the original forward direction, forward speed and landfall location data, it has been observed that the correlation between forward direction and the original landfall location is 0.54 and the correlation between forward speed and the original landfall location is 0.23, results that match the correlations calculated by [71]. Therefore, the shifting approach to generate a larger sample of hurricane data is valid, but considering the original correlation between the three variables mentioned would represent better the hurricane characteristics of the domain considered.

Finally, the Bayesian Network has been tested by comparing the values of the surge obtained in Delft3D FM to the surge values obtained after inferring hurricane variables in the Bayesian Network. The storm surge has been estimated for the 21 hurricanes of the validation data set. The Bayesian Network provides the uncertainty of the estimation by giving a normal distribution of the surge. The slope of the best fit line for the mean surge values is 0.861, with an R^2 of 0.885. Moreover, the average standard deviation of the estimations is 1.16 meters. These results indicate a reasonable estimation of the surge by means of the Bayesian Network. This estimation can be made in the order of seconds.

8.2 Recommendations and further research

Based on the key findings and the limitations of the models described in the discussion, further research is recommended in the following topics:

- **Finer resolution of the unstructured mesh and topography when simulating overland flood**: In case coastal flood is simulated, it is recommended the use of high resolution Digital Terrain Models for the topography (e.g. cellsize of 5 meter by 5 meter) and an unstructured mesh of similar resolution. However, it should be noted that this resolution would increase noticeably the computational time of the simulations.
- **Size of the hurricane data set**: In order to achieve a more robust Bayesian Network, the hurricane data set should be extended. By analyzing the characteristics of the hurricanes at different locations, it is possible to develop an algorithm to generate synthetic hurricane tracks that are representative from each region. Actually, one of the objectives of building the BN for this project was generating synthetic storms , but also including the surge variable apart from wind and location parameters.
- **Consideration of other physical variables in the BN**: In view of the application of a BN to predict storm surge in other world regions, additional variables could be included in the model. For instance, the

bathymetry gradient is key for the enhancement of the storm surge.

- **Alternative methods for the calculation of joint probabilities in a BN:** The adequate representation of tail dependencies is limited when using normal copulas. Currently, the methods to solve joint distributions that represent tail dependency are not feasible for a Bayesian Network (e.g. sampling).Therefore, further investigation is encouraged in the development of methods to solve tail dependent copulas in a shorter computational time, in order to improve the accuracy of the estimation in those joint distributions that show tail dependence.
- **Applicability of Dynamic BN in hurricane-induced surge problems:**: Most of the physical phenomena that can be observed in nature are not detected based on a particular point in time, but they can be described by a multiple state of observations that yield a judgement of one complete final event [51]. This is also the case of hurricanes. At a specific time step, the variation of one variable can influence the value of another variable in the following time steps. This kind of relationships are only considered if Dynamic Bayesian Networks are used, by which the temporal dimension is added to the BN.

APPENDIX A

Phase lag between simulations and observations

During the simulation of different hurricanes, it has been observed that the the simulations in Delft3D FM present a time lag with respect to the observations at the tidal gauges (Figure A.1). In Table A.1, there are shown the times at which the maximum surge was achieved at every station for observations and simulations, for Hurricane Katrina and Hurricane Gustav. The time lags are also calculated.

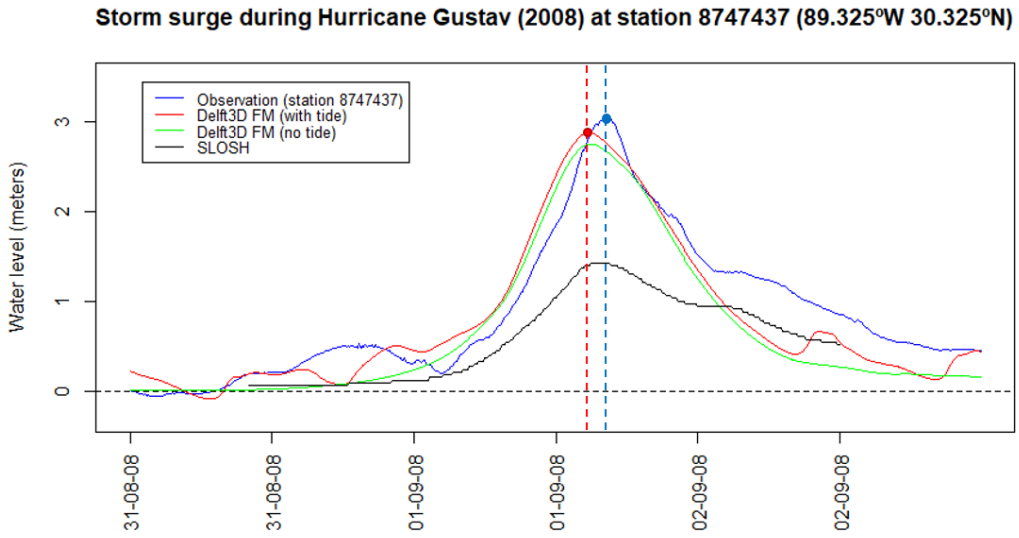

Figure A.1: Storm surge validation at the Bay Waveland Yacht Club station (ID: 8747437) for Hurricane Gustav (2008).

The time lag of the observations with respect to the simulations is explained by the faster propagation of the hurricanes in the simulations than in reality, as a result of the linear interpolation of the hurricane forward speed made by Delft3D FM. The data time interval of the hurricane input (best hurricane track) as given in the HURDAT2 database is generally 6 hours, while the time step of the imposition of external forcing (*User time step*) is 6 minutes. To show this phenomenon, general diagrams $x - t$ and $v - t$ are used (Figure A.2 and Figure A.3).

As a result of the linear interpolation applied in the hurricane forward speed between two points of the hurricane track, the slope of the forward speed in the simulation is constant (red line in Figure A.3). However, in reality the forward speed of the hurricane increases more smoothly, as shown by the blue line in Figure A.3. Therefore, the hurricane forward speed of the real hurricane is smaller than the forward speed of the simulated hurricane

Hurricane	Station	Source	Date & Time surge peak	Time lag
Katrina	8760922	Observation	29/08/2005 09:30:00	36 min
Katrina	8760922	Simulation	29/08/2005 08:54:00	
Gustav	8760922	Observation	01/09/2008 11:36:00	0 min
Gustav	8760922	Simulation	01/09/2008 11:36:00	
Gustav	8747437	Observation	01/09/2008 16:12:00	1 h 12 min
Gustav	8747437	Simulation	01/09/2008 15:00:00	

Table A.1: Time lag between the maximum storm surge obtained from simulation and from the observations for Hurricane Katrina and Gustav, at Pilots East Station (ID: 8760922) and Waveland Yacht Club Station (ID: 8747437).

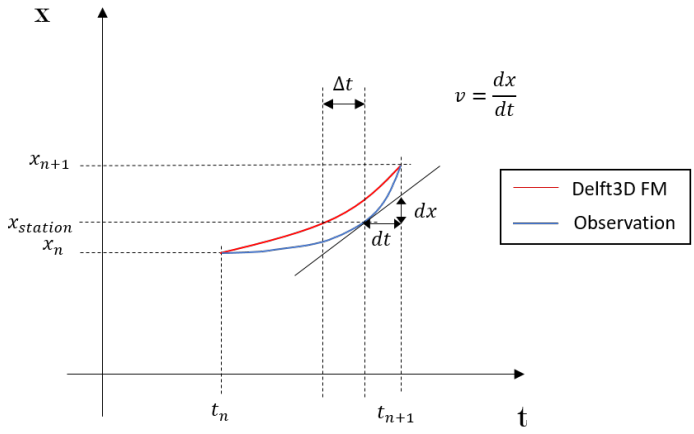

Figure A.2: General diagram of the trajectory (x-t) of the simulated and the real hurricanes.

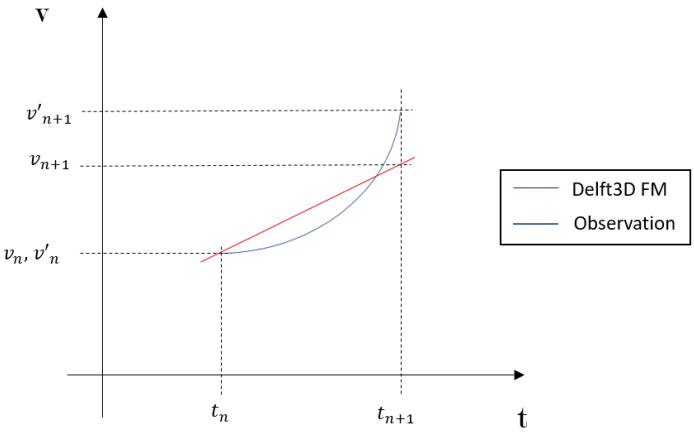

Figure A.3: General diagram of the velocity (v-t) of the hurricanes.

for a certain time span after the time step n. If the peak of the surge falls in this certain time span between time step n and time step $n+1$, the simulated hurricane would arrive before than the real hurricane to a specific station, causing the time lag Δt shown in Figure A.3.

To corroborate this explanation, it is provided the information given on the HURDAT2 database with respect to the best track of Hurricane Katrina. The time steps n and $n+1$ correspond to the immediate time-step before and after the storm surge peak:

$$\text{Pilots East Station (Katrina)} = \begin{cases} t_n = 29/08/2005\ \ 06{:}00{:}00 \\ t_{n+1} = 29/08/2005\ \ 11{:}00{:}00 \\ x_n = (-89.6, 28.2) \\ x_{n+1} = (-89.6, 29.3) \\ x_{station} = (-89.4, 28.9) \\ v_n = 19.96\ \ km/h \\ v_n = 23.70\ \ km/h \end{cases} \tag{A.1}$$

The surge peak at Pilots East Station during Hurricane Katrina is registered on August 29, 2005 at 8.54 AM for the simulation and at 9.30 AM for the observation. This record falls right in between the time step n (6.00 AM) and the time step $n + 1$ (11.00 AM). The time lag observed is 36 minutes.

APPENDIX B

Validation of the Eastcoast 2001 database at Gulfport Harbour

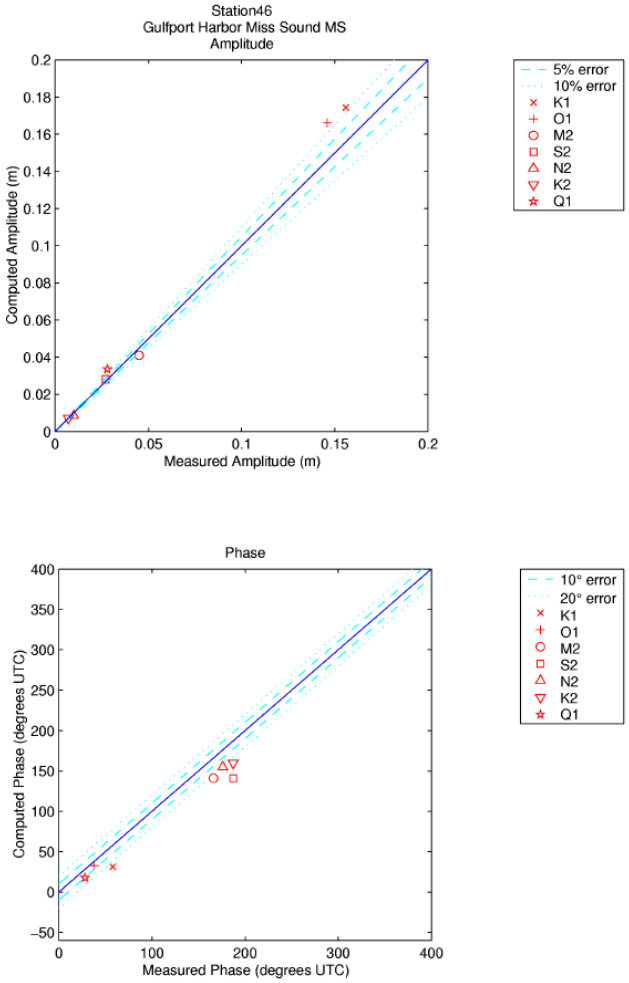

Figure B.1: Scatter plot with the comparison between the computed vs harmonic tidal constituents at the Gulfport Harbor (central coast of Mississippi) by using the Eastcoast2001 database [54].

APPENDIX C

Hydraulic roughness

MS-GAP Class	Description	Manning's n
1	Agriculture	0.05
2	Fresh water	0.025
3	Aquaculture	0.045
4	Estuarine water	0.025
6	Farmed wetlands	0.035
7	Estuarine emergent	0.05
8	Estuarine woody	0.14
9	Palustrine emergent	0.06
10	Bottomland hardwood	0.14
11	Riverine swamp	0.14
12	Pine savannah	0.09
13	Fresh water shrub/scrub	0.075
14	Palustrine non-vegetated	0.035
15	Transportation	0.032
16	High density urban	0.15
24	Urban fresh water	0.025
25	Wet soil/water/shadow	0.04
26	Urban pine	0.18
27	Urban hardwood	0.16
28	Urban low herbaceous	0.07
29	Urban grassy/pasture	0.055
30	Bare urban I	0.12
31	Bare urban II	0.12
32	Clear cuts	0.036
50	Low density pine	0.16
51	Medium density pine	0.18
52	High density pine	0.2
53	Medium density hardwood	0.17
54	High density hardwood	0.17
55	Mixed forest	0.16
56	Recent harvest	0.045
57	Cypress/tupelo	0.18
60	Agriculture	0.05
61	Grassy/pasture/range	0.05
62	Low herbaceous vegetation	0.05
63	Evergreen shrub	0.08
71	Wetland	0.05
80	Bare	0.035
81	Sand bar/beach	0.03

Figure C.1: Hydraulic roughness values proposed by [5] for the coast of Mississippi and Louisiana.

APPENDIX D

Development of Hurricane Katrina

D.1 Air pressure at MSL

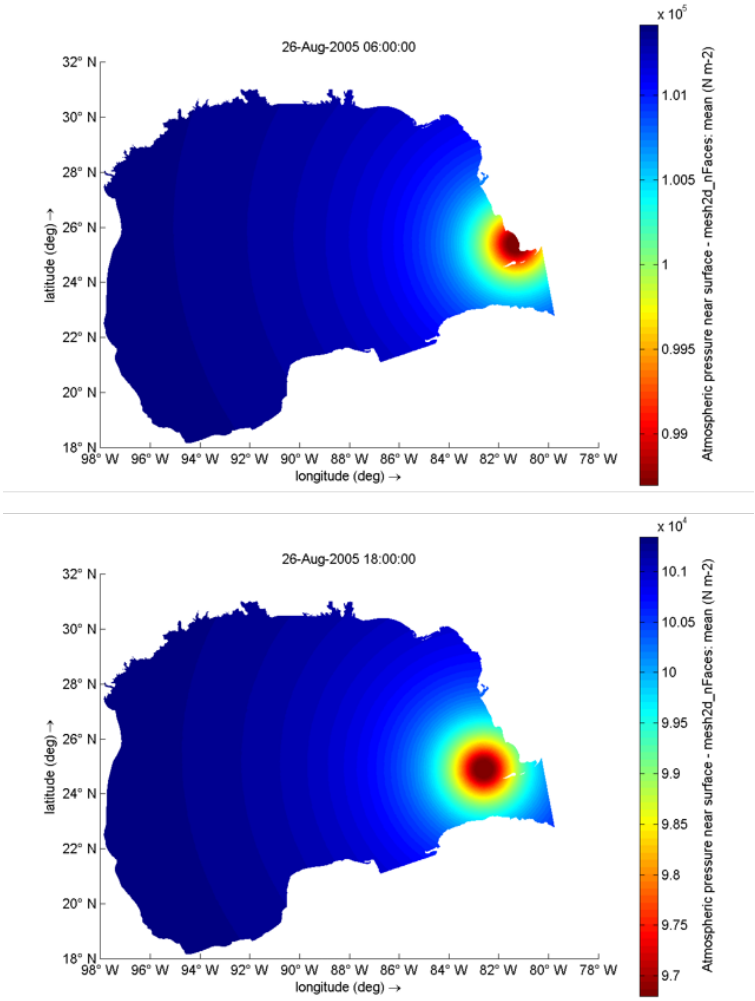

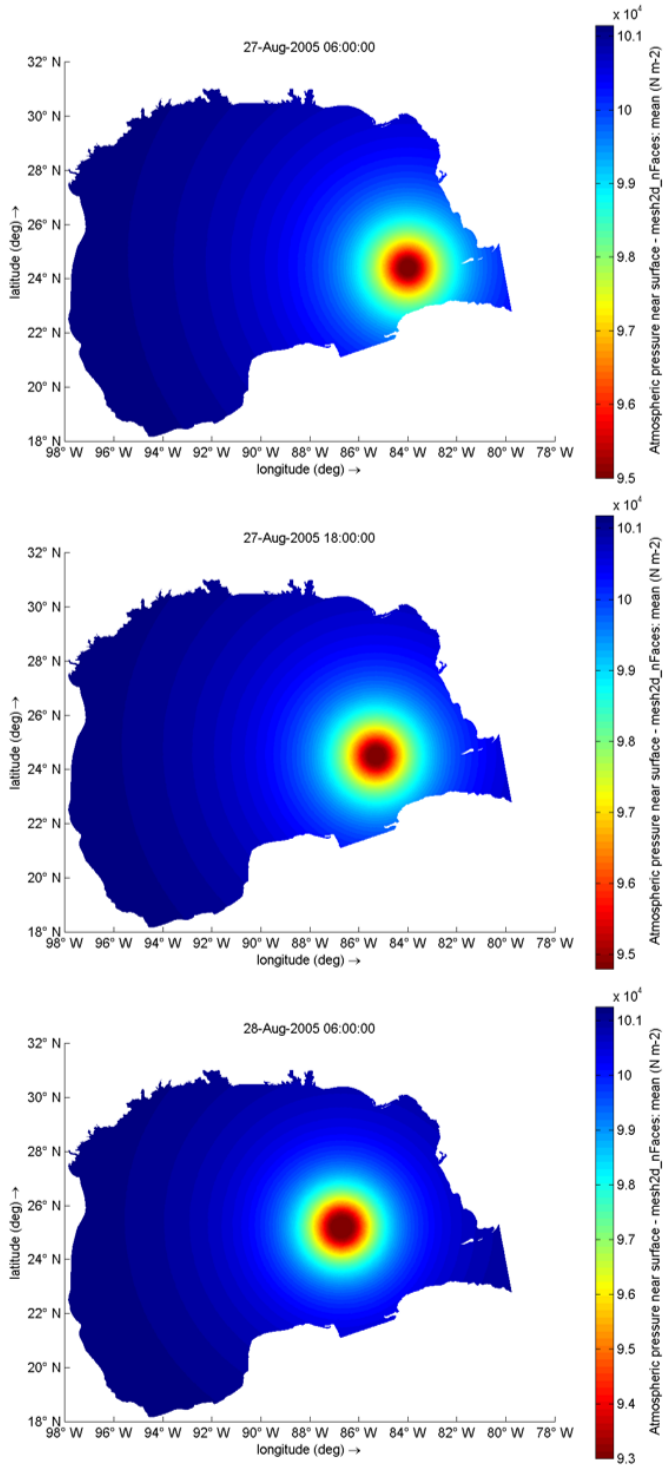
27-Aug-2005 06:00:00
27-Aug-2005 18:00:00
28-Aug-2005 06:00:00
latitude (deg) →
longitude (deg) →
32° N
30° N
28° N
26° N
24° N
22° N
20° N
18° N
98° W
96° W
94° W
92° W
90° W
88° W
86° W
84° W
82° W
80° W
78° W
x 10^4
10.1
10
9.9
9.8
9.7
9.6
9.5
9.4
9.3
Atmospheric pressure near surface - mesh2d_nFaces: mean (N m-2)

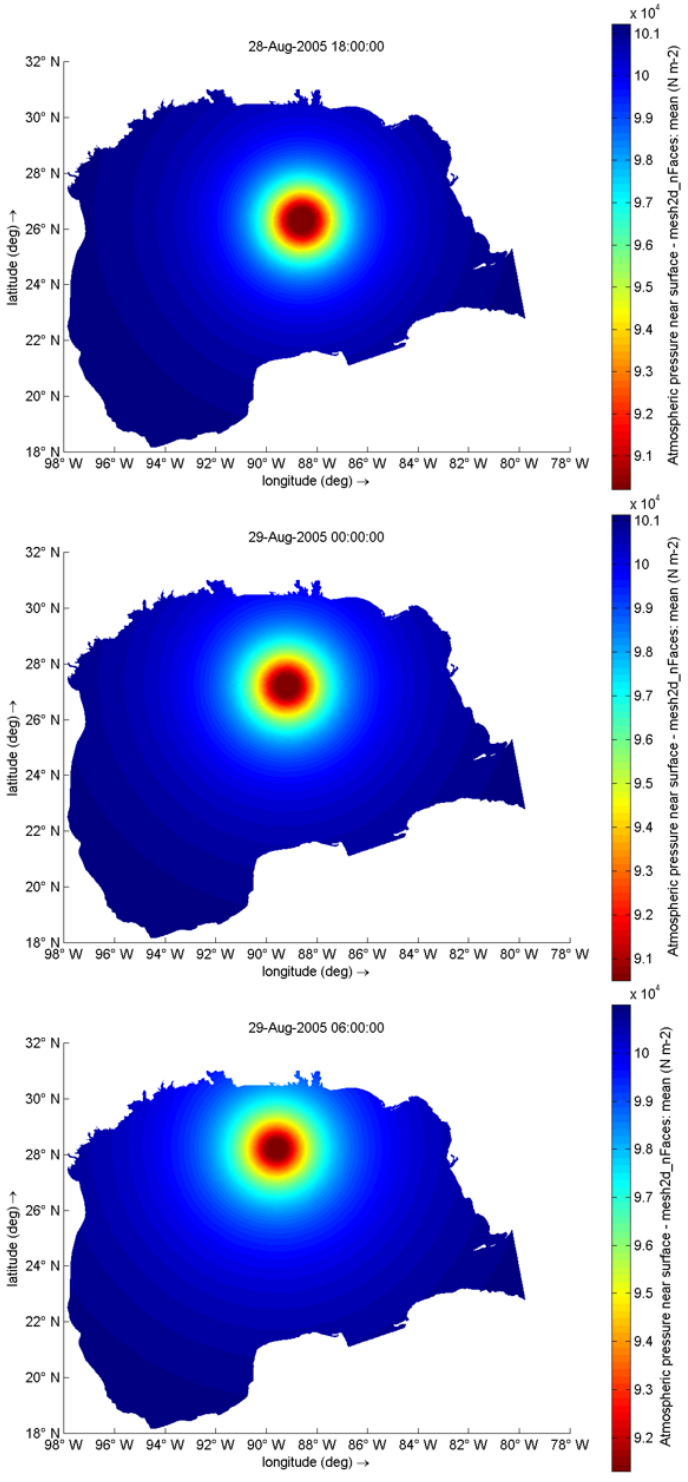
28-Aug-2005 18:00:00
29-Aug-2005 00:00:00
29-Aug-2005 06:00:00
latitude (deg) →
longitude (deg) →
32° N
30° N
28° N
26° N
24° N
22° N
20° N
18° N
98° W
96° W
94° W
92° W
90° W
88° W
86° W
84° W
82° W
80° W
78° W
x 10^4
10.1
10
9.9
9.8
9.7
9.6
9.5
9.4
9.3
9.2
9.1
Atmospheric pressure near surface - mesh2d_nFaces: mean (N m-2)

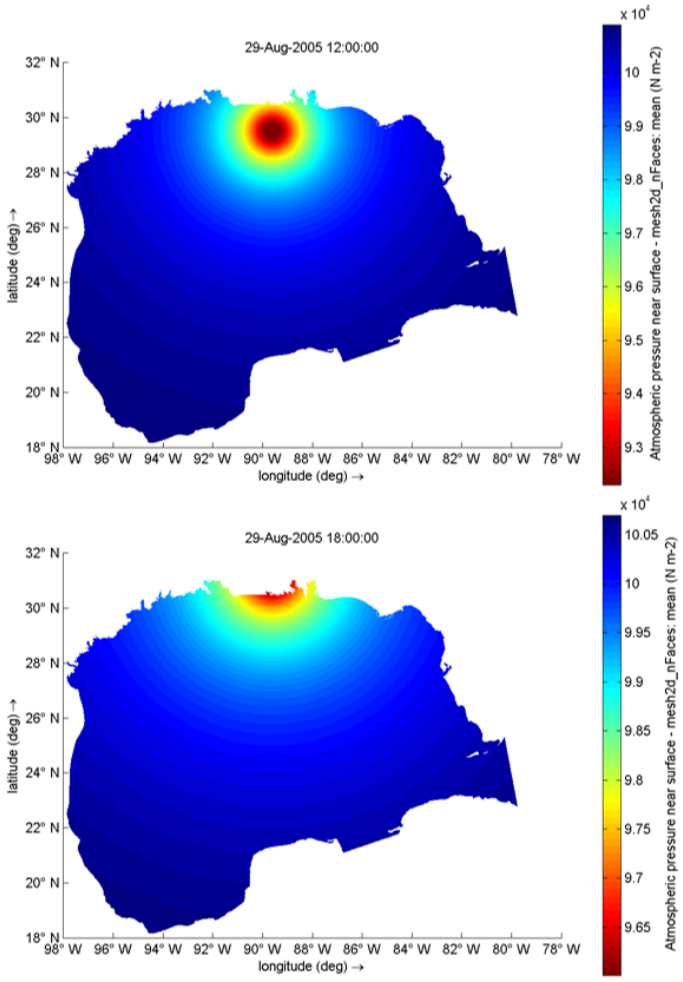
29-Aug-2005 12:00:00
32° N
30° N
28° N
26° N
24° N
22° N
20° N
18° N
latitude (deg) →
98° W 96° W 94° W 92° W 90° W 88° W 86° W 84° W 82° W 80° W 78° W
longitude (deg) →
x 10^4
10
9.9
9.8
9.7
9.6
9.5
9.4
9.3
Atmospheric pressure near surface - mesh2d_nFaces: mean (N m-2)
29-Aug-2005 18:00:00
32° N
30° N
28° N
26° N
24° N
22° N
20° N
18° N
latitude (deg) →
98° W 96° W 94° W 92° W 90° W 88° W 86° W 84° W 82° W 80° W 78° W
longitude (deg) →
x 10^4
10.05
10
9.95
9.9
9.85
9.8
9.75
9.7
9.65
Atmospheric pressure near surface - mesh2d_nFaces: mean (N m-2)

D.2 Wind speed (y-component)

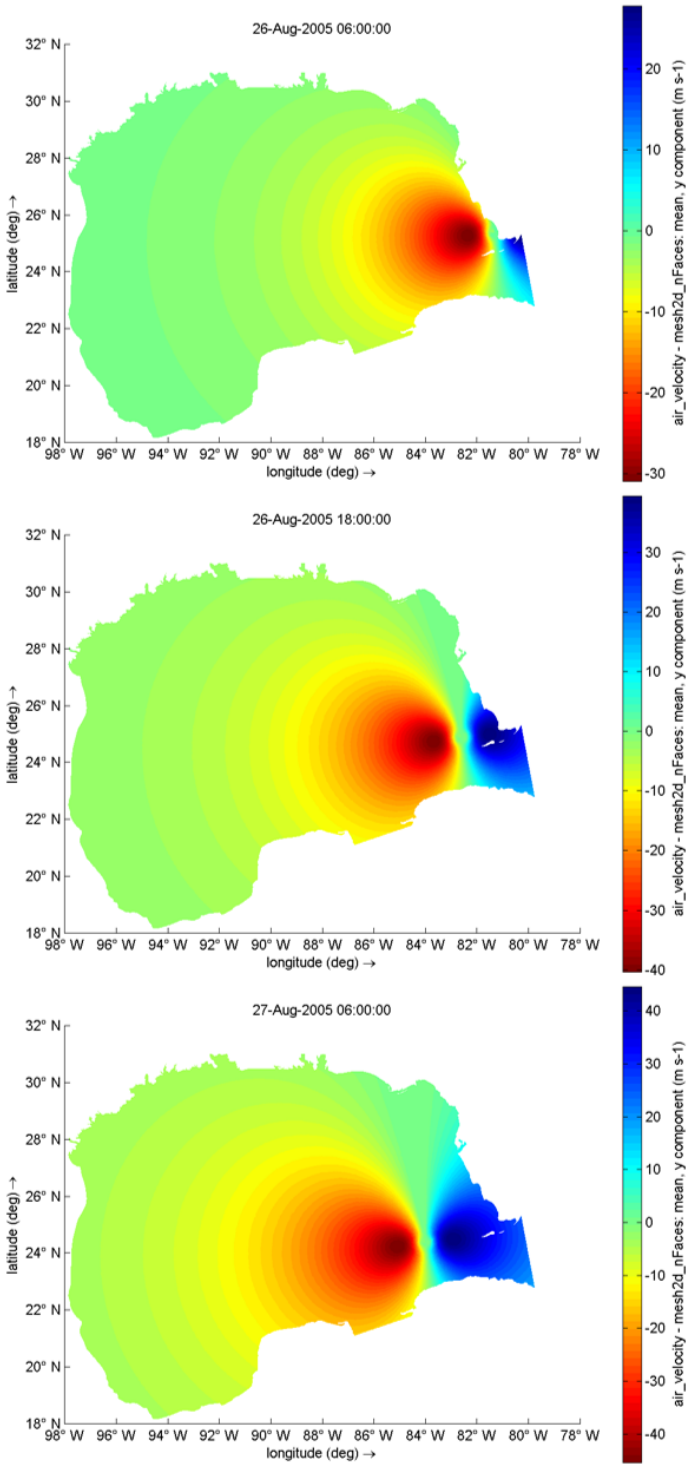

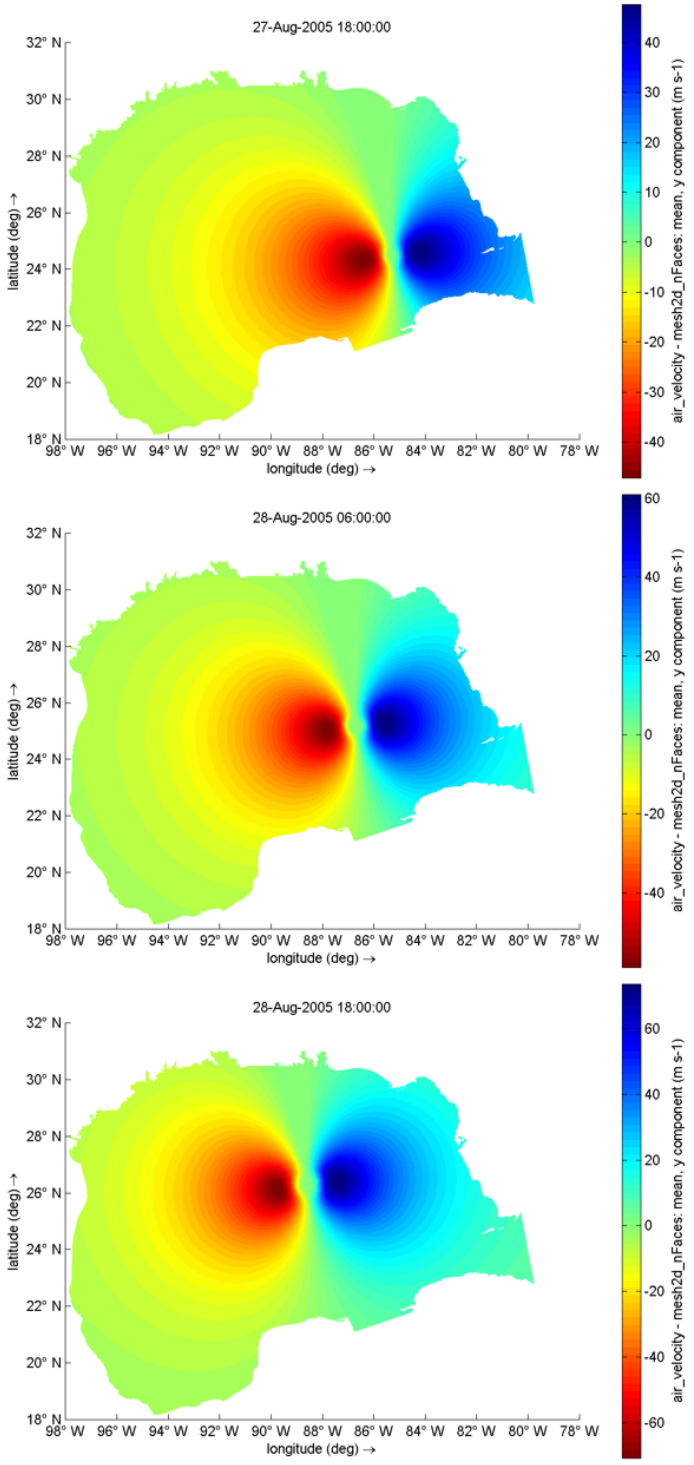
27-Aug-2005 18:00:00
28-Aug-2005 06:00:00
28-Aug-2005 18:00:00
latitude (deg) →
longitude (deg) →
32° N
30° N
28° N
26° N
24° N
22° N
20° N
18° N
98° W
96° W
94° W
92° W
90° W
88° W
86° W
84° W
82° W
80° W
78° W
air_velocity - mesh2d_nFaces: mean, y component (m s-1)
40
30
20
10
0
-10
-20
-30
-40
60
-60

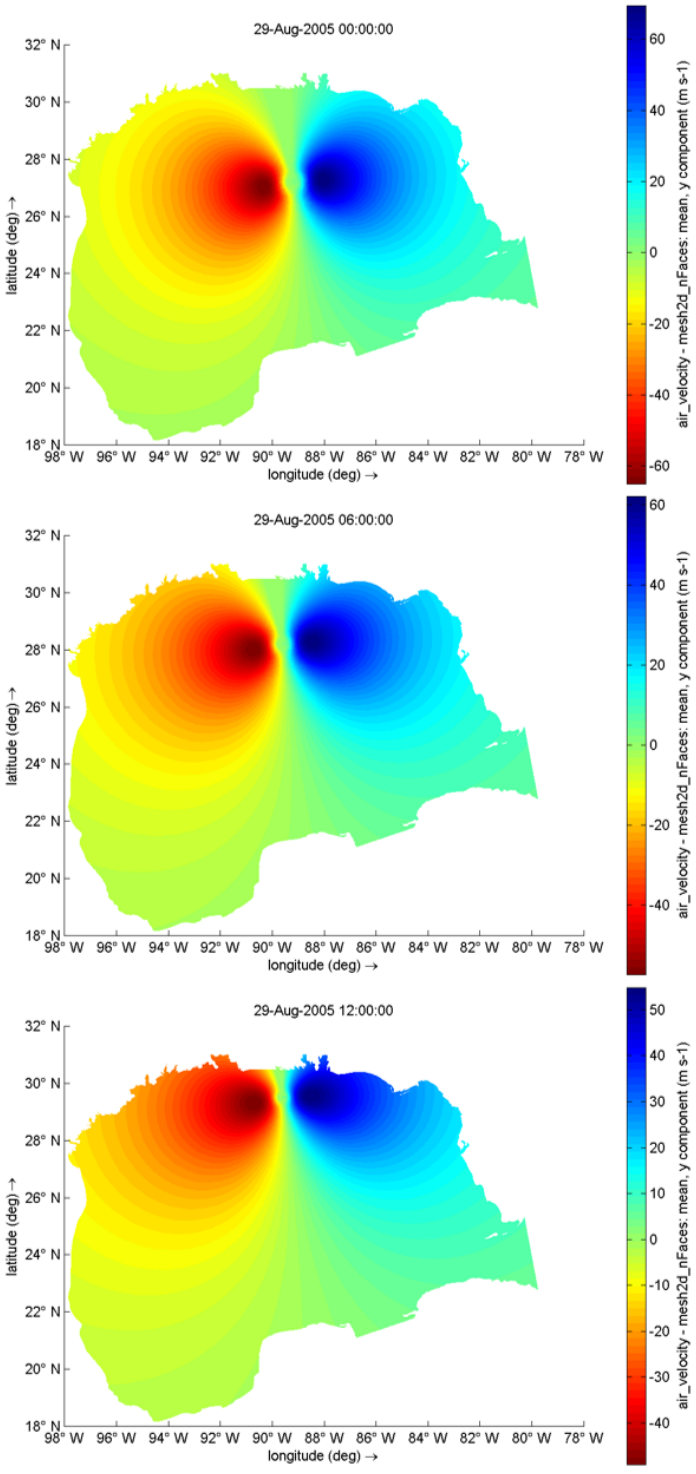
29-Aug-2005 00:00:00
32° N
30° N
28° N
26° N
24° N
22° N
20° N
18° N
latitude (deg) →
98° W 96° W 94° W 92° W 90° W 88° W 86° W 84° W 82° W 80° W 78° W
longitude (deg) →
60
40
20
0
-20
-40
-60
air_velocity - mesh2d_nFaces: mean, y component (m s-1)
29-Aug-2005 06:00:00
32° N
30° N
28° N
26° N
24° N
22° N
20° N
18° N
latitude (deg) →
98° W 96° W 94° W 92° W 90° W 88° W 86° W 84° W 82° W 80° W 78° W
longitude (deg) →
60
40
20
0
-20
-40
air_velocity - mesh2d_nFaces: mean, y component (m s-1)
29-Aug-2005 12:00:00
32° N
30° N
28° N
26° N
24° N
22° N
20° N
18° N
latitude (deg) →
98° W 96° W 94° W 92° W 90° W 88° W 86° W 84° W 82° W 80° W 78° W
longitude (deg) →
50
40
30
20
10
0
-10
-20
-30
-40
air_velocity - mesh2d_nFaces: mean, y component (m s-1)

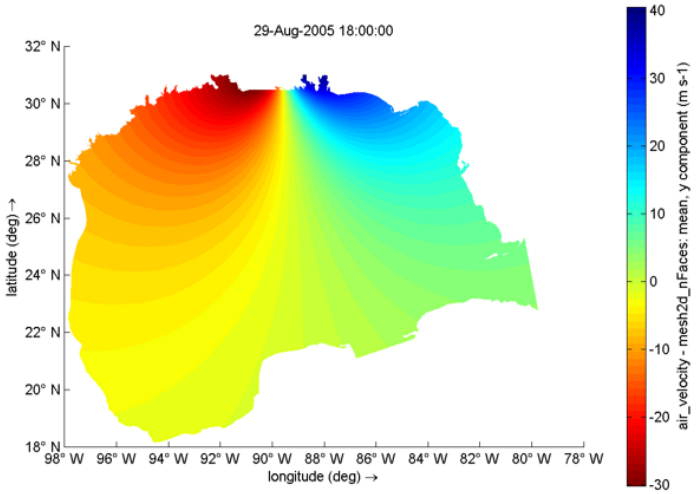
29-Aug-2005 18:00:00
32° N
30° N
28° N
26° N
24° N
22° N
20° N
18° N
latitude (deg) →
98° W
96° W
94° W
92° W
90° W
88° W
86° W
84° W
82° W
80° W
78° W
longitude (deg) →
40
30
20
10
0
-10
-20
-30
air_velocity - mesh2d_nFaces: mean, y component (m s-1)

D.3 Water level

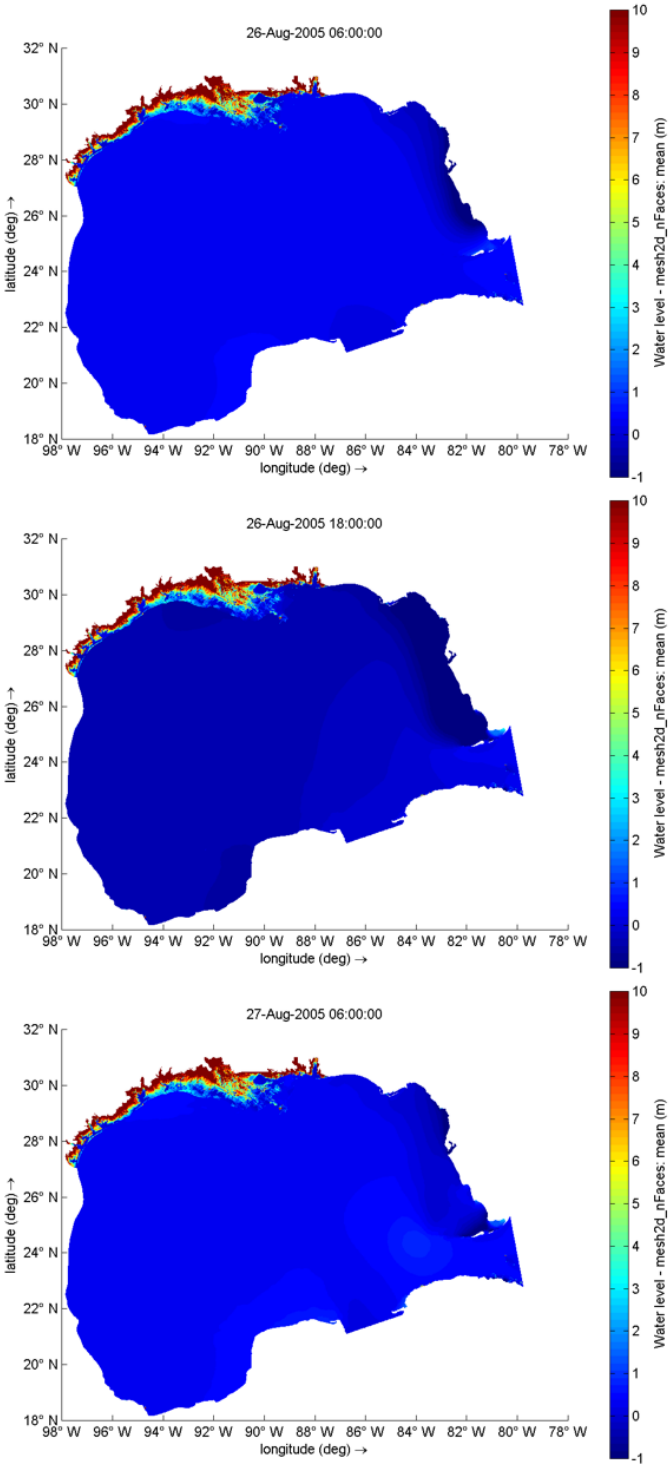

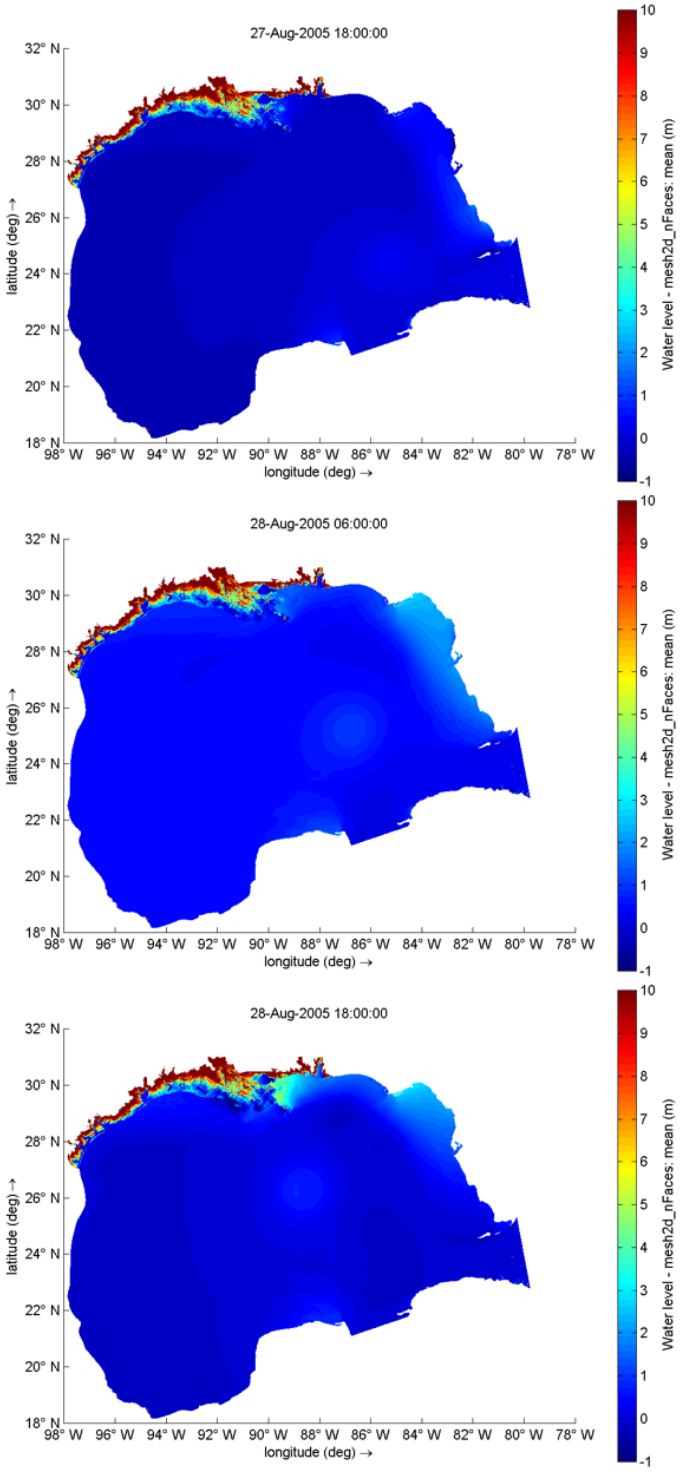
27-Aug-2005 18:00:00
28-Aug-2005 06:00:00
28-Aug-2005 18:00:00
latitude (deg) →
longitude (deg) →
32° N
30° N
28° N
26° N
24° N
22° N
20° N
18° N
98° W
96° W
94° W
92° W
90° W
88° W
86° W
84° W
82° W
80° W
78° W
Water level - mesh2d_nFaces: mean (m)
10
9
8
7
6
5
4
3
2
1
0
-1

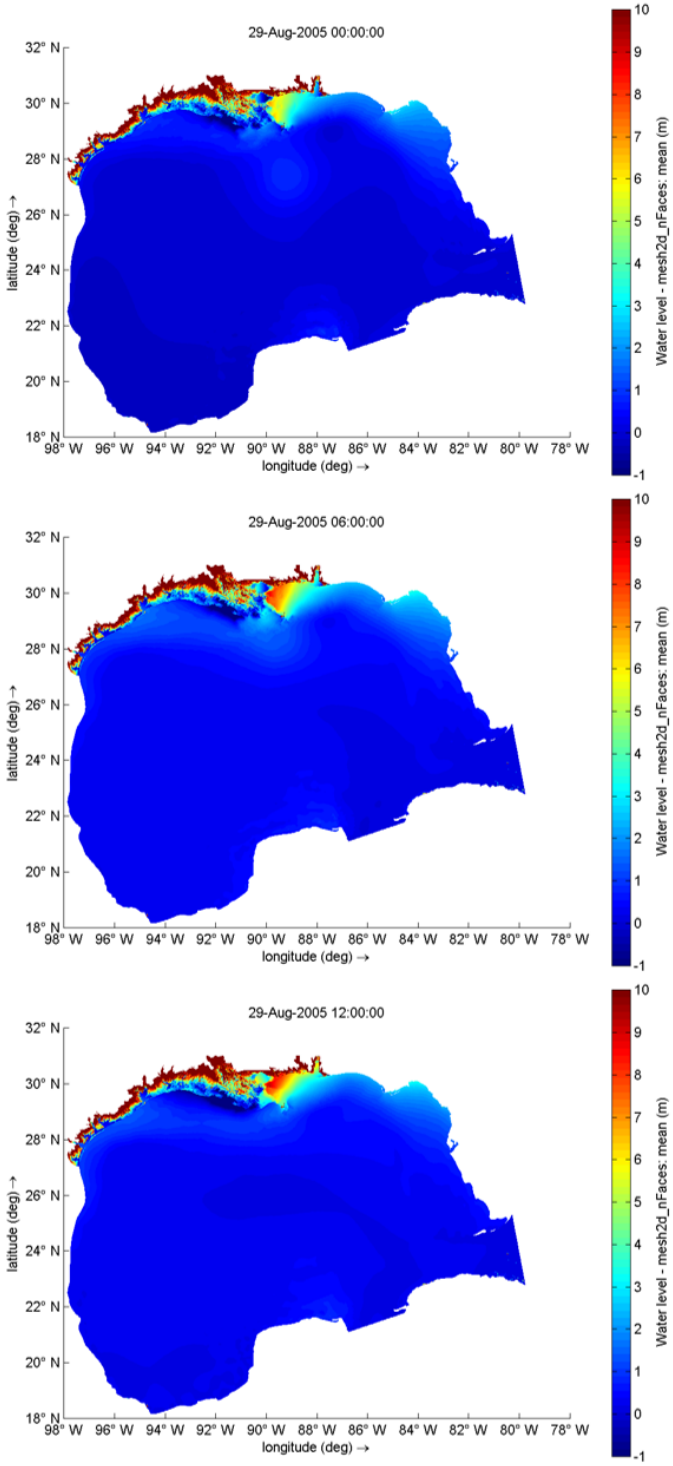
29-Aug-2005 00:00:00
29-Aug-2005 06:00:00
29-Aug-2005 12:00:00
latitude (deg) →
longitude (deg) →
32° N
30° N
28° N
26° N
24° N
22° N
20° N
18° N
98° W
96° W
94° W
92° W
90° W
88° W
86° W
84° W
82° W
80° W
78° W
Water level - mesh2d_nFaces: mean (m)
10
9
8
7
6
5
4
3
2
1
0
-1

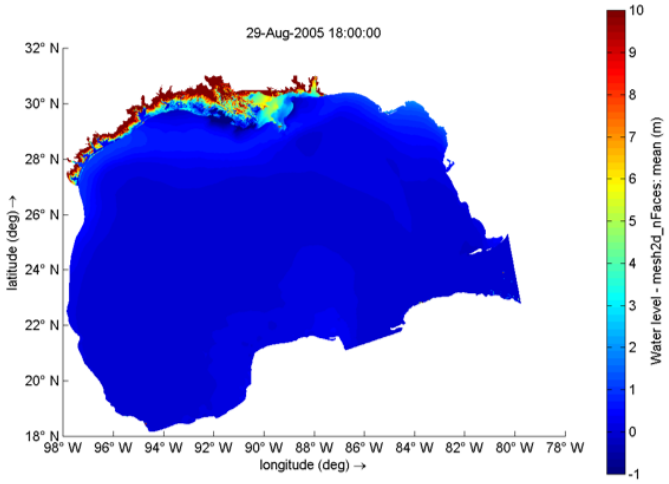
29-Aug-2005 18:00:00
32° N
30° N
28° N
26° N
24° N
22° N
20° N
18° N
latitude (deg) →
98° W
96° W
94° W
92° W
90° W
88° W
86° W
84° W
82° W
80° W
78° W
longitude (deg) →
10
9
8
7
6
5
4
3
2
1
0
-1
Water level - mesh2d_nFaces: mean (m)

APPENDIX E

Historical hurricanes making landfall in Mississippi (22 hurricanes)

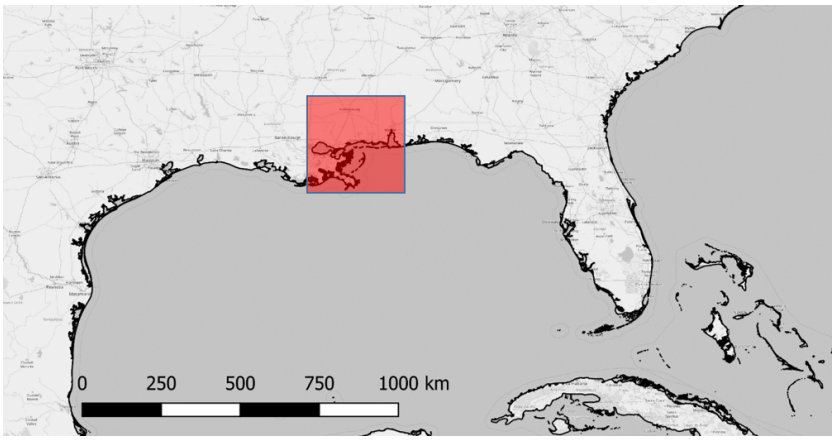

Figure E.1: Geographical domain considered for the selection of hurricanes (red shadowed rectangle).

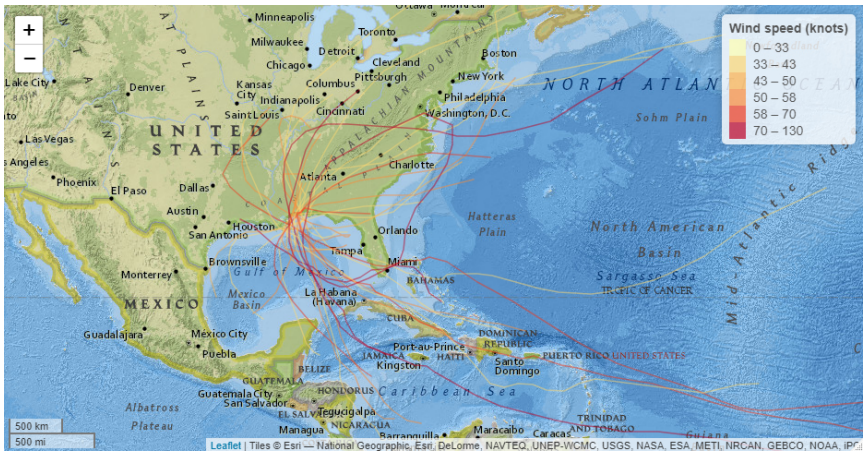

Figure E.2: Hurricane best tracks of the 22 events that fall in the 120-kilometer alongshore region surrounding Gulfport Harbour.

Bibliography

[1] C. Blain, R. Linzell, P. Chu, and C. Massey. Validation test report for the ADvanced CIRCulation Model (ADCIRC). https://pdfs.semanticscholar.org/d2a3/84d19a9fdfc980e90a48db9b4c7270e3183b.pdf, 2010.

[2] M. Browne, B. Castelle, D. Strauss, R. Tomlinson, M. Blumenstein, and C. Lane. Near-shore swell estimation from a global wind-wave model: Spectral process, linear and artificial neuronal network models. *Coastal Engineering*, 54 (5):445–460, 2007.

[3] K. Bryant and M. Akbar. An exploration of wind stress calculation techniques in hurricane storm surge modeling. *Journal of Maritime Science*, 58(4), 2016.

[4] S. Bunya, J. Dietrich, J. Westerink, B. Ebersole, J. Smith, J. Atkinson, R. Jensen, D. Resio, R. Luettich, C. Dawson, V. Cardone, A. Cox, M. Powell, H. Westerink, and H. Roberts. A high-resolution coupled riverine flow, tide, wind, wind wave and storm surge model for Southern Louisiana and Mississippi: Prt II - Model Development and Validation. *Monthly Weather Review*, 2010.

[5] S. Bunya, J. Dietrich, J. Westerink, B. Ebersole, J. Smith, J. Atkinson, R. Jensen, D. Resio, R. Luettich, C. Dawson, V. Cardone, A. Cox, M. Powell, H. Westerink, and H. Roberts. A high-resolution coupled riverine flow, tide, wind, wind wave and storm surge model for Southern Louisiana and Mississippi: Part I - Model Development and Validation. *Monthly Weather Review*, 2010.

[6] A. Castro, F. Pinto, and G. Iglesias. Artificial intelligence applied to plane wave reflection at submerged breakwaters. *Journal of Hydraulic Research*, 49 (4):465–472, 2011.

[7] Center for Climate and Energy Solutions. Hurricanes and climate change. https://www.c2es.org/content/hurricanes-and-climate-change/, 2019.

[8] H. Charnock. Wind stress on a water surface. *Quarterly Journal of the Royal Meteorological Society*, 81:639–640, 1955.

[9] J. Davies. Geographical variation in coastal development. *Longman*, 1980.

[10] A. De Sherbinn, A. Schiller, and A. Pulsipher. The vulnerability of global cities to climate hazards. https://journals.sagepub.com/doi/pdf/10.1177/0956247807076725, 2007.

[11] D. Dee. Guidelines for documenting the validity of computational modelling software. https://towardsdatascience.com/beginners-ask-how-many-hidden-layers-neurons-to-use-in-artificial-neural-networks-51466afa0d3e, 1994.

[12] Deltares. Deltares: Enabling delta life. https://www.deltares.nl/en/, 2011.

[13] Deltares. D-Flow Flexible Mesh User Manual. page 58, 2019.

[14] Deltares Systems. Validation document Delft3D Flexible Mesh Suite. 2017.

[15] J. C. Dietrich, S. Tanaka, J. J. Westerink, C. N. Dawson, R. A. Luettich, M. Zijlema, L. H. Holthuijsen, J. M. Smith, L. G. Westernik, and H. J. Westerink. Performance of the unstructured mesh SWAN+ADCIRC model in computing hurricane waves and surge. *Springer*, 2012.

[16] K. Dresback, R. Kolar, and J. Dietrich. On the form of the momentum equation for shallow water models based on the generalized wave continuity equation. https://www.sciencedirect.com/science/article/pii/S0309170804002088, 2005.

[17] V. Dvorak. Tropical cyclone intensity analysis and forecasting from satellite imagery. *Monthly weather review (NOAA)*, 103:420–430, 1975.

[18] Federal Emergency Management Agency. Wave setup. *Analysis and Mapping Guidelines - Focused Study Report*, 2005.

[19] Federal Emergency Management Agency. Wave setup, runup, and overtopping. *Guidelines and Specifications for Flood Hazard Mapping Partners*, 2005.

[20] M. Francis. Hurricanes on Earth, hurricanes on Jupiter. `https://galileospendulum.org/2011/08/29/hurricanes-on-earth-hurricanes-on-jupiter/`, 2011.

[21] J. Freer, K. Beven, J. Neal, G. Schumann, J. Hall, and P. Bates. Flood risk and uncertainty. *Risk and Uncertainty Assessment for Natural Hazards, Cambridge (UK)*, pages 190–233, 2011.

[22] General Bathymetric Chart of the Oceans. Global ocean and land terrain models. `https://www.gebco.net/data_and_products/gridded_bathymetry_data/`, 2019.

[23] C. Genest and A. C. Favre. Everything you always wanted to know about copula modeling but were afraid to ask. *Journal of hydrologic engineering*, 2007.

[24] C. Genest and L. Rivest. On the multivariate probability integral transformation. *Statistics Probability Letters*, 53(4):391–399, 2001.

[25] S. Graham and H. Riebeek. Hurricanes: the greatest storms on Earth. *NASA*, 2006.

[26] W. M. Gray. Global view of the origin of tropical disturbances and storms. 96:669–700, 1968.

[27] A. Grzegorzewski, M. Cialone, A. Lansen, M. van Ledden, J. Smith, and T. Wamsley. The influence of barrier islands on hurricane-generated storm surge and waves in Louisiana and Mississippi. `https://www.researchgate.net/publication/265003326_THE_INFLUENCE_OF_BARRIER_ISLANDS_ON_HURRICANE-_GENERATED_STORM_SURGE_AND_WAVES_IN_LOUISIANA_AND_MISSISSIPPI`, 2009.

[28] B. Gutierrez, N. Plant, and E. Thieler. A Bayesian network to predict coastal vulnerability to sea level rise. *Journal of Geophysical Research*, 2011.

[29] A. Hanea, M. Gheorghe, and D. Ababei. Non-parametric Bayesian networks for parameter estimation in reservoir simulation: A graphical take on the ensemble Kalman filter. *Computational Geosciences*, 2013.

[30] A. Hanea, O. Morales-Napoles, and D. Ababei. Non-parametric Bayesian Networks: Improving theory and reviewing applications. *Elsevier*, 144:265–284, 2015.

[31] E. L. Harp, M. Castañeda, and M. D. Held. Landslides triggered by Hurricane Mitch in Tegucigalpa, Honduras. *USGS*, 2002.

[32] B. Harper. Tropical cyclone parameter estimation in the Australian region: Wind–pressure relationships and related issues for engineering planning and design. *Woodside Australian Energy*, 2002.

[33] Z. Hausfather. Explainer: How climate change is accelerating sea level rise. `https://www.carbonbrief.org/explainer-how-climate-change-is-accelerating-sea-level-rise`, 2019.

[34] G. J. Holland. An analytic model of the wind and pressure profiles in hurricanes. *Monthly Weather Review*, 108:1212–1218, 1980.

[35] Y. Huang, R. Weisberg, L. Zheng, and M. Zijlema. Gulf of Mexico hurricane wave simulations using SWAN : Bulk formula-based drag coefficient sensitivity for Hurricane Ike. *Journal of Geophysical Research*, 118:3916–3938, 2013.

[36] J. Irish, Y. Song, and K. Chang. Probabilistic hurricane surge forecasting using parameterized surge response functions. *Geophysical Research Letters*, 38:L03606, 2011.

[37] C. Jelesnianski, J. Chen, and W. Shaffer. Sea lake and overland surge from hurricanes: Display training. `https://slosh.nws.noaa.gov/slosh/SLOSH-Display-Training.pdf`, 2003.

[38] S. Jonkman, M.-N. O. Steenbergen, R.D.J.M, J. Vrijling, and A. Vrouwenvelder. Probabilistic design: Risk and reliability. *Delft University of Technology*, 2015.

[39] M.-R. Keim, B.D and G. Stone. Spatiotemporal patterns and return periods of tropical storm and hurricane strikes from texas to maine. https://journals.ametsoc.org/doi/pdf/10.1175/JCLI4187.1, 2006.

[40] P. Kerr, J. Westerink, J. Dietrich, R. Martyr, S. Tanaka, D. Resio, J. Smith, H. Westerink, L. Westerink, T. Tamsley, M. van Ledden, and W. de Jong. Surge generation mechanisms in the lower mississippi river and discharge dependency. *Journal of waterway, port, coastal and ocean engineering*, 139(4), 2013.

[41] J. P. Kossin, J. A. Knaff, H. I. Berger, D. C. Herndon, T. A. Cram, C. S. Velden, R. J. Murnane, and J. D. Hawkins. Estimating hurricane wind structure in the absence of aircraft reconnaissance. *Weather forecast*, 22, 89-101.

[42] C. Kousky and E. Michel-Kerjan. Examining flood insurance claims in the United States: six key findings. *The journal of risk and insurance*, 2015.

[43] A. Laing and J. L. Evans. Introduction to tropical meteorology. *University Corporation for Atmospheric Research*, 8:90, 2013.

[44] C. Landsea and J. Beven. The revised Atlantic hurricane database (HURDAT2). https://www.aoml.noaa.gov/hrd/hurdat/hurdat2-format.pdf, 2019.

[45] C. Landsea and J. Franklin. Atlantic hurricane database uncertainty and presentation of a new database format. *Monthly weather review (NOAA)*, 141:3576–3592, 2012.

[46] M. Lopez and G. Iglesias. Artificial intelligence for estimating infragravity energy in a harbour. *Elsevier (Ocean Engineering)*, 57:56–63, 2013.

[47] V. Makin. A note on the drag of the sea surface at hurricane winds. *Boundary-Layer Meteorology*, 115:169–176, 2005.

[48] J. Malilay. The public health consequences of disasters. tropical cyclones. *Oxford University Press*, pages 207–227, 1997.

[49] D. L. Malmquist and A. F. Michaels. Severe storms and the insurance industry. *Routledge hazards and disaster series*, 1:54–69, 2000.

[50] K. L. McInnes, G. D. Hubbert, S. E. Oliver, and D. J. Abbs. A numerical modelling study of coastal flooding. *Meteorology and Atmospheric Physics*, 80:217–233, 2002.

[51] V. Mihajlovic and M. Petkovic. Dynamic Bayesian Networks: A State of the Art. https://ris.utwente.nl/ws/portalfiles/portal/27679465/0000006a.pdf, 2001.

[52] S. Miller, R. Muir-Wood, and A. Boissonnade. An exploration of trends in normalized weather-related catastrophe losses. *Climate extremes and society*, pages 225–247, 2008.

[53] O. Morales-Napoles, D. Worm, P. van den Haak, A. Hanea, W. Courage, and S. Miraglia. Introduction to Bayesian Networks. *TNO*, 2013.

[54] A. Mukai, J. Westerink, R. Luettich, and D. Mark. Eastcoast 2001, a tidal constituent database for Western North Atlantic, Gulf of Mexico and Caribbean Sea. *Coastal Inlets Research Program*, 2002.

[55] T. Murty. Storm surges-meteorological ocean tides. *Canadian Bulletin of Fisheries and Aquatic Sciences*, 212:876–897, 1984.

[56] National Hurricane Center. Tropical Cyclone Report: Hurricane Katrina. https://www.nhc.noaa.gov/data/tcr/AL122005_Katrina.pdf, 2005.

[57] National Hurricane Center. Observed waterlevels at Bay Waveland Yacht Club, MS. https://tidesandcurrents.noaa.gov/waterlevels.html?id=8747437&units=metric&bdate=20191023&edate=20191024&timezone=GMT&datum=MSL&interval=6&action=, 2019.

[58] National Oceanic and Atmospheric Administration. Potential storm surge flooding. https://www.nhc.noaa.gov/surge/PotentialStormSurgeTips-media.pdf.

[59] National Oceanic and Atmospheric Administration. Coastal engineering 2008. https://www.aoml.noaa.gov/hrd/tcfaq/G16.html, 2014.

[60] National Oceanic and Atmospheric Administration. Best track data (HURDAT2). https://www.nhc.noaa.gov/data/, 2018.

[61] National Oceanic and Atmospheric Administration. International best track archive for climate stewardship (IBTrACS). https://www.ncdc.noaa.gov/ibtracs/index.php?name=ib-v4-access, 2018.

[62] National Oceanic and Atmospheric Administration. Glossary of National Hurricane Center terms. https://www.nhc.noaa.gov/aboutgloss.shtml, 2019.

[63] NHC: Storm Surge Unit. Introduction to storm surge. https://www.nhc.noaa.gov/surge/surge_intro.pdf, 2003.

[64] S. Pearson, C. Storlazzi, A. van Dongeren, M. Tissier, and A. Reniers. A Bayesian-based system to assess wave driven flooding hazards on coral reef-lined coasts. *Journal of Geophysical Research: Oceans*, 122:10999–10117, 2017.

[65] M. Powell, P. Vickery, and T. Reinhold. Reduced drag coefficient for high wind speeds in tropical cyclones. *Nature*, pages 279–283, 2003.

[66] M. Powell, P. Vickery, and T. Reinhold. Drag coefficient distribution and wind speed dependence in tropical cyclones. *Final Report to the National Oceanic Atmospheric Administration (NOAA) Joint Hurricane Testbed (JHT) Program*, 2006.

[67] S. Quiring, A. Schumacher, C. Labosier, and L. Zhu. Variations in mean annual tropical cyclone size in the Atlantic. *Journal of Geophysical Research*, 116, 2011.

[68] H. Saffir and R. Simpson. Saffir-Simpson hurricane wind scale. https://www.nhc.noaa.gov/aboutsshws.php, 1970.

[69] R. Schloemer. Analysis and synthesis of hurricane wind patterns over Lake Okechobee, FL. *Hydromet*, 30 (70:31):31–49, 1954.

[70] School of Ocean and Earth Science and Technology (SOEST): University of Hawaii at Manoa. Met 200 atmospheric processes and phenomena. https://www.soest.hawaii.edu/MET/Faculty/businger/courses/notes200/10Forces&Wind.pdf, 2013.

[71] A. Sebastian, E. Dupuits, and O. Morales-Napoles. Applying a Bayesian network based on Gaussian copulas to model the hydraulic boundary conditions for hurricane flood risk analysis in a coastal watershed. *Elsevier: Coastal Engineering*, 125:42–50, 2017.

[72] J. Smith. Coastal engineering 2008. *Proceedings of the 31st International Conference*, 2008.

[73] S. Smith and E. Banke. Variation of the sea surface drag coefficient with wind speed. *Quarterly Journal of the Royal Meteorological Society*, 101:665–673, 1975.

[74] S. R. Stewart. Tropical Cyclone Report Hurricane Cindy 3 – 7 July 2005. https://www.nhc.noaa.gov/data/tcr/AL032005_Cindy.pdf, 2005.

[75] D. Stromberg. Natural disasters, economic development and humanitarian aid. *Journal of economic perspectives*, 21:199–222, 2007.

[76] C. Szpilka. ADCIRC_db_extract_2012.F90, 2013.

[77] J. Teng, A. Jakeman, J. Vaze, B. Croke, D. Dutta, and S. Kim. Flood inundation modelling: A review of methods, recent advances and uncertainty analysis. *Environmental Modelling and Software*, 90:201–216, 2017.

[78] UniNet. Uninet help. https://d1rkab7tlqy5f1.cloudfront.net/EWI/Over%20de%20faculteit/Afdelingen/Applied%20Mathematics/Applied%20Probability/Risk/Download/UninetHelp.pdf, 2019.

[79] US Department of Homeland Security. Final coastal and riverine high water mark collection for Hurricane Katrina in Mississipi. *FEMA-1604-DR-MS, Task Orders 413 and 420*, 2006.

[80] D. Vatvani, N. Zweers, M. van Ormondt, A. Smale, H. de Vries, and V. Makin. Storm surge and wave simulations in the gulf of mexico using a consistent drag relation for atmospheric and storm surge models. *Natural Hazards and Earth System Sciences*, 12:2399–2410, 2012.

[81] A. Veltcheva and Y. Uchiyama. Investigation of the typhoon pressure and wind field with application for storm surge estimation. *Report of the port and airport research institute*, 41(2), 2002.

[82] H. Verhaeghe, J. De Rouck, and J. van der Meer. Combined classifier-quantifier model: a 2-phases neuronal model for prediction of wave overtopping at coastal structures. *Coastal Engineering*, 55 (5):357–374, 2008.

[83] Q. Wang, J. Chen, and K. Hu. Storm surge prediction for louisiana coast using artificial neuronal networks. 2016.

[84] J. Williams. The weather book. *Vintage Books*, 1997.

[85] L. Xie, H. Liu, Liu, and S. Bao. A numerical study of the effect of hurricane wind asymmetry on storm surgeand inundation. *Elsevier*, 36:71–79, 2011.

[86] M. Zijlema. Computational modelling of flow and transport. *Delft University of Technology*, 2015.


TU Delft
Delft
University of
Technology


AXA